

# Contents

<i>Preface</i> . . . . .	vii
<i>Statement</i> . . . . .	viii
<i>Acknowledgements</i> . . . . .	ix
<i>Summary</i> . . . . .	x
<b>I Introduction</b>	<b>xiii</b>
<b>1 Temperature Measurement in the Industrial Environment</b>	<b>1</b>
1.1 Introduction . . . . .	1
1.2 The Emission of Radiation from Real Surfaces . . . . .	4
1.2.1 Blackbody Radiators . . . . .	4
1.2.2 Non-Blackbodies . . . . .	4
1.2.3 Radiation Thermometry . . . . .	5
1.2.4 Kirchhoff's Law . . . . .	6
1.2.5 Real Surface Effects . . . . .	8
1.3 Oxidation of Iron . . . . .	9
1.3.1 Formation of Wustite . . . . .	11
1.3.2 Formation of Magnetite . . . . .	13
1.3.3 Formation of Haematite . . . . .	13
1.3.4 2-D Structures of Adsorbed Layers . . . . .	14

1.4	Electrical Properties of Iron and its Oxides . . . . .	16
1.4.1	Magnetic Effects . . . . .	16
1.4.2	Dielectric Constants . . . . .	17
1.4.3	Conductivity . . . . .	17
<b>II</b>	<b>The Optical Problem-Plane Surfaces</b>	<b>19</b>
<b>2</b>	<b>Reflection and Refraction from Plane Surfaces</b>	<b>21</b>
2.1	Introduction . . . . .	21
2.2	Smooth Surface Scattering - A Review . . . . .	22
2.3	The Need for Further Development . . . . .	24
2.4	Plane Waves in Material Media . . . . .	25
2.4.1	Maxwell's Equations in a Conducting Medium . . . . .	26
2.4.2	Plane Wave Solution . . . . .	28
2.5	Boundary Conditions at an interface . . . . .	32
<b>3</b>	<b>Interference in Plane Layered Media</b>	<b>35</b>
3.1	Introduction . . . . .	35
3.2	Electromagnetic Approach . . . . .	36
3.2.1	Single Layer Case . . . . .	36
3.2.2	Multiple Layer Case . . . . .	45
3.3	The Reflected Field . . . . .	47
3.3.1	Unoxidised Surfaces . . . . .	47
3.3.2	Oxidised Surfaces . . . . .	50
3.3.3	Instability of Emissivity at low thickness of Scale . . . . .	54
<b>4</b>	<b>Numerical Solutions for Smooth Surfaces</b>	<b>57</b>
4.1	The Numerical Scheme . . . . .	57
4.2	Multi-Layer Oxide Films . . . . .	58

4.3	Interpretation and Discussion of Results . . . . .	60
4.3.1	Comparison to Experimental Data . . . . .	60
4.3.2	Comparison of One-Layer and Three-Layer Models . . . . .	62
4.3.3	Emissivity Change with Thickness . . . . .	63
4.3.4	Emissivity Change with Wavelength . . . . .	66
4.3.5	Emissivity Variation with Temperature . . . . .	67
4.3.6	Final Conclusions for the Smooth Case . . . . .	68
<b>III</b>	<b>The Optical Problem-Irregular Surfaces</b>	<b>71</b>
<b>5</b>	<b>Rough Surfaces</b>	<b>73</b>
5.1	Introduction . . . . .	73
5.2	The Nature of Rough Surfaces . . . . .	74
5.3	The Rayleigh Criterion . . . . .	75
5.4	Scattering Characteristics of Rough Surfaces . . . . .	77
5.5	Rough Surface Types . . . . .	79
5.6	Rough Surface Statistics . . . . .	80
5.7	Physical and Geometrical Optics . . . . .	81
5.7.1	Geometrical Optics . . . . .	81
5.7.2	Physical Optics and Diffraction . . . . .	82
5.8	Fresnel and Fraunhofer Diffraction . . . . .	83
5.9	Multiple Scattering and Surface Shadowing . . . . .	83
5.10	Influence of Scattering Regions . . . . .	84
5.11	The Emissivity of Rough Surfaces - A Review to Date . . . . .	86
5.11.1	Optical Roughness ratios $\sigma/\lambda > 1$ . . . . .	87
5.11.2	Optical Roughness ratios $\sigma/\lambda \ll 1$ . . . . .	88
5.11.3	Rough Filmed Surfaces . . . . .	92
5.12	Review of Electromagnetic Scattering Approaches . . . . .	95

5.12.1	Differential Methods . . . . .	95
5.12.2	Integral Methods . . . . .	95
5.12.3	Rayleigh Method . . . . .	96
5.12.4	Perturbation Theory . . . . .	96
5.12.5	Integral Equation Methods . . . . .	96
5.12.6	Variational Methods . . . . .	97
5.12.7	Other Methods . . . . .	97
5.13	The Purpose of Further Research . . . . .	97
<b>6</b>	<b>Kirchhoff Theory</b>	<b>99</b>
6.1	Introduction . . . . .	99
6.2	The Helmholtz Representation . . . . .	101
6.2.1	The Interior Problem in $R^3$ . . . . .	101
6.2.2	The Exterior Problem in $R^3$ . . . . .	102
6.2.3	Existence and Uniqueness . . . . .	105
6.3	Beckmann's Theory . . . . .	106
6.3.1	Preliminary Problem Construction . . . . .	106
6.4	The Scattering Integral . . . . .	115
6.4.1	The Kirchhoff Solution in the Fraunhofer Zone . . . . .	117
6.4.2	The Determination of Rough Surface Emissivity . . . . .	118
<b>7</b>	<b>Unoxidised Rough Steel Surfaces</b>	<b>121</b>
7.1	Introduction . . . . .	121
7.1.1	Non-Periodic Surfaces . . . . .	121
7.1.2	Periodic Surfaces . . . . .	122
7.2	The Extension to Infinite Surfaces . . . . .	125
7.3	Non-Periodically Rough Surfaces . . . . .	126
7.3.1	Smooth Surface $\zeta' = 0$ . . . . .	127
7.3.2	Non-Periodic, Perfectly Conducting Surface . . . . .	128

7.4	Rough Periodic Functions . . . . .	131
7.5	Simplifications of the Kirchhoff Integral . . . . .	131
7.5.1	Periodicity of $\zeta(x)$ . . . . .	132
7.5.2	Main Integral (non-edge terms) . . . . .	132
7.5.3	Edge Terms . . . . .	134
7.5.4	Complete Solution . . . . .	134
7.6	Perfect Conductivity . . . . .	135
7.6.1	Main Integral . . . . .	135
7.6.2	Edge Terms . . . . .	136
7.6.3	Total Solution . . . . .	136
7.6.4	Even Functions . . . . .	137
7.6.5	Odd Functions . . . . .	139
7.6.6	Solution in Terms of $\theta_I, \theta_S$ . . . . .	140
7.6.7	Total Solutions : Even and Odd Functions . . . . .	141
7.7	Mean Plane Reflection Coefficient . . . . .	142
7.8	Varying Surface Reflection coefficient . . . . .	142
7.8.1	Main Integral . . . . .	142
7.8.2	The Case $\theta_S = \theta_I = 0$ . . . . .	144
7.8.3	Edge Terms . . . . .	146
7.9	Specific Periodic Surface Profiles . . . . .	147
7.9.1	Solution Simplifications, $A = 0, T \rightarrow \infty$ . . . . .	148
7.9.2	The Main Integral . . . . .	149
7.9.3	Convergence Criteria for a Valid Solution . . . . .	149
7.9.4	Evaluation of the Integral $\int_0^{2\pi} \cos^{2m} x_0 e^{ik_z^- A \sin x_0} dx_0$ . . . . .	151
7.9.5	The Edge Terms . . . . .	152
7.9.6	The Complete Solution . . . . .	154
7.9.7	Comparison to Perfect Conducting Case . . . . .	155
7.9.8	The Approximate Solution . . . . .	155

7.9.9	Consequences of the Periodic Solution . . . . .	157
7.9.10	Closer Analysis of the second order term $1/4N_2(2\pi A/T)^2$ . . . . .	160
<b>8</b>	<b>Oxidised Rough Surfaces</b>	<b>163</b>
8.1	Introduction . . . . .	163
8.2	Constraints of the Method . . . . .	165
8.2.1	Fresnel Coefficients . . . . .	167
8.3	Solution for Periodically Rough Surfaces . . . . .	170
8.3.1	Consequences of the Oxidised Film Solution . . . . .	171
<b>9</b>	<b>Numerical Solution Scheme for Rough Surfaces</b>	<b>175</b>
9.1	Interpretation and Discussion of Numerical Results : Unoxidised Surfaces . . . . .	176
9.1.1	Conclusions . . . . .	178
9.2	Interpretation and Discussion of Numerical Results : Oxidised Surfaces . . . . .	179
9.3	Conclusions . . . . .	184
9.3.1	Summary . . . . .	185
9.4	Future Directions in Research . . . . .	186
<b>A</b>		<b>189</b>
A.1	Derivatives of odd and even functions . . . . .	189
A.2	Derivatives of Reflection Coefficients . . . . .	190
A.3	Properties of Bessel Functions . . . . .	193
A.4	Tangent Plane Criterion . . . . .	195
	<b>Bibliography</b>	<b>198</b>

## **Preface**

This thesis is submitted as the full requirement for the degree of Master of Science in Applied Mathematics.

Frank Bierbrauer

## Statement

This thesis contains no material which has been accepted for the award of any other degree or diploma in any university and, to the best of the author's knowledge, no material previously published or written by another person, except when due reference is made in the text of the thesis.

Frank Bierbrauer



## **Acknowledgements**

I would like to thank both my thesis supervisor Dr Andrew Prentice (mathematics department) and Dr John Chen (BHP Research Laboratories). John for his generous pep talks that were all too necessary at certain times, as well as for his friendship and enthusiasm. Andrew for his willingness to make numerous changes in my thesis direction during the years, and most of all for his help at times of need.

## Summary

This thesis "A Theoretical Investigation into Steel Surface Emissivity", arose out of a need from industry to more fully comprehend how the surface emissivity, an important parameter in the non-contact measurement of steel surface temperature, varied with the steel object's surface structure and its electrical properties. As well, the variation of emissivity with temperature and wavelength are required.

The surface emissivity of an object is directly related to its reflectivity. The industrial problem becomes an investigation of the reflective properties of a surface covered by iron-oxide layers of irregular configuration. It is thus an optics problem in the interference and scattering of electromagnetic waves.

The thesis is divided into three parts : Part 1, deals with an introduction to the thesis problem, see chapter 1; Part 2, considers the analysis of the optical problem from a multilayer interference viewpoint, see chapters 2, 3 and 4; Part 3 considers the scattering of electromagnetic radiation from layered surfaces, refer to chapters 5, 6, 7, 8 and 9.

Chapter 1 is an introduction to the area of non-contact temperature measurement (thermometry). Optical Pyrometry and millimetre wave Radiometry, the current method of temperature measurement, is discussed as well as the concept of emissivity. It discusses the formation of oxide layers on steel at high temperatures, their structure and electrical properties, the growth of layers and the structures possible in an industrial environment. Chapter 2, 3 and 4 analyse the Optical problem of the reflection characteristics of the combined steel/oxide structure. The theoretical aspects of reflection and refraction from these plane surfaces is discussed, as well as a review of current research in this topic.

Chapters 5 and 6 deal with the theoretical aspects of surface roughness and the scattering of radiation from such surfaces. Chapter 6 outlines the scattering approach used in this thesis. The theory of Beckmann (a modified version of Kirchhoff theory) used in the thesis problem is given, leading to a scattering integral and the determination of rough surface emissivity.

Chapters 7 and 8 are devoted to analytical solutions of the scattering integral for both unoxidised (ch 7) and oxidised (ch 8) surfaces. The fundamental work of this thesis is then outlined : the solution of the Beckmann scattering integral for dielectric periodic surfaces. The solution includes the influence of surface edges. It gives a simple formulation of both oxidised and unoxidised scattering coefficients in terms of the smooth reflectivity and a multiplier making up the roughness contribution. This simple expression gives rise to the complete scattering behaviour of the rough surface.

General conclusions for the entire thesis are then made in section 9.3, with a discussion of further possible research covered in section 9.4. Most of this thesis contains original work which contributes as follows :

1. Previous research on scattering of radiation assumed a single non-absorbing layer of oxide of constant low conductivity, when in fact :
  - Oxides are highly absorbing, section 1.4.
  - The oxides are semiconductors at high temperatures, section 1.4.
  - More than one layer of oxide exists, they are wustite, magnetite and haematite, section 1.3.
2. Previous work concentrated on rough perfectly conducting surfaces and complex numerical models. The solution of this problem is made as follows :
  - A simple analytic solution is found with a straightforward physical interpretation for both oxidised and unoxidised surfaces, sections 7.8, 7.9, 8.3.
  - The solution specifically treats dielectric surfaces having finite conductivity, sections 7.8, 8.3.
  - The solution is easily extended to surfaces of infinite dimensions, section 7.2

For both the flat surface interference case and the rough surface case numerical simulation confirm the theoretical solutions, chapter 4 and 9.



## Part I

# Introduction



# Chapter 1

# Temperature Measurement in the Industrial Environment

## 1.1 Introduction

In the steel industry temperature determines to a great extent the quality and type of steel produced as a final product for use in many varied technologies. Therefore, the temperature of steel needs to be known to a fair degree of accuracy. In addition, it needs to be controlled in the processing of steel.

So, temperature is one of the most important parameters to measure and control in industry. In order to measure the temperature of steel surfaces in industry two standard ways are in everyday use. One, is by the use of direct or contact means, where this implies the direct measurement of surface temperature through the use of a thermocouple attached to the steel surface itself. Contact means are not always applicable. If for instance the object under investigation is in motion, is inaccessible, or may be damaged as a result of contact, [68]. To circumvent this problem non-contact temperature measurement has become a very popular method in industry. This method entails the measurement of surface temperature through the measurement of the radiation emitted from the steel object

## 2CHAPTER 1. TEMPERATURE MEASUREMENT IN THE INDUSTRIAL ENVIRONMENT

under consideration. This is made possible by the fact that any object above  $0^{\circ}\text{K}$  produces thermal radiation. This radiation is received, and indirectly, the temperature may be measured.

The most commonly used technology for non-contact, on-line temperature measurement is Infrared (IR) pyrometry. Another useful technology is microwave radiometry which offers some unique advantages such as seeing through smoke, measuring sub-surface temperatures and so on. In both cases the emissivity variation (to be defined) significantly affects the measurement results. The emissivity itself is dependent on the steel object's material composition, surface structure, measurement frequency and body temperature. This implies two areas of investigation low and high temperatures. The characteristics of the emissivity are quite different at low temperatures ( $200 - 600^{\circ}\text{C}$ ) as compared to higher ones ( $800 - 1400^{\circ}\text{C}$ ).

In the steel industry, specifically the rolling of hot steel, the temperatures are often rather high, typically above  $600^{\circ}\text{C}$ . It is therefore important to study the variation of emissivity with the variables mentioned above.

Metallurgical studies indicate that at elevated temperatures up to three layers of iron-oxide form on steel, [19]. The process of oxide growth is rapid and influences, to a marked degree, temperature measurement. Since IR pyrometry and microwave radiometry range over a wide spectrum, not only must one investigate surface emissivity as a function of temperature,  $800 - 1300^{\circ}\text{C}$ , but also the wavelengths of measurement radiation,  $0.5 - 20\mu\text{m}$  up to millimetre and centimetre wavelengths. Additionally each surface is disturbed by rough undulations, this too adds an extra factor to emissivity characteristics.

In order to get a clear idea of what industrial temperature measurement entails, we will discuss several topics necessary to define the problem of emissivity determination for real surfaces.

First it must be made clear what we mean by the emission of radiation from surfaces, how to measure this radiation and consequently the temperature of the surface. How to evaluate the emissivity from such data, and what specific characteristics of the material



and its surface, influence the emissivity.

A brief introduction to radiative properties is given and then the oxidation characteristics of iron are considered.

Previous research included the effect of oxide layers on a metal surface but it was restricted to single layers of haematite for which

1. Only non-absorbing layers of oxide were considered, ie oxides with zero absorption coefficient. This is not valid at high temperatures when absorption effects must be considered since the oxide is no longer a simple dielectric but a semiconductor. This effect has not been previously considered and will be taken into account in this thesis.
2. Previous work, even if it did consider oxide absorption of radiation, did not allow for the large increase in conductivity present at high temperatures of the oxides. This effect will also be analysed here.
3. To the authors knowledge, the influence of oxide layers has always been restricted to consideration only of the oxide  $Fe_2O_3$  when in fact there are always three layers of oxide present at high temperatures. That is, wustite, haematite and magnetite. So multilayer structures should be investigated because each of the oxides possess different electrical properties which may lead to qualitatively and quantitatively different behaviour.
4. In fact, it is important to note that the most prevalent oxide is wustite not haematite as previously thought.

There are then several new contributions to be made for the study of smooth surface emissivity. In summary :

- The absorption of iron-oxides are taken into account
- Three layers  $FeO$ ,  $Fe_3O_4$ ,  $Fe_2O_3$  of iron-oxide are analysed.

- The semiconducting properties of each of the oxides is included.

## 1.2 The Emission of Radiation from Real Surfaces

### 1.2.1 Blackbody Radiators

Consider a body that is capable of absorbing all radiation incident upon it, so no radiation is either transmitted or reflected. However it can still emit radiation merely by the fact that it is a hot body above 0°K. Now, when a state of equilibrium exists between the energy received and emitted then this total absorber must emit radiant energy at the same rate it receives it, otherwise its temperature would either rise or fall again eventually producing an equilibrium situation, [37]. This complete absorber is called a blackbody and emits radiant energy related to its temperature and wavelength of radiation by Planck's law :

$$L(\lambda, T) = \frac{c_1}{\lambda^5 (e^{c_2/\lambda T} - 1)} \quad (1.1)$$

where  $L(\lambda, T)$  is the time rate of emission of radiant energy per unit interval of wavelength,  $\lambda$ , through  $2\pi$  steradians per unit area of a blackbody at absolute temperature  $T$ . This is also called the hemispherical spectral radiant intensity per unit area of a blackbody. The constants  $c_1 = 3.7413 \times 10^{-16} \text{Wm}^2$  and  $c_2 = 1.4387 \times 10^{-2} \text{mK}$  are the first and second radiation constants respectively, [37].

### 1.2.2 Non-Blackbodies

Any body which is not a perfect absorber is called a non-blackbody. This of course includes all real materials since perfect absorption is not strictly possible, although good approximations exist. In that case define the ratio of spectral radiance of a non-blackbody to that of a blackbody at that temperature and wavelength by the ratio

$$\epsilon = \frac{L(\lambda, T)_{nbb}}{L(\lambda, T)_{bb}} \quad (1.2)$$

where the subscripts  $bb$  = blackbody and  $nbb$  = non-blackbody. This ratio, which measures the ability of a non-blackbody to emit radiant energy with respect to a perfect emitter (absorber), is called the spectral emittance of the body. This value must always lie between 0 and 1, 0 being the poorest emitter and 1 the perfect emitter as close to a blackbody as is possible. Then we may define the time rate of emission of radiant energy for a non-blackbody as

$$L(\lambda, T)_{nbb} = \epsilon L(\lambda, T)_{bb} \quad (1.3)$$

or using equation (1.1)

$$L(\lambda, T)_{nbb} = \epsilon \frac{c_1}{\lambda^5 (e^{c_2/\lambda T} - 1)} \quad (1.4)$$

notice that the emittance  $\epsilon$  is a function of both wavelength and temperature as a consequence of the definition above. That is

$$\epsilon = \epsilon(\lambda, T) \quad (1.5)$$

So once the radiant energy  $L(\lambda, T)$  has been measured and the wavelength of the emitted radiation is known then it is possible to calculate from (1.4) the temperature, provided the emittance of the object is known. Some way must be found to calculate or measure this variable.

### 1.2.3 Radiation Thermometry

The scientific technique of the measurement of temperature via the reception of spectral radiation is called Radiation Thermometry. The detection of such radiant energy is achieved with the use of either a radiation pyrometer or radiometer. The two devices measure radiant energy over different wavelength ranges. The radiation pyrometer detecting energy in the range from visible to infrared and the radiometer up to millimetre and centimetre wavelengths, [37]. Why these particular ranges? The atmosphere surrounding the radiant object and the measuring device consists of a variety of gases such as Nitrogen, Oxygen, water vapour and Carbon Dioxide. All of these gases absorb, reemitt and

scatter radiation passing into them. This presents a problem as to the radiation allowed to pass through the atmosphere to be received by the radiometer or pyrometer. There are however spectral regions in which the atmosphere does not absorb radiation. These regions are called atmospheric windows and are free of atmospheric interference. They are clearly observable in the Figure 1.2.1 as wide peaks in the transmittance of radiation through the types of gases present in air. It is fairly obvious that the regions over which the clearest observation is possible occurs over the ranges  $\sim 0 - 1\mu\text{m}$  and  $\sim 8 - 14\mu\text{m}$ , [68]. Similarly this is true at longer wavelengths such as *mm* and *cm*. Then we have

- Optical Pyrometry  $0 - 1\mu\text{m}$ ,  $8 - 14\mu\text{m}$
- Radiometry  $0.5 - 3\text{mm}$ ,  $\text{cm}$

#### 1.2.4 Kirchhoff's Law

When electromagnetic radiation is incident on a body it is either transmitted through the body (at least partially), reflected off the surface or absorbed by the body. This is required by conservation of energy. Call the intensity of radiation received  $I_0$ , that transmitted  $I_t$ , that reflected  $I_r$  and that absorbed  $I_a$ . Then we have

$$I_0 = I_r + I_t + I_a \quad (1.6)$$

or

$$1 = r + t + a \quad (1.7)$$

where  $r = I_r/I_0$ ,  $t = I_t/I_0$  and  $a = I_a/I_0$ , being the amount reflected, transmitted and absorbed respectively. Usually these terms are known as the spectral reflectance, transmittance and absorptance' [52]. These terms relate to non-blackbodies and as such depend upon the spectral distribution of the impinging radiation [37] and so upon the temperature of the source of the radiation. Now when the source of the impinging (blackbody) radiation has the same temperature as that of the body for which the above terms apply,

then the total emittance is equal to the total absorptance. That is

$$\epsilon_{total} = a_{total} \quad (1.8)$$

For bodies which are opaque, ie where the transmittance is zero,  $t \simeq 0$ , we find

$$\epsilon = 1 - r \quad (1.9)$$

in other words the emittance may be calculated from the reflectance of the object. Since the reflectance of most real objects is measured by the use of reflected radiation from its surface, it must depend critically on the wavelength of the incident radiation, its electrical properties such as conductivity and the surface characteristics of the surface such as its chemical and physical structure. The emittance will now depend on many aspects other than just the wavelength and temperature.

### **Reflectivity, Emissivity, Transmittivity**

It is best to clarify some terms in common usage. The aforesaid radiant characteristics of material bodies : the reflectance, transmittance, absorptance and emittance are properties of 'real' specimens, regardless of the body's thickness or surface condition', [89]. Then the reflectance from a non-optically smooth or inhomogeneous material is called reflectance, whereas the property of reflection from an optically smooth surface that is opaque is the reflectivity. Similarly the transmittivity is the transmission characteristic of a perfectly smooth and homogeneous body. The transmittance is the ratio of transmitted intensity to incident intensity of the real body with whatever optical properties and surface structure it has. Also, the absorptivity is again that of an optically perfect specimen which is opaque. The same applies to the emissivity. It is common that these terms are interchanged in the literature with many works referring to the emittance as emissivity and reflectance as reflectivity and so on. It will be assumed forthwith that we are always referring to the real substance but shall frequently refer to radiative properties by their common names.

### 1.2.5 Real Surface Effects

By real surfaces we mean surfaces possessing characteristics such as surface roughness, inhomogeneities in the bulk structure and so on. These real surface characteristics can strongly influence the determination of the reflectivity (reflectance) of a surface, [89]. They may be divided into three separate categories : Topographical, Chemical and Physical.

#### Physical

The physical characteristics include such structures as the crystal lattice orientation, particle size, strain and the like. For a surface free of surface layers, such as oxides on steel, the reflectance characteristics are governed by a thin surface layer a few hundred angstroms deep. In this layer several features can alter the reflection properties such as adsorbed gas atoms, lattice imperfections and crystalline plane variations. This also includes processes such as polishing and other mechanical manipulations. In our case this would include the action of a roller when hot steel is rolled.

#### Chemical

By chemical characteristics we refer to the presence of inhomogeneities and contaminants in surface layers on the steel. These surface layers could include grease or other common industrial contaminants. Most often this layer will be constituted of the oxide(s) of the metal in question. This would mean the presence of various oxides such as ferric oxide ( $Fe_2O_3$ ) or wustite ( $FeO$ ). In the case of steel, since it usually consists also of alloys, it will often have oxides of Chromium, Silicon and Nickel as well.

Other than oxidation, several reactions are possible with gases, including hydrogen, carbon-monoxide/dioxide and sulphurous gases such as  $H_2S$ ,  $S_2$  and  $SO_2$ , [33]. These reactions are called decarburisation, carburisation and sulfidation. These extra reaction products will not concern us in this thesis. Since their presence is minimal compared with the

iron-oxides only these will be dealt with.

These oxide layers do not make a smooth join with the base metal or for that matter grow in a regular way. The growth depends on surface structure, temperature and oxygen partial pressure. This of course produces variations in the reflectance via the refractive index of the material. The effect of these coatings on the metal can completely change the emittance characteristics from that of a metal to that of a dielectric, [89].

### **Topographical**

The topographical characteristics describe the the surface profile of the steel. That is, its boundary with the surrounding atmosphere. Generally the shapes of real metal surfaces are always irregular in some way, be it the surface of the metal itself with no oxide present or when oxide is present. This variation is commonly referred to as surface roughness, which consists of peaks and valleys about the mean surface plane. Its effects are well known to drastically change the emittance of real surfaces, [72]. The most commonly noticed trait being a marked rise in emittance compared with a perfectly clean regular surface.

The chemical and topographical characteristics will be those considered in this thesis.

## **1.3 Oxidation of Iron**

Iron and Steel oxidise at high temperatures very rapidly. The higher the temperature the faster the oxidation reaction. This depends also upon the partial pressure of oxygen. The reaction of oxygen with a metal is usually quite complex and may occur via several possible mechanisms. We start with a clean metal surface. Oxygen is adsorbed onto the metal surface and then can dissolve into the metal. Oxide is formed on the surface as either a film or as separate oxide nuclei, [44]. Both adsorption and initial Scale formation

depend on the surface orientation, crystal defects in the surface, surface preparation and impurities present in the surface and the gas. Once these islands of oxide exist they can expand over the whole metal surface covering it in an oxide film, often called "Scale". Then, in summary, the growth phase is

- Adsorption of oxygen on the surface
- Formation of oxide nuclei which grow laterally to form a continuous film
- Further growth of the film perpendicular to the surface

Note, that if the oxidation takes place at atmospheric pressure, as it surely does in hot rolling of steel, then the first two stages above occur too rapidly to be observed. The portion of the process that can be seen is the actual thickening of the film. For a detailed analysis of iron oxidation see [71]

The actual layer structure is often in the form of flat planes following the crystal structure of the particular oxide. These planes are not necessarily flat on the surface but may form terraces, ledges and kinks all of which contribute to an irregular surface shape. This process of forming planes, is however, restricted to high densities of atoms, other structures are possible. To some degree the metal is now separate from the gas. Once a uniform film covers the metal further reactions can only take place through solid state diffusion of the reactants through the film, [44]. In our case, when quite thick films may form, this rate of reaction is determined by the chemical potential gradient across the Scale, see Figure 1.3.2, [19].

At times, porous Scales form which do not prevent further adsorption as in the case of solidstate diffusion. In this case, reactions may be limited by processes occurring at phase boundaries, [44]. At high temperatures the oxides may actually melt and form further structures.

In each type of metal the reaction and formation of Scale will depend on the history of the metal itself, that is, whatever previous treatment the metal had been subjected to, the temperature, gas composition, pressure and the time for which the reaction was allowed



to take place.

Generally, three types of oxide or Scale form on iron or steel (excluding Chromium, Silicon etc), they are Wustite,  $FeO$ , Magnetite,  $Fe_3O_4$  and Haematite,  $Fe_2O_3$ . The rate at which they form and their dependence on oxygen content and temperature are shown in the phase diagram in Figure 1.3.1, [38], with a modern version in Figure 1.3.2, [19]. Their thicknesses form in the ratios

$$FeO : Fe_3O_4 : Fe_2O_3 \quad (1.10)$$

$$1 : 0.04 : 0.009 \quad (1.11)$$

### 1.3.1 Formation of Wustite

The formation of a Scale layer of Wustite takes place via the reaction



This wustite phase is only stable above  $570^\circ\text{C}$ . We are dealing with temperatures well in excess of this stability point, for example in the range  $700 - 1200^\circ\text{C}$ . Below this critical temperature the wustite breaks down into magnetite via the equation, [35].



Although some haematite is also present, [90].

The wustite constitutes usually up to 95% of the total Scale formed, [90]. The growth of Scale is determined by diffusion of oxygen into the iron and can be described by a parabolic rate law

$$\left(\frac{\Delta m}{A}\right)^2 = kt \quad (1.14)$$

where  $t$  is the time for the reaction,  $\Delta m$  the mass of oxide formed,  $A$ , a constant and  $k$ , the rate constant of formation. The growth is quite fast above  $700^\circ\text{C}$  with thicknesses in excess of several  $100 \mu\text{m}$  forming in a few hours. It can be seen however, [19], that the Scale formation can be very rapid indeed, with the thickness depending on the equation

$$d = K\sqrt{te^{-\frac{40500}{RT}}} \quad (1.15)$$

see Table 1.3.1, [19] for the speed at which layers form.

Table 1.3.1 Iron-oxide layer growth over 1000 seconds at increasing temperature

The formation of the first layer of oxide is well demonstrated by the diagram of Hauffe, [38], which shows how each Scale layer forms. There is an initial rate of oxide growth above  $800^{\circ}\text{C}$  which produces a compact layer of  $FeO$  about  $0.01\ \mu\text{m}$  thick, which then crystallises with a definite crystal arrangement with many grain boundaries. Further growth of another layer of  $FeO$  continues through the cavities produced from the earlier Scale formation.

Note that wustite itself is metal deficient this means its structure is often written as  $Fe_{1-y}O$ , this is usually called non-stoichiometry meaning a variation in the ideal molecular formula, [33]. This non-stoichiometry decreases the higher the temperature so its stability increases at higher temperatures, with the value of  $y$  being very small (0.05) between  $800$  and  $1250^{\circ}\text{C}$  at the iron/wustite boundary. It is this non-stoichiometry which allows self diffusion of iron which allows further reaction of iron with oxygen once these iron

molecules have migrated to the surface of the layer, [44]. Further oxidation to magnetite and haematite is now possible.

### 1.3.2 Formation of Magnetite

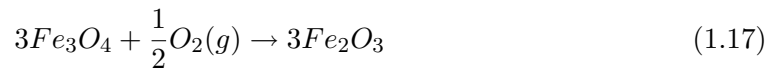
The reaction governing the formation of magnetite is



As for wustite the formation of magnetite obeys a parabolic rate law, the law mentioned above (1.15) is general for all iron-oxides except for the different rate constants. These are shown in Table 1.3.1, [38]. Magnetite is also non-stoichiometric so this is written  $Fe_{3-y}O_4$ . The value of  $y$  increases as temperature increases allowing further diffusion and formation of the other oxide, haematite. Note that because of this diffusion ability the protective action of the oxide layers is small, [78]. This means oxidation continues to occur even when the iron seems to be protected from further oxidation by the layer itself. The total percentage of magnetite composition comes to about 4%, considerably less than wustite, although it is predominant below about 570°C. During the formation of this phase, cracking occurs continuously caused by the mechanical stresses that exist between different phases, [90].

### 1.3.3 Formation of Haematite

Haematite  $Fe_2O_3$  forms on top of magnetite via



It is thought that the motion of oxygen through pores and cracks in both haematite and wustite allows further growth in both of these inner layers and the relatively minimal growth of haematite which occupies only about 1% or so of the total Scale layers. The non-stoichiometry of haematite is very low, [44], and the oxide may be oxygen deficient,

as such, any diffusion is very weak which leads to the previously mentioned fact that further layer growth under the haematite layer is only possible through migration of oxygen molecules via cracks and pores.

### 1.3.4 2-D Structures of Adsorbed Layers

Usually, most of the oxygen atoms are adsorbed preferentially on sites with the highest density of surface atoms. Thus the shape of oxide surfaces rely on the crystal planes present on the metal substrate. A variety of structures may be formed not only on metal crystal planes, but also as a rearrangement of surface atoms to form new configurations. Since different crystal faces adsorb oxygen differently the surface film structure may form striations or facets. These facets are known to change surface oxygen diffusion and alter the further formation of new layers.

The growth of oxide films takes place via a spreading out from oxide nuclei, this lateral spreading is temperature dependent. The size and shape of these nuclei influence the profile of the eventual film formed. Once this nucleation has taken place the film starts to thicken. This increase in film depth occurs very rapidly to begin with and then drops off to a gradual increase.

Various phases of both iron and its oxides exist, [87]. This phase or modification is a clarification of the change in crystal structure at different temperatures and pressures. For iron it exists in an  $\alpha$  phase until it converts to its  $\gamma$  phase at about  $912^\circ\text{C}$ . The phase influences the reflection properties of iron for example  $\alpha$  iron has a reflectivity about 3% lower than  $\gamma$  iron, [90]. Iron undergoes a further transition to  $\delta$  iron at  $1394^\circ\text{C}$ . At very high temperature eg  $1538^\circ\text{C}$  the first phase has its melting point.

The oxides also form in different phases.  $FeO$  consists mainly of phase III at high temperatures ( $\sim 1000^\circ\text{C}$ ). The phases of magnetite are  $\gamma - Fe_3O_4$  and haematite  $\alpha, \gamma - Fe_2O_3$  phase, these phases also allow labelling of transitions in electrical properties.

In fact, a great variety of structures are possible from plane facets to needle like structures.

Typical sections through pieces of iron covered in oxide are shown in Figures 1.3.3 to 1.3.6. Cavities, platelets, pores, ridges, whiskers and blades are all possible growth structures which give rise to a wide variety of surface roughness characteristics.

### Surface Defects & Structures

The defects and unusual surface structures vary widely from simple planes to blades and whiskers. These structures form the basis for a rough surface either for iron itself or as the surface profile of the oxide on it. Included in the roughness characterisation are grain boundaries Figures 1.3.9, 1.3.10, 1.3.13, which act as scattering elements inside the oxide, [78]. This particular form of roughness will not be considered although it can be taken into account with the use of the so-called Maxwell Garnett equations, [50]. Further possible structures include the formation of bubbles or cavities underneath the oxide, Figures 1.3.11, 1.3.12. Surface porosity adds to the variation and is difficult to consider in scattering, Figures 1.3.6-1.3.9. Stresses in oxide formation can produce cracks and a breaking off of Scale. Similarly, in the process of cracking off of Scale, when water is applied during hot rolling, spalling produces ridges and curled up layers of Scales in patches. All of these effects can significantly alter the intrinsic roughness of the steel/iron and so change the way radiation is scattered from real steel surfaces.

We will restrict ourselves mainly to periodic surfaces generally for theoretical reasons but also because the overall large scale roughness structure approximates an undulations akin to a sinusoidal shape, see Figures 1.3.3-1.3.6. These other extra roughness producing structures may be of a small enough size that longer measurement wavelengths will not be aware of them. Our structures then, are films of oxide on steel having a kind of average periodicity around 50-150  $\mu\text{m}$  with amplitudes of the order of 1-2 $\mu\text{m}$ , Figure 1.3.5.

Although the structures mentioned above can, to some extent, be considered to be periodic with amplitude  $A$  and period  $T$ , the surface is only approximately so. It was already mentioned that the formation of oxide takes place in a plane layering process so surfaces having a step-like profile are also possible, not to mention saw-tooth shapes. Lastly, there

is some evidence to suggest that surfaces undergoing corrosion (for us, oxidation) form fractal surfaces which have structure on all scales. These approximations to real surfaces could take into account the more unusual forms such as dendrites, whiskers (Figure 1.3.14) and platelets mentioned previously, [53], [32]. This could be the subject of further study.

## 1.4 Electrical Properties of Iron and its Oxides

The electrical properties of iron and its oxides contribute to their refractive indices which influence the scattering of radiation from the surface of oxidised steel. The three separate electrical properties : permeability, accounting for magnetic effects, permittivity, also written as the dielectric constant, and the conductivity, which accounts for the ability of materials to conduct electricity. Of these, the one we are most concerned with will be the conductivity. Before discussing this aspect we will briefly outline the effects of both permittivity and permeability.

### 1.4.1 Magnetic Effects

#### Iron

Iron and steel are ferromagnetic substances. This means they exhibit strong magnetic fields without the need for the presence of an imposed magnetic field. So, their permeabilities are large and can strongly effect the absorption, reflection and transmission of radiation. However, magnetic materials possess a temperature called the Curie point beyond which their ferromagnetism converts to paramagnetism. This condition randomises the magnetic moments of the previously ferromagnetic substance (magnetic moments aligned) and thereby reduces the permeability significantly. For iron, this temperature is about 768°C. Below this temperature its magnetic properties cannot be ignored. However at elevated temperatures, prevalent for hot rolled steel, 800 - 1300°C, the permeability can be assumed to be that of free space with little loss of accuracy. So, for us, iron will have  $\mu = \mu_0$ , the permeability of free space.

### Oxides

The only truly magnetic oxide is magnetite, as its name implies it too is strongly magnetic at lower temperatures. At high temperatures it becomes virtually non-magnetic allowing us to express the respective permeabilities of the oxides as that of free space.

So we have that  $\mu_{FeO} \simeq \mu_{Fe_2O_3} \simeq \mu_{Fe_3O_4} \simeq \mu_0$

#### 1.4.2 Dielectric Constants

It is possible for the permittivity of materials to become significant. The ability of a material to react to impinging radiation via the introduction of the polarisation of the material leads to complex permittivities and gives rise to extra conductive effects. These effects can be considered and section (2.4.2) takes some note of their properties. Currently most of the relevant literature assume the dielectric constants of iron, and its oxides, to be that of free space,  $\epsilon_0$ , we also will implement this assumption throughout. Therefore the permittivities of each material are defined by :

$$\epsilon_{FeO} \simeq \epsilon_{Fe_2O_3} \simeq \epsilon_{Fe_3O_4} \simeq \epsilon_0 \quad (1.18)$$

#### 1.4.3 Conductivity

##### Iron

It is well known that the conductivity of iron decreases with increasing temperature. Although its conductivity is very high at low temperatures eg at 200°C it has a conductivity of about  $5 \times 10^6 (\Omega\text{m})^{-1}$ . Its conductivity quickly declines until at 800°C its conductivity is only  $1 \times 10^6 (\Omega\text{m})^{-1}$ , nevertheless still a significant value. The graph of resistivity (1/conductivity) variation with temperature is shown in Figure 1.4.1 and demonstrates this decline. The results of this graph will be used as the information for a table of  $\sigma = \sigma(T)$  for use in the equations employed to calculate the refractive index of iron, [26].

## Oxides

All of the oxides of iron are actually semiconducting ceramics and as such have the rather unusual property of increasing their conductivities with increasing temperature. For wustite its conductivity increases, see, [84], [93] and, [2]. Its conductivity may go as high as  $10^4 (\Omega\text{m})^{-1}$ . Its conductivity is p-type but undergoes a transition to n-type depending on the oxygen pressure, [44]. Magnetite has a very slowly increasing conductivity with temperature but is slightly higher than that of wustite. It may also reach conductivities in the range  $10^4 (\Omega\text{m})^{-1}$  for temperatures in excess of  $900^\circ\text{C}$ . It is an n-type semiconductor, [44]. Similarly the conductivity of haematite increases with temperature but at a much faster rate than either of the other two oxides. It may reach conductivities of the order of  $10^5 (\Omega\text{m})^{-1}$ , [2]. Its conductivity varies, it is a n-type conductor in the temperature range  $650\text{-}800^\circ\text{C}$  and a p-type at higher temperatures, [44]. All of their conductive properties are described by the graph of Adler, [2]. His results were used to construct conductivity functions for use in this thesis.

For the case of iron and magnetite no simple formulae exist to describe their conductivities. Instead, a Spline algorithm was used to fit to the graphs of Davis, [26], and Adler, [2], see Figure 1.4.2. In the case of both wustite and haematite two simple equations may be used. Their conductivities obey an exponential decay relation.

For wustite, the relation is

$$\sigma_{FeO} = 2.5769e^{-\frac{810.168}{T+273}} \quad (1.19)$$

For haematite, it is

$$\sigma_{Fe_2O_3} = 5.623e^{-\frac{2.129}{T+273}} \quad (1.20)$$

The 273 of course a conversion to  $^\circ\text{C}$ .



## Part II

# The Optical Problem-Plane Surfaces



## Chapter 2

# Reflection and Refraction from Plane Surfaces

### 2.1 Introduction

Smooth Surface scattering has a long history and the major contributions to such scattering is considered in the first section. A brief review is given concentrating on the work of Tanaka & DeWitt, [82], which is typical of the investigations in this vain. They studied the smooth surface reflection for oxidised metal surfaces experimentally and theoretically. This work provides a starting point for our more involved investigation and as a check with experimental data. This section is kept brief because of the already significant literature available on the topic.

The second section gives a quick introduction to the use of electromagnetic theory in scattering concentrating on the electrical properties of materials and their origin. This is important for the subsequent investigation. It is included for completeness even though many standard texts cover the material, although several specialist topics such as dispersion are not standard by any means.

Included in the last section are the boundary conditions for two material interfaces, these

conditions being vital, as they are needed for a proper solution of the smooth surface problem.

## 2.2 Smooth Surface Scattering - A Review

A good deal of work has been done in the investigation of smooth surface scattering. As regards the problem of oxide formation on steel, the major contribution is that of Tanaka & DeWitt, [82], who conducted an experimental and theoretical study into emissivity variation with oxide growth. The theoretical study investigated the smooth surface film effects for a single layer of  $Fe_2O_3$  (haematite), assumed non-absorbing over the wavelength range  $0 - 3\mu\text{m}$ . No account was taken of the absorption properties of the oxide layer and the conductive temperature dependence was not considered. It was assumed the oxide present was haematite when the dominant layer present at high temperatures is in fact wustite with completely different electrical properties. This is not such a bad assumption however, since only temperatures up to about  $630^\circ\text{C}$  were considered, wustite breaks down to magnetite and haematite below  $570^\circ\text{C}$ . Tanaka & DeWitt also carried out experimental work at two separate wavelengths,  $1.6\ \mu\text{m}$  and  $3.0\ \mu\text{m}$ . They oxidised a clean polished steel specimen of carbon steel (not iron as in our case) at specified temperatures :  $427 - 627\ ^\circ\text{C}$ . The variation of emissivity over time at the specific wavelengths was measured. This was equivalent to recording the emissivity as a function of oxide layer thickness (cf section (1.3.1)). They obtained the graphs shown in Figures 2.2.1, 2.2.2 and 2.2.4. Obvious initial increase in emissivity as the oxide layer grows and interference effects after the emissivity reaches a value close to one. The experimental results were supported by theory, although no direct conclusions were drawn, except that the ‘ discrepancy between simulation and experiment increases as oxidation proceeds ’. Although the theoretical model was quite useful in predicting emissivities, [82]. Considering the fact that the true conditions of oxide growth were not included in their theoretical model these conclusions are to be expected, other than the given reason : the presence of roughness, which of

course cannot be ignored.

Other contributors to the smooth film on a steel substrate model include, Brannon & Goldstein, [16], who took experimental measurements of the emissivity of aluminium coated in a layer of aluminium oxide at temperatures up to 200°C they compared their results to theoretical models similar to Tanaka & DeWitt's, [82], except for the inclusions of the absorption properties of the oxide layer. They found the initial increase in emissivity at small thicknesses of oxide until a constant value was reached. They also noted a discrepancy in theoretical and experimental results. The experimental results always had a greater emissivity than the theoretical ones. This was considered due to scattering in the layer itself, no mention was made of surface roughness. The simulation results, Figure 2.2.3, did approximate closely the experimental results for small oxide thickness and followed the same general trend.

Experimental research conducted by Iuchi et al, [43], found that the emissivity of rolled steel increased very slightly in a linear fashion as the temperature was increased from 300 - 800°C. In fact, it was clearly stated that  $\epsilon \propto \sqrt{T}$ , compare with Figure 2.2.6. Each reading indicated an increase in emissivity for smaller wavelengths see Figure 2.2.5. The variation of emissivity with wavelength was seen to be of the form  $\epsilon \propto \lambda^{-1}$  or  $\lambda^{-1/2}$  reaching a constant value for longer wavelengths. High emissivities were recorded in the visible range and low ones in the infrared.

Siegel & Howell, [72], support the previous results and state categorically that an oxide thickness of even a few microns involves a substantial increase in emissivity. Typical graphs are shown in Figure 2.2.7 and 2.2.10. They also show that the temperature dependence is to the half power at wavelengths greater than about  $5\mu\text{m}$ . There is a direct relationship for emissivity increase with temperature and resistivity (inverse of conductivity). This implies that oxide layers, being more conductive at higher temperatures, should produce lower emissivities as the temperature increases. This effect is reversed at short wavelengths  $\sim 1\mu\text{m}$ . Similarly emissivity is known to decrease with increase in wavelength and vice versa, for a decrease, [72], Figure 2.2.8, 2.2.9.

**Summary**

In summary the experimental characteristics of plane layered surfaces are :

1. When compared to the unoxidised case there is a distinct increase in emissivity at small wavelengths.
2. As the wavelength is increased the emissivity decreases as  $\epsilon \propto \lambda^{-1/2}$  becoming constant and small at very long wavelengths.
3. For emissivity verses thickness of oxide layer, there is an initial increase from a very low emissivity to one close to 1.
4. There are oscillations observed when the layer thickness is comparable to the wavelength.
5. After the oscillation the emissivity remains constant
6. The emissivity is proportional to the square root of temperature.
7. The emissivity is high in the visible spectrum and low in the IR.

The theoretical results show discrepancies with experimental data

1. The emissivity is always lower than the corresponding experimental result.
2. Thicker oxide layers show greater variation from the experimental.
3. Certain assumptions are usually made to account for discrepancies such as roughness.

**2.3 The Need for Further Development**

As can be seen from the summary above there is a need to account for theoretical and experimental discrepancies. In some cases the theoretical results show reasonable agreement and in others they don't produce the desired characteristics of the experimental results at

all. For example, the usual reason given for the discrepancies are that the result must be due to roughness when in fact there is no need to extend the theory this far. Consideration should be taken of simpler added contributions such as extra oxide layers, the absorption properties of the oxides and their conduction increases at high temperatures.

It is quite possible to account for the extra emissivity in this way. Absorption may be the likely contributor. The variation in experimental and theoretical results at longer oxidation times is most likely due to the extra layers of oxide formed having quantitatively different electrical properties.

Therefore, there is a need for the extension of previous work into these heretofore neglected aspects of smooth, flat surface, multilayer, scattering. This provides the reason for the purpose of the present study before any extra consideration of properties such as roughness are required. Any deviation from this point onwards will then merit such a study.

## 2.4 Plane Waves in Material Media

Since steel in industry is usually covered fully or partially in layers of iron-oxide we must consider what effect these layers have on the reflection of plane waves from this multilayer surface. It would be expected that both the thickness of each layer and each successive layers' electrical properties would contribute to the scattering characteristics of the reflected field.

Both the layers, represented by the iron-oxides : Magnetite, Haematite and Wustite, and the steel, represented by iron (for simplicity), must be considered absorbing, that is, absorbing incident radiation of wavelength  $\lambda$  through the conductivity  $\sigma_c$ . This means their refractive indices must be complex (see section (2.4.2)).

### 2.4.1 Maxwell's Equations in a Conducting Medium

In each layer and substrate the electric and magnetic fields must obey Maxwell's equations. In a lossy medium which is homogeneous, linear and isotropic the equations are defined by

$$\nabla \times \mathbf{E} = -\frac{\partial \mathbf{B}}{\partial t} \quad (2.1)$$

$$\nabla \cdot \mathbf{D} = 0 \quad (2.2)$$

$$\nabla \times \mathbf{H} = \mathbf{J} + \frac{\partial \mathbf{D}}{\partial t} \quad (2.3)$$

$$\nabla \cdot \mathbf{B} = 0 \quad (2.4)$$

describing the behaviour for electric,  $\mathbf{E}$ , and magnetic,  $\mathbf{H}$ , field vectors, which are related by the constitutive relations  $\mathbf{D} = \varepsilon \mathbf{E}$  and  $\mathbf{B} = \mu \mathbf{H}$ . As is usual take the curl of the first equation and using (2.3) and the constitutive relations we get

$$\nabla \times \nabla \times \mathbf{E} = -\mu \frac{\partial \mathbf{J}}{\partial t} - \mu \varepsilon \frac{\partial^2 \mathbf{E}}{\partial t^2} \quad (2.5)$$

using the identity  $\nabla \times \nabla \times \mathbf{E} = \nabla(\nabla \cdot \mathbf{E}) - \nabla^2 \mathbf{E}$  and equation (2.2), we have

$$\nabla^2 \mathbf{E} - \mu \varepsilon \frac{\partial^2 \mathbf{E}}{\partial t^2} = \mu \frac{\partial \mathbf{J}}{\partial t} + \nabla \left( \frac{\rho}{\varepsilon} \right) \quad (2.6)$$

where  $\mathbf{J} = \sigma \mathbf{E}$  is the conduction current in the medium, and  $\rho$  the charge density in the medium. There is a similar equation for the magnetic field

$$\nabla^2 \mathbf{H} - \mu \varepsilon \frac{\partial^2 \mathbf{H}}{\partial t^2} = \nabla \times \mathbf{J} \quad (2.7)$$

Now substituting for the conduction current in each medium and assuming no sources,  $\rho = 0$ , we find, in a lossy material medium, the wave equations

$$\nabla^2 \mathbf{E} - \mu \varepsilon \frac{\partial^2 \mathbf{E}}{\partial t^2} - \sigma \mu \frac{\partial \mathbf{E}}{\partial t} = 0 \quad (2.8)$$

$$\nabla^2 \mathbf{H} - \mu \varepsilon \frac{\partial^2 \mathbf{H}}{\partial t^2} - \sigma \mu \frac{\partial \mathbf{H}}{\partial t} = 0 \quad (2.9)$$



The last terms  $\sigma\mu\frac{\partial\mathbf{E}}{\partial t}, \sigma\mu\frac{\partial\mathbf{H}}{\partial t}$  attenuate the propagating wave in the medium so it loses some of its energy, ie it is absorbed. Notice that the equation above could have been written in the form

$$\nabla^2\mathbf{E} - \mu\frac{\partial}{\partial t}\left(\frac{\partial\mathbf{D}}{\partial t} + \mathbf{J}\right) = 0 \quad (2.10)$$

where the first term in brackets is the displacement current and the second the conduction current. It is known that media with displacement current much greater than conduction current are lossless and an EM wave will propagate through the medium such that its velocity through that medium is determined by the quantities  $\mu, \varepsilon$  in the following manner

$$v = \frac{1}{\sqrt{\mu\varepsilon}} = \frac{1}{\sqrt{\mu_r\varepsilon_r}} \frac{1}{\sqrt{\mu_0\varepsilon_0}} = \frac{c}{\sqrt{\mu_r\varepsilon_r}} = \frac{c}{N} \quad (2.11)$$

where  $\mu_r = \mu/\mu_0, \varepsilon_r = \varepsilon/\varepsilon_0, N = \sqrt{\mu_r\varepsilon_r}$  are the relative permeability, relative permittivity and refractive index of the medium,  $c$  is the speed of light in a vacuum. So the wave equation in a lossless medium (eg free space, air, dielectrics) reads

$$\nabla^2\mathbf{E} - \frac{1}{v^2}\frac{\partial^2\mathbf{E}}{\partial t^2} = 0 \quad (2.12)$$

For media which have the conduction current much greater than the displacement current the wave equation can be replaced by a diffusion equation where the EM wave is strongly attenuated and may eventually be completely absorbed in the medium. The equation in a conductor becomes

$$\nabla^2\mathbf{E} - \sigma\mu\frac{\partial\mathbf{E}}{\partial t} = 0 \quad (2.13)$$

for all intents and purposes the equation governing the propagation of an EM wave in iron is (2.13). For the iron oxides which are good conductors at high temperatures, it would seem that, at first, they too would be described by (2.13). However, their conductivity is quite small at lower temperatures and always less than that of iron. Also, some of the iron oxides possess other ‘conductive’ loss mechanisms which are controlled by both their permittivity and their permeability. So the entire equation (2.8) must be used in their case.

### 2.4.2 Plane Wave Solution

Substituting for a plane wave

$$\mathbf{E} = E_0 e^{i(\mathbf{k}\cdot\mathbf{r} - \omega t)} \hat{\mathbf{e}} \quad (2.14)$$

with unit vector  $\hat{\mathbf{e}}$  in the direction of  $\mathbf{E}$ . Note that the analogous plane wave for the magnetic field can be expressed in terms of the electric field as

$$\mathbf{H} = \frac{1}{\mu\omega} \mathbf{k} \times \mathbf{E} = \frac{N}{c\mu} \hat{\mathbf{k}} \times \mathbf{E} \quad (2.15)$$

where  $N$  is the refractive index of the medium and  $\mathbf{k} = k\hat{\mathbf{k}} = (N/c\omega)\hat{\mathbf{k}}$  is the wave vector in the direction of the plane wave  $\mathbf{E}$ . We get an equation of the form

$$-k^2 \mathbf{E} + \mu\epsilon\omega^2 \mathbf{E} + i\sigma\mu\omega \mathbf{E} = 0 \quad (2.16)$$

or

$$k^2 = \omega^2 \mu\epsilon + i\omega\sigma\mu = \omega^2 \mu \left( \epsilon + \frac{i\sigma}{\omega} \right) \quad (2.17)$$

where the dispersion relation for the wavenumber  $k$  can be complex since  $\omega$  is real. This value of  $k$  is often called the complex phase propagation constant and the expression

$$k = \pm [Re(k) + iIm(k)] = \pm(\alpha + i\beta) \quad (2.18)$$

defines the real and imaginary parts given by

$$\alpha = \omega \sqrt{\frac{\mu\epsilon}{2}} \sqrt{\sqrt{1 + \left(\frac{\sigma}{\omega\epsilon}\right)^2} + 1} \quad (2.19)$$

$$\beta = \omega \sqrt{\frac{\mu\epsilon}{2}} \sqrt{\sqrt{1 + \left(\frac{\sigma}{\omega\epsilon}\right)^2} - 1} \quad (2.20)$$

notice that the second term  $\beta$  is only non-zero if  $\omega \neq 0$  so the extra complex term is the factor which produces the absorption. Both the velocity and wavelength of the initial EM wave are decreased by the factors

$$v_{medium} = \frac{\omega}{\alpha} \quad (2.21)$$

$$\lambda_{medium} = \frac{2\pi}{\alpha} \quad (2.22)$$

then the medium is dispersive. This gives rise to attenuation defined by the skin depth

$$\Delta = \frac{1}{\beta} = \frac{2\alpha}{\omega\mu\sigma} \quad (2.23)$$

for a purely conducting medium this is more often seen written as

$$\Delta = \sqrt{\frac{2}{\omega\mu\sigma}} \quad (2.24)$$

This describes the decay of the wave in the medium.

We may also express the refractive index of the medium in terms of the real and imaginary parts of the wavenumber  $k$  by

$$N = \frac{c}{v} = \frac{ck}{\omega} = \left(\frac{c\alpha}{\omega}\right) + i\left(\frac{c\beta}{\omega}\right) \quad (2.25)$$

$$= Re(N) + Im(N) \equiv N_r + iN_i \equiv n + i\eta \quad (2.26)$$

where

$$Re(N) = \frac{c\alpha}{\omega} = c\sqrt{\frac{\mu\varepsilon}{2}} \sqrt{\sqrt{1 + \left(\frac{\sigma}{\omega\varepsilon}\right)^2} + 1} \quad (2.27)$$

$$Im(N) = \frac{c\beta}{\omega} = c\sqrt{\frac{\mu\varepsilon}{2}} \sqrt{\sqrt{1 + \left(\frac{\sigma}{\omega\varepsilon}\right)^2} - 1} \quad (2.28)$$

this second imaginary part of the refractive index is often called the attenuation factor  $\eta$ . Note that since  $\omega = 2\pi v/\lambda$ , where  $v$  is the attenuated velocity in the medium, the above indices can be expressed in terms of the wavelength instead of the angular frequency,  $\omega$ . This analysis can be extended further by investigating the actual motion of electrons in the medium of interest with the use of the differential equation

$$\mathbf{F} = m\mathbf{a} = -e\mathbf{E} - \xi\mathbf{v} \quad (2.29)$$

where the net force  $\mathbf{F} = m\mathbf{a}$  on the electron of charge  $e$  is due to the electric field  $\mathbf{E}$  of the incident radiation and a frictional force described by the parameter  $\xi$ . Defining the static value of conductivity as

$$\sigma_0 = \frac{\mathcal{N}e^2}{\xi} \quad (2.30)$$

where  $\mathcal{N}$  is the number of electrons per unit volume. Substituting for a plane wave and finding a solution in terms of  $\mathbf{v} = \mathbf{v}_0 e^{-i\omega t}$  and defining a free current density  $\mathbf{J}_f = -\mathcal{N}e\mathbf{v} = \sigma\mathbf{E}$  we get

$$\sigma(\omega) = \frac{\sigma_0}{1 - i(\sigma_0 m \omega / \mathcal{N} e^2)} \quad (2.31)$$

(see, [94]). This may also be expressed in terms of real and complex conductivities as

$$\sigma = \sigma_r + i\sigma_i = \frac{\sigma_0}{[1 + (\sigma_0 m \omega / \mathcal{N} e^2)^2]} \left[ 1 + i \left( \frac{\sigma_0 m \omega}{\mathcal{N} e^2} \right) \right] \quad (2.32)$$

as before, the extra complex conductivity can be incorporated into the equations (2.27) and (2.28) as follows

$$\alpha = \omega \sqrt{\frac{\mu(\varepsilon - \sigma_i/\omega)}{2}} \sqrt{\sqrt{1 + \left( \frac{\sigma_r}{\omega(\varepsilon - \sigma_i/\omega)} \right)^2} + 1} \quad (2.33)$$

$$\beta = \omega \sqrt{\frac{\mu(\varepsilon - \sigma_i/\omega)}{2}} \sqrt{\sqrt{1 + \left( \frac{\sigma_r}{\omega(\varepsilon - \sigma_i/\omega)} \right)^2} - 1} \quad (2.34)$$

or

$$\alpha = \omega \sqrt{\frac{\mu\varepsilon}{2}} \left[ \left( 1 - \frac{\sigma_i}{\omega\varepsilon} \right) + \sqrt{\left( 1 - \frac{\sigma_i}{\omega\varepsilon} \right)^2 + \left( \frac{\sigma_r}{\omega\varepsilon} \right)^2} \right]^{\frac{1}{2}} \quad (2.35)$$

$$\beta = \omega \sqrt{\frac{\mu\varepsilon}{2}} \left[ - \left( 1 - \frac{\sigma_i}{\omega\varepsilon} \right) + \sqrt{\left( 1 - \frac{\sigma_i}{\omega\varepsilon} \right)^2 + \left( \frac{\sigma_r}{\omega\varepsilon} \right)^2} \right]^{\frac{1}{2}} \quad (2.36)$$

then the refractive index is defined by

$$Re(N) = c \sqrt{\frac{\mu\varepsilon}{2}} \left[ \left( 1 - \frac{\sigma_i}{\omega\varepsilon} \right) + \sqrt{\left( 1 - \frac{\sigma_i}{\omega\varepsilon} \right)^2 + \left( \frac{\sigma_r}{\omega\varepsilon} \right)^2} \right]^{\frac{1}{2}} \quad (2.37)$$

$$Im(N) = c \sqrt{\frac{\mu\varepsilon}{2}} \left[ - \left( 1 - \frac{\sigma_i}{\omega\varepsilon} \right) + \sqrt{\left( 1 - \frac{\sigma_i}{\omega\varepsilon} \right)^2 + \left( \frac{\sigma_r}{\omega\varepsilon} \right)^2} \right]^{\frac{1}{2}} \quad (2.38)$$

retrieving the case  $\sigma = \sigma_r$  when  $\sigma_i = 0$ . We now have the conductivity depending on the frequency  $\omega$  reducing back to  $\sigma_0$  if  $\omega = 0$ . Also the current density and electric field are not in phase any more. The real part of  $\sigma$  gives a current in phase with the electric field but the complex part  $\sigma_i$  produces one completely out of phase. We have

- large friction  $\Rightarrow \sigma \simeq \sigma_0$  a constant, this holds mainly for metals such as iron. This holds for frequencies into the microwave region so we may approximate the conductivity of iron as a constant  $\sigma_0, \sigma_i \simeq 0$ .
- Small friction  $\Rightarrow$  a plasma not considered here.

It is possible to further extend the investigation of conductivity in terms of a force equation on charge carriers as above, with the inclusion of a mechanical restoring force on an electron  $\mathbf{F}_m = -m_e\omega_0^2\mathbf{r}$  depending on position ( $\omega_0$  the natural frequency of oscillation of the charge), frictional damping  $\mathbf{F}_d = -m_e\gamma\mathbf{v}$  and a Lorentz force  $\mathbf{F}_l = -e(\mathbf{E}_p + \mathbf{v} \times \mathbf{B}_m)$  where  $\mathbf{E}_p$  and  $\mathbf{B}_m$  are the induced fields. Now the refractive index is given generally by

$$n + i\eta = \sqrt{\kappa_m \left( \kappa_e + \frac{i\sigma}{\omega\varepsilon_0} \right)} \quad (2.39)$$

where  $\kappa_m = 1 + \chi_m = \mu_r$  or  $\mu = \kappa_m\mu_0$  is the relative permeability and  $\kappa_e = 1 + \chi_e = \varepsilon_r$  or  $\varepsilon = \kappa_e\varepsilon_0$ . Then the general dispersion theory with the inclusion of free electrons gives for the refractive indices

$$n^2 - \eta^2 = 1 + \frac{\mathcal{N}}{\varepsilon_0} \sum_j \frac{n_j(e^2/m_e)(\omega_j^2 - \omega^2)}{(\omega_j^2 - \omega^2)^2 + (\gamma_j\omega)^2} - \frac{\sigma_0^2 m_e / \mathcal{N}_0 \varepsilon_0 e^2}{1 + (\sigma_0 m_e \omega / \mathcal{N}_0 e^2)^2} \quad (2.40)$$

$$2n\eta = \frac{\mathcal{N}}{\varepsilon_0} \sum_j \frac{n_j(e^2/m_e)\gamma_j\omega}{(\omega_j^2 - \omega^2)^2 + (\gamma_j\omega)^2} + \frac{(\sigma_0/\omega\varepsilon_0)}{1 + (\sigma_0 m_e \omega / \mathcal{N}_0 e^2)^2} \quad (2.41)$$

where  $\mathcal{N}$  is the number of molecules per unit volume,  $n_j$  is the no of electrons characterised by the natural frequency  $\omega_j$  and damping constant  $\gamma_j$ . We have summed over all types of electrons of the above frequencies. Note that this is the result for  $\kappa_m = 1$  no magnetic effects are included. Often these effects are incorporated into the permittivity by the addition of a factor  $\varepsilon''$  ie

$$\varepsilon = \varepsilon' - i\varepsilon'' - \frac{i\sigma}{\omega} \quad (2.42)$$

a similar procedure is adopted for magnetic losses characterised by an analogous expression

$$\mu = \mu' - i\mu'' \quad (2.43)$$

these two contributions represent the  $\kappa_e$  and  $\kappa_m$  factors present in the refractive index equation (2.39) above. This is the representation for a general lossy medium. Here we involve the natural frequencies of vibration of the electrons in the medium. For metals at low frequencies no noticeable difference is found from the constant conductivity case but the differences start to show up in the infrared and visible portions of the spectrum. These frequencies start to be comparable to the natural frequencies of some of the bound electrons. If this is the case we must deal with the general expressions (2.40) and (2.41), [94].

## 2.5 Boundary Conditions at an interface

A plane wave travelling in a medium of electrical properties  $\mu_1, \varepsilon_1, \sigma_1$  is incident upon a second medium separated from the first by an interface  $S$  having boundary curve  $C$ . The second medium is characterised by  $\mu_2, \varepsilon_2, \sigma_2$ . Then the boundary conditions for the electric and magnetic fields across  $C$  are given by (see for example, [63])

$$\hat{\mathbf{n}} \times (\mathbf{E}_2 - \mathbf{E}_1) = 0 \quad (2.44)$$

$$\hat{\mathbf{n}} \cdot (\varepsilon_2 \mathbf{E}_2 - \varepsilon_1 \mathbf{E}_1) = 0 \quad (2.45)$$

$$\hat{\mathbf{n}} \times (\mathbf{H}_2 - \mathbf{H}_1) = 0 \quad (2.46)$$

$$\hat{\mathbf{n}} \cdot (\mu_2 \mathbf{H}_2 - \mu_1 \mathbf{H}_1) = 0 \quad (2.47)$$

for linear isotropic and homogeneous media 1 and 2, where  $\hat{\mathbf{n}}$  is the unit normal to  $C$  taken from region 1 into region 2. The first and third conditions merely state that the tangential electric and magnetic field vectors on both sides of the surface are continuous. The other two state that the normal components of the electric and magnetic flux densities are continuous across  $C$ . These boundary conditions are true for media without surface charges or currents on the surface  $S$ . They apply to static or time varying fields and as such are applicable to the propagation of EM waves through several different media.

They will be used in conjunction with an incident plane wave to describe the reflection properties of iron-oxide layers on an iron substrate.





## Chapter 3

# Interference in Plane Layered Media

### 3.1 Introduction

The first section is devoted to the detailed derivation of singlefilm interference phenomena by the use of Maxwell's equations of electromagnetics. This is detailed because of some delicate manipulations of the electric and magnetic fields as well as an investigation of phase changes in the oxide film. This developed theory is then extended straightforwardly to multilayer films, the main object of investigation. It must be remembered that we are dealing with several oxide films, not just one, as has already been considered in the literature.

There is an additional note on Snell's law which has been found non-applicable to finite surfaces unless certain conditions are satisfied. Quite reasonably, Snell's law has always been considered valid and it is shown to be true here as well.

The final section considers the consequences of a flat surface solution comparing a smooth unoxidised one to an oxidised one. The three specific areas which are addressed include how the emissivity varies with thickness of oxide layer, ie interference properties, how it

changes with wavelength and the effect temperature has. All of these areas are fundamental questions worth asking and is at least part of the purpose of the investigation. The final section analyses the numerical data and compares it to the theoretical interpretations of the previous section.

## 3.2 Electromagnetic Approach

In order to simplify the treatment of electromagnetic wave interference we will, for the moment, restrict ourselves to the case of one film of oxide on an iron substrate rather than three. This will be rectified by a straightforward extension of the one layer theory later on in the analysis.

### 3.2.1 Single Layer Case

We are given that a monochromatic plane wave travelling in air of refractive index  $N_1 = 1$ , i.e. with free space electrical properties  $\mu_1 = \mu_0, \varepsilon_1 = \varepsilon_0, \sigma_1 = \sigma_0 = 0$ , is incident upon a thin dielectric (oxide) film between two linear isotropic and homogeneous media (also true of film). Consider Figure 3.2.1. The film has electrical properties  $\mu_2, \varepsilon_2, \sigma_2, N_2$  and the substrate has  $\mu_3, \varepsilon_3, \sigma_3, N_3$  both refractive indices of which may be complex.

Then it is obvious that the electric and magnetic field vectors are constituted of incident, reflected and transmitted waves. The boundary conditions at the interfaces 1 are given by (N.B. the unit normal at both interface 1 and 2 is the same always in the  $z$ -direction)

$$\hat{\mathbf{n}} \times (\mathbf{E}_{I1} + \mathbf{E}_{R1}) = \hat{\mathbf{n}} \times (\mathbf{E}_{T1} + \mathbf{E}'_{R2}) \quad (3.1)$$

$$\hat{\mathbf{n}} \times (\mathbf{H}_{I1} + \mathbf{H}_{R1}) = \hat{\mathbf{n}} \times (\mathbf{H}_{T1} + \mathbf{H}'_{R2}) \quad (3.2)$$

$$\varepsilon_1 \hat{\mathbf{n}} \cdot (\mathbf{E}_{I1} + \mathbf{E}_{R1}) = \varepsilon_2 \hat{\mathbf{n}} \cdot (\mathbf{E}_{T1} + \mathbf{E}'_{R2}) \quad (3.3)$$

$$\mu_1 \hat{\mathbf{n}} \cdot (\mathbf{H}_{I1} + \mathbf{H}_{R1}) = \mu_{2,3} \hat{\mathbf{n}} \cdot (\mathbf{H}_{T1} + \mathbf{H}'_{R2}) \quad (3.4)$$

At boundary 2

$$\hat{\mathbf{n}} \times (\mathbf{E}_{I2} + \mathbf{E}_{R2}) = \hat{\mathbf{n}} \times \mathbf{E}_{T2} \quad (3.5)$$

$$\hat{\mathbf{n}} \times (\mathbf{H}_{I2} + \mathbf{H}_{R2}) = \hat{\mathbf{n}} \times (\mathbf{H}_{T2} + \mathbf{H}'_{R2}) \quad (3.6)$$

$$\varepsilon_2 \hat{\mathbf{n}} \cdot (\mathbf{E}_{I2} + \mathbf{E}_{R2}) = \varepsilon_3 \hat{\mathbf{n}} \cdot \mathbf{E}_{T2} \quad (3.7)$$

$$\mu_2 \hat{\mathbf{n}} \cdot (\mathbf{H}_{I2} + \mathbf{H}_{R2}) = \mu_3 \hat{\mathbf{n}} \cdot \mathbf{H}_{T2} \quad (3.8)$$

Figure 3.2.1 The interaction of an incident electromagnetic wave with a single layer film on a substrate

following the earlier equations (2.44)-(2.47). Where  $I, R, T$  stand for incident reflected and transmitted waves respectively. Note that all field vectors stand for the resultant sum of waves travelling in their particular direction at that point in the medium. For simplicity we will deal with a plane wave which is polarised perpendicularly with respect to the plane of incidence defined as the plane constructed from the incident wave vector  $\mathbf{k}_{I1}$  and the unit vector in the  $z$  direction,  $\hat{\mathbf{k}}$ . This arbitrary choice is completely general. We use the notation of Hect & Zajac, [40].

The incident angles at each interface are written  $\theta_{I1}, \theta_{I2}$ , the refraction angles  $\theta_{T1}, \theta_{T2}$ , the reflection angles  $\theta_{R1}, \theta_{R2}$  notice that  $\theta_{T1} = \theta_{I2}$ . The " ' " superscripts refer to secondary reflections and transmissions at the film/air interface ( $2 \rightarrow 1$ ). For example the incident angle that the reflected wave  $E'_{R2}$  makes at the interface as it travels from the film into the air is designated by  $\theta'_{I2}$ , note  $\theta'_{I2} = \theta_{R2}$ .

Then at boundary 1 using the boundary condition above, that is, that the tangential components of  $E$  are equal on the interface where the normal  $\hat{\mathbf{n}} = \hat{\mathbf{k}}$

$$E_1 = E_{I1} + E_{R1} = E_{T1} + E'_{R2} \quad (3.9)$$

using the fact that  $\mathbf{H} = \frac{N}{c\mu} \hat{\mathbf{k}} \times \mathbf{E}$  and since  $\mathbf{E}$  is already tangent to the interface

$$H_1 = H_{I1(\text{tang})} + H_{R1(\text{tang})} = H_{T1(\text{tang})} + H'_{R2(\text{tang})} \quad (3.10)$$

then define normal and tangential unit vectors  $\hat{\mathbf{t}} = \hat{\mathbf{i}}, \hat{\mathbf{n}} = \hat{\mathbf{k}}$ . Then, since the electric field is perpendicular to the plane of incidence,  $\hat{\mathbf{t}} = \hat{\mathbf{E}}_{I1} \times \hat{\mathbf{n}}$ , we find

$$\mathbf{H}_{I1} \cdot \hat{\mathbf{t}} = \frac{N_1}{c\mu_1} (\hat{\mathbf{k}}_{I1} \times \mathbf{E}_{I1}) \cdot (\hat{\mathbf{E}}_{I1} \times \hat{\mathbf{n}}) \quad (3.11)$$

$$= \frac{N_1}{c\mu_1} [(\mathbf{k}_{I1} \cdot \mathbf{E}_{I1})(\mathbf{E}_{I1} \cdot \mathbf{n}) - (\mathbf{k}_{I1} \cdot \mathbf{n})(\mathbf{E}_{I1} \cdot \mathbf{E}_{I1})] \quad (3.12)$$

$$= -\frac{E_{I1}N_1}{c\mu_1} (\mathbf{k}_{I1} \cdot \mathbf{n}) \quad (3.13)$$

since  $\mathbf{k}_{I1} \cdot \mathbf{E}_{I1} = 0$  (perpendicular to each other)

$$H_{I1} = -\frac{E_{I1}N_1}{c\mu_1} \cos(\pi - \theta_{I1}) \quad (3.14)$$

$$= \frac{E_{I1}N_1}{c\mu_1} \cos \theta_{I1} \quad (3.15)$$

similarly

$$H_{R1} = \frac{E_{R1}N_1}{c\mu_1} \cos(\pi - \theta_{R1}) \quad (3.16)$$

$$= -\frac{E_{R1}N_1}{c\mu_1} \cos \theta_{R1} \quad (3.17)$$

therefore we find

$$H_{I1(tang)} + H_{R1(tang)} \quad (3.18)$$

$$= \frac{N_1}{c\mu_1} (E_{I1} \cos \theta_{I1} - E_{R1} \cos \theta_{I1}) \quad (3.19)$$

since by the laws of reflection  $\theta_{R1} = -\theta_{I1}$ , also for the RHS

$$H_{T1} = \frac{E_{T1}N_2}{c\mu_2} \cos \theta_{T1} \quad (3.20)$$

now since  $\theta_{T1} = \theta_{R2} = \theta'_{I2} = \theta_{I2}$  then

$$H_{T1} = \frac{E_{T1}N_2}{c\mu_2} \cos \theta'_{I2} \quad (3.21)$$

similarly

$$H'_{R2} = -\frac{E'_{R2}N_2}{c\mu_2} \cos \theta'_{I2} \quad (3.22)$$

so the RHS is

$$H_{T1(tang)} + H'_{R2(tang)} = \frac{N_2}{c\mu_2} (E_{T1} - E'_{R2}) \cos \theta'_{I2} \quad (3.23)$$

finally at boundary 1

$$\frac{N_1}{c\mu_1} (E_{I1} \cos \theta_{I1} - E_{R1} \cos \theta_{I1}) = \frac{N_2}{c\mu_2} (E_{T1} - E'_{R2}) \cos \theta'_{I2} \quad (3.24)$$

a similar procedure at boundary 2 leads to :

$$E_2 = E_{I2} + E_{R2} = E_{T2} \quad (3.25)$$

$$H_{2(tang)} = H_{I2(tang)} + H_{R2(tang)} = H_{T2(tang)} \quad (3.26)$$

$$= \frac{N_2}{c\mu_2} (E_{I2} - E_{R2}) \cos \theta_{I2} = \frac{N_3}{c\mu_3} E_{T2} \cos \theta_{T2} \quad (3.27)$$

(NB :  $\mathbf{E}$  components are already tangent to the boundary).

**Phase Changes in the Film**

Observe Figure 3.2.2

Figure 3.2.2 Phase changes inside the one-layer film

The distance travelled inside the film from boundary 1 to boundary 2 is given by

$$\cos \theta_{I2} = \frac{d}{b} \quad (3.28)$$

or

$$b = \frac{d}{\cos \theta_{T1}} \quad (3.29)$$

the optical path difference for the first two reflected rays is

$$h = N_2(AB + BC) - N_1AD \quad (3.30)$$

using  $AB = BC = b$

$$h = \frac{2N_2d}{\cos \theta_{T1}} - N_1AD \quad (3.31)$$

now the distance  $c$  is given by

$$c = b \sin \theta_{I2} = d \tan \theta_{T1} \quad (3.32)$$

now  $AC = 2c$

$$AD = AC \sin \theta_{I1} = \frac{2d \tan \theta_{T1}}{\sin \theta_{I1}} \quad (3.33)$$

but using Snell's law  $N_1 \sin \theta_{I1} = N_2 \sin \theta_{T1}$

$$AD = \frac{2dN_2 \sin^2 \theta_{T1}}{N_1 \cos \theta_{T1}} \quad (3.34)$$

therefore

$$h = \frac{2N_2d}{\cos \theta_{T1}} (1 - \sin^2 \theta_{T1}) \quad (3.35)$$

$$= 2N_2d \cos \theta_{T1} \quad (3.36)$$

the phase shift is then calculated by  $\delta = kh$  for a single traversing of the film. The phase shift will be

$$kh = kN_2d \cos \theta_{I2} \quad (3.37)$$

since  $\theta_{T1} = \theta_{I2}$ . Then each of the electric fields  $E_{I2}$  and  $E'_{R2}$  will have experienced this phase shift thus they may be written

$$E_{I2} = E_{T1} e^{-ikh} \quad (3.38)$$

$$E'_{R2} = E_{R2} e^{-ikh} \quad (3.39)$$

Now substitute for these in equations (3.25) we get

$$E_2 = E_{I2} + E_{R2} \quad (3.40)$$

or

$$E_{T1} e^{-ikh} + E'_{R2} e^{ikh} = E_{T2} \quad (3.41)$$

similarly

$$H_2 = \frac{N_2}{c\mu_2}(E_{T1}e^{-ikh} - E'_{R2}e^{ikh}) \cos \theta_{I2} = \frac{N_3}{c\mu_3}E_{T2} \cos \theta_{T2} \quad (3.42)$$

therefore

$$\frac{N_2}{c\mu_2}(E_{T1}e^{-ikh} - E'_{R2}e^{ikh}) \cos \theta_{I2} = \frac{N_3}{c\mu_3}(E_{T1}e^{-ikh} + E'_{R2}e^{ikh}) \cos \theta_{T2} \quad (3.43)$$

then we have two equations which may be solved for  $E_{T1}$  and  $E'_{R2}$ . Rewrite these to make the calculation easier we have

$$E_2 = E_{T1}e^{-ikh} + E'_{R2}e^{ikh} \quad (3.44)$$

$$H_2 = \frac{N_2}{c\mu_2}(E_{T1}e^{-ikh} - E'_{R2}e^{ikh}) \cos \theta_{I2} \quad (3.45)$$

multiply (3.44) by  $\frac{N_2}{c\mu_2} \cos \theta_{I2}$  and add to eliminate  $E'_{R2}$  we get

$$H_2 + \left(\frac{N_2}{c\mu_2} \cos \theta_{I2}\right) E_2 = \frac{2N_2}{c\mu_2} \cos \theta_{I2} E_{T1} e^{-ikh} \quad (3.46)$$

also multiply  $\frac{N_2}{c\mu_2} \cos \theta_{I2}$  by  $E_2$  and subtract  $H_2$

$$\left(\frac{N_2}{c\mu_2} \cos \theta_{I2}\right) E_2 - H_2 = \frac{2N_2}{c\mu_2} \cos \theta_{I2} E'_{R2} e^{ikh} \quad (3.47)$$

Now using the previous two equations substitute from (3.44) and (3.45) above

$$E_1 = E_{T1} + E'_{R2} \quad (3.48)$$

$$= \left(\frac{c\mu_2 e^{ikh}}{2N_2 \cos \theta_{I2}}\right) \left[H_2 + \left(\frac{N_2}{c\mu_2} \cos \theta_{I2}\right) E_2\right] + \left(\frac{c\mu_2 e^{-ikh}}{2N_2 \cos \theta_{I2}}\right) \left[\left(\frac{N_2}{c\mu_2} \cos \theta_{I2}\right) E_2 - H_2\right] \quad (3.49)$$

$$= \left(\frac{e^{ikh} + e^{-ikh}}{2}\right) E_2 + \left(\frac{c\mu_2}{N_2 \cos \theta_{I2}}\right) \left(\frac{e^{ikh} - e^{-ikh}}{2}\right) H_2 \quad (3.50)$$

$$= E_2 \cos kh + H_2 \left(\frac{c\mu_2}{N_2 \cos \theta_{I2}}\right) i \sin kh \quad (3.51)$$

and for  $H_1$

$$H_1 = \frac{N_2}{c\mu_2} \cos \theta'_{I2} (E_{T1} - E'_{R2}) \quad (3.52)$$

$$= \frac{N_2}{c\mu_2} \cos \theta'_{I2} \left\{ \left(\frac{c\mu_2 e^{ikh}}{2N_2 \cos \theta_{I2}}\right) \left[H_2 + \left(\frac{N_2}{c\mu_2} \cos \theta_{I2}\right) E_2\right] - \right.$$



$$\left( \frac{c\mu_2 e^{-ikh}}{2N_2 \cos \theta_{I2}} \right) \left[ \left( \frac{N_2}{c\mu_2} \cos \theta_{I2} \right) E_2 - H_2 \right] \} \quad (3.53)$$

$$= H_2 \cos kh + E_2 i \sin kh \left( \frac{N_2 \cos \theta_{I2}}{c\mu_2} \right) \quad (3.54)$$

or

$$E_1 = E_2 \cos kh - H_2 \left( \frac{c\mu_2}{N_2 \cos \theta_{I2}} \right) i \sin kh$$

$$H_1 = -E_2 \left( \frac{N_2 \cos \theta_{I2}}{c\mu_2} \right) i \sin kh + H_2 \cos kh$$

or

$$\begin{bmatrix} E_1 \\ H_1 \end{bmatrix} = \begin{bmatrix} \cos kh & \frac{-i \sin kh}{\gamma_2} \\ -i\gamma_2 \sin kh & \cos kh \end{bmatrix} \begin{bmatrix} E_2 \\ H_2 \end{bmatrix} \quad (3.55)$$

or

$$\begin{bmatrix} E_1 \\ H_1 \end{bmatrix} = M_1 \begin{bmatrix} E_2 \\ H_2 \end{bmatrix} \quad (3.56)$$

where  $\gamma_2 = \frac{N_2}{c\mu_2} \cos \theta_{I2}$  and  $M_1$  is the characteristic matrix of the film. Note that upon the use of (3.9) and (3.25) we get

$$\begin{bmatrix} E_{I1} + E_{R1} \\ \gamma_1 (E_{I1} - E_{R1}) \end{bmatrix} = M_1 \begin{bmatrix} E_{T2} \\ \gamma_3 E_{T2} \end{bmatrix} \quad (3.57)$$

which leads to the definition of the reflection and transmission coefficients  $R$  and  $T$  :

$$R = \frac{E_{R1}}{E_{I1}} \text{ and } T = \frac{E_{T2}}{E_{I1}} \quad (3.58)$$

and thus we get :

$$\begin{bmatrix} R + 1 \\ \gamma_1 (1 - R) \end{bmatrix} = M_1 \begin{bmatrix} T \\ \gamma_3 T \end{bmatrix} \quad (3.59)$$

or

$$R^\perp = \frac{\gamma_1 m_{11} + \gamma_1 \gamma_3 m_{12} - m_{21} - \gamma_3 m_{22}}{\gamma_1 m_{11} + \gamma_1 \gamma_3 m_{12} + m_{21} + \gamma_3 m_{22}} \quad (3.60)$$

$$T^\perp = \frac{2\gamma_1}{\gamma_1 m_{11} + \gamma_1 \gamma_3 m_{12} + m_{21} + \gamma_3 m_{22}} \quad (3.61)$$

where  $\gamma_1 = \frac{N_1}{c\mu_1} \cos \theta_{I1}$ ,  $\gamma_3 = \frac{N_3}{c\mu_3} \cos \theta_{I3}$  and the  $m_{ij}$ 's refer to the elements of  $M_1$ .

A similar set of equations may be derived for the case of  $\mathbf{E}$  parallel to the plane of incidence, giving the matrix equation :

$$\begin{bmatrix} E_1 \\ H_1 \end{bmatrix} = M_1 \begin{bmatrix} E_2 \\ H_2 \end{bmatrix} \quad (3.62)$$

identical to the perpendicular case except that

$$\gamma_2 = \frac{N_2}{c\mu_2 \cos \theta_{I2}}, \quad \gamma_3 = \frac{N_3}{c\mu_3 \cos \theta_{I3}} \quad (3.63)$$

that is

$$R^{\parallel} = - \left( \frac{\gamma_1 m_{11} + \gamma_1 \gamma_3 m_{12} - m_{21} - \gamma_3 m_{22}}{\gamma_1 m_{11} + \gamma_1 \gamma_3 m_{12} + m_{21} + \gamma_3 m_{22}} \right) \quad (3.64)$$

$$T^{\parallel} = \frac{2\gamma_1 \left( \frac{\cos \theta_{I1}}{\cos \theta_{I3}} \right)}{\gamma_1 m_{11} + \gamma_1 \gamma_3 m_{12} + m_{21} + \gamma_3 m_{22}} \quad (3.65)$$

Note that we may express the reflection and transmission coefficients in a slightly different way, [13], by considering the flat surface reflection coefficients for each boundary and replacing the matrix elements by these. That is

$$r = \frac{r_1 + r_2 e^{2i\delta}}{1 + r_1 r_2 e^{2i\delta}} \quad (3.66)$$

$$t = \frac{t_1 t_2 e^{i\delta}}{1 + r_1 r_2 e^{2i\delta}} \quad (3.67)$$

where  $r_{1,2}$  and  $t_{1,2}$  are the reflection and transmission coefficients at each interface 1 and 2. They are given by

$$r_{1,2}^{\perp} = \frac{N_{2,3} \cos \theta_{I(1,2)} - N_{1,2} \cos \theta_{T(1,2)}}{N_{2,3} \cos \theta_{I(1,2)} + N_{1,2} \cos \theta_{T(1,2)}} \quad (3.68)$$

$$t_{1,2}^{\perp} = \frac{2N_{1,2} \cos \theta_{I(1,2)}}{N_{2,3} \cos \theta_{I(1,2)} + N_{1,2} \cos \theta_{T(1,2)}} \quad (3.69)$$

$$r_{1,2}^{\parallel} = \frac{N_{1,2} \cos \theta_{I(1,2)} - N_{2,3} \cos \theta_{T(1,2)}}{N_{1,2} \cos \theta_{I(1,2)} + N_{2,3} \cos \theta_{T(1,2)}} \quad (3.70)$$

$$t_{1,2}^{\parallel} = \frac{2N_{2,3} \cos \theta_{I(1,2)}}{N_{1,2} \cos \theta_{I(1,2)} + N_{2,3} \cos \theta_{T(1,2)}} \quad (3.71)$$

for each kind of polarisation.

### 3.2.2 Multiple Layer Case

Now this analysis may be extended to the case of multiple layers. Dealing for the moment only with the perpendicularly polarised waves. The matrix  $M_1$  relates the fields at the two adjacent boundaries, then we may say for two films

$$\begin{bmatrix} E_2 \\ H_2 \end{bmatrix} = M_2 \begin{bmatrix} E_3 \\ H_3 \end{bmatrix} \quad (3.72)$$

and similarly for three films :

$$\begin{bmatrix} E_3 \\ H_3 \end{bmatrix} = M_3 \begin{bmatrix} E_4 \\ H_4 \end{bmatrix} \quad (3.73)$$

or

$$\begin{bmatrix} E_1 \\ H_1 \end{bmatrix} = M_1 M_2 \begin{bmatrix} E_3 \\ H_3 \end{bmatrix} \quad (3.74)$$

using (3.62) continuing this procedure to  $p$  films we get

$$\begin{bmatrix} E_1 \\ H_1 \end{bmatrix} = M_1 M_2 M_3 \dots M_p \begin{bmatrix} E_{p+1} \\ H_{p+1} \end{bmatrix} \quad (3.75)$$

where

$$M_1 M_2 M_3 \dots M_p = M = \begin{pmatrix} m_{11} & m_{12} \\ m_{21} & m_{22} \end{pmatrix} \quad (3.76)$$

for the specific case of three layers we obtain

$$M_j = \begin{pmatrix} \cos kh_j & \frac{-i \sin kh_j}{\gamma_j} \\ -i\gamma_j \sin kh_j & \cos kh_j \end{pmatrix} \quad (3.77)$$

where  $h_j = N_j d_j \cos \theta_{ij}$ . Note that Snells law allows the calculation of the angles  $\theta_{Tj}$  easily. For  $\theta_{T1}$  we have

$$N_1 \sin \theta_{I1} = N_2 \sin \theta_{T1} \quad (3.78)$$

or

$$\sin \theta_{T1} = \frac{N_1}{N_2} \sin \theta_{I1} \quad (3.79)$$

and for  $\theta_{T2}$

$$\sin \theta_{T2} = \frac{N_2}{N_3} \sin \theta_{T1} = \frac{N_1}{N_3} \sin \theta_{I1} \quad (3.80)$$

so generally

$$\sin \theta_{Tj} = \frac{N_1}{N_{j+1}} \sin \theta_{I1} \quad (3.81)$$

so it follows  $\cos \theta_{Tj} = \sqrt{1 - \sin^2 \theta_{Tj}}$ ,  $\gamma_j = \frac{N_j}{c\mu_j} \cos \theta_{Ij}$  and  $j = \{1, 2, 3, 4, 5\}$ . Following a similar procedure we get :

$$R_{\perp} = \frac{\gamma_1 m_{11} + \gamma_1 \gamma_5 m_{12} - m_{21} - \gamma_5 m_{22}}{\gamma_1 m_{11} + \gamma_1 \gamma_5 m_{12} + m_{21} + \gamma_5 m_{22}} \quad (3.82)$$

$$T_{\perp} = \frac{2\gamma_1}{\gamma_1 m_{11} + \gamma_1 \gamma_5 m_{12} + m_{21} + \gamma_5 m_{22}} \quad (3.83)$$

and for the case of parallel polarisation :

$$R_{\parallel} = - \left( \frac{\gamma_1 m_{11} + \gamma_1 \gamma_5 m_{12} - m_{21} - \gamma_5 m_{22}}{\gamma_1 m_{11} + \gamma_1 \gamma_5 m_{12} + m_{21} + \gamma_5 m_{22}} \right) \quad (3.84)$$

$$T_{\parallel} = \frac{2\gamma_1 \left( \frac{\cos \theta_{I1}}{\cos \theta_{I5}} \right)}{\gamma_1 m_{11} + \gamma_1 \gamma_5 m_{12} + m_{21} + \gamma_5 m_{22}} \quad (3.85)$$

With  $\gamma_j = \frac{N_j}{c\mu_j \cos \theta_{Ij}}$ . The 3-layer substrate system is now ordered as follows :  $N_1$  is air (= 1),  $N_2$  is haematite,  $N_3$  is magnetite,  $N_4$  is Wustite and  $N_5$  iron. All angles are completely analogous to the one layer case.

The reflectance and transmittance can then be calculated as follows :

$$R_y = RR^* \text{ and } T_y = TT^* \quad (3.86)$$

where "\*" indicates the complex conjugate. The total reflectance can be expressed as an average of the two kinds of polarisation :

$$R_y = \frac{R_{y\parallel} + R_{y\perp}}{2} \text{ and } T_y = \frac{T_{y\parallel} + T_{y\perp}}{2} \quad (3.87)$$

then emittance is easily calculated as

$$\epsilon = 1 - R_y \quad (3.88)$$

where we have assumed that the transmission coefficient will tend to zero once the wave passes into the steel substrate which is of course highly absorbing and infinitely thick.

**Note on Snells Law**

The use of Snells law in the determination of angles of refraction has recently been shown to be valid only when considering a plane wave incident on a surface of infinite dimensions, [39]. If the surface is finite then the size of the surface, the angle of incidence and the polarisation of the incident wave produce deviations in Snell's law. Note that if the surface dimensions are relatively large compared to the wavelength of the incident radiation this problem is circumvented since the surface can then be taken as approximately infinite.

The same reasoning applies to rough surfaces where each scattering facet is of course not infinite. However if each of these elements is very large in comparison to the wavelength then we may use Snells law. This statement is supported by Bleistein & Handelsman, [12], who show Snells law relations can be derived from the Kirchoff solution for rough surface scattering and state that Snell's law is valid ' . . . for wavelengths small compared to the fundamental body dimensions '.

Snell's law shall be assumed applicable in this thesis.

**3.3 The Reflected Field**

To get a feel for the difference in the reflection coefficients for a plane surface and that of a layered one, we will consider the effect of an unlayered surface on the surface emissivity of iron (steel).

**3.3.1 Unoxidised Surfaces**

Let the thickness of the layer tend to zero ( $h \rightarrow 0$ ) and choose the incidence angle as normal ( $\theta_{I1} = 0$ ), then the reflection coefficient of a substrate (iron) with a single layer ( $FeO$ ) is

$$R = \frac{r_1 + r_2}{1 + r_1 r_2} \quad (3.89)$$

where

$$r_1^\perp = \frac{N_2 - N_1}{N_2 + N_1} \quad (3.90)$$

$$r_1^\parallel = \frac{N_1 - N_2}{N_1 + N_2} \quad (3.91)$$

$$r_2^\perp = \frac{N_3 - N_2}{N_3 + N_2} \quad (3.92)$$

$$r_2^\parallel = \frac{N_2 - N_3}{N_2 + N_3} \quad (3.93)$$

then for perpendicular polarisation

$$R^\perp = \frac{N_3 - N_1}{N_3 + N_1} \quad (3.94)$$

$$R^\parallel = -\frac{N_3 - N_1}{N_3 + N_1} \quad (3.95)$$

of course independent of  $N_2$  as expected. Now,  $N_1 = 1$  since it is air then we have

$$R^\perp = \frac{N_3 - 1}{N_3 + 1} \quad (3.96)$$

$$R^\parallel = -\frac{N_3 - 1}{N_3 + 1} \quad (3.97)$$

and  $N_3$  is the complex refractive index of iron, that is, it has the structure

$$N_3 = n_3 + i\eta_3 \quad (3.98)$$

therefore

$$R^\perp = \frac{(n_3 - 1) + i\eta_3}{(n_3 + 1) + i\eta_3} \quad (3.99)$$

$$R^\parallel = -\frac{(n_3 - 1) + i\eta_3}{(n_3 + 1) + i\eta_3} \quad (3.100)$$

rationalise both to get

$$R^\perp = \frac{(n_3^2 + \eta_3^2 - 1) + 2i\eta_3}{(n_3 + 1)^2 + \eta_3^2} \quad (3.101)$$

$$R^\parallel = -\frac{(n_3^2 + \eta_3^2 - 1) + 2i\eta_3}{(n_3 + 1)^2 + \eta_3^2} \quad (3.102)$$

the reflectivity is defined by

$$R_y^\perp = R^\perp R^{\perp*} \quad (3.103)$$

$$R_y^\perp = \frac{(n_3^2 + \eta_3^2 - 1)^2 + 4\eta_3^2}{[(n_3 + 1)^2 + \eta_3^2]^2} \quad (3.104)$$

$$R_y^\parallel = \frac{(n_3^2 + \eta_3^2 - 1)^2 + 4\eta_3^2}{[(n_3 + 1)^2 + \eta_3^2]^2} \quad (3.105)$$

the average is

$$R_y = \frac{R_y^\perp + R_y^\parallel}{2} \quad (3.106)$$

$$= \frac{(n_3^2 + \eta_3^2 - 1)^2 + 4\eta_3^2}{[(n_3 + 1)^2 + \eta_3^2]^2} \quad (3.107)$$

which gives an emissivity of

$$\epsilon = 1 - \frac{(n_3^2 + \eta_3^2 - 1)^2 + 4\eta_3^2}{[(n_3 + 1)^2 + \eta_3^2]^2} \quad (3.108)$$

How does the emissivity vary with the wavelength and the temperature ? Substitute for the values of  $n_3$  and  $\eta_3$  from (2.27) and (2.28), that is

$$n_3 = \frac{1}{\sqrt{2}} \left[ \sqrt{1 + \left( \frac{\sigma}{\omega\epsilon_0} \right)^2} + 1 \right]^{1/2} \quad (3.109)$$

$$\eta_3 = \frac{1}{\sqrt{2}} \left[ \sqrt{1 + \left( \frac{\sigma}{\omega\epsilon_0} \right)^2} - 1 \right]^{1/2} \quad (3.110)$$

then  $\epsilon$  becomes

$$\epsilon = 1 - \frac{\left( \frac{\sigma}{\omega\epsilon_0} \right)^2}{\left[ \sqrt{1 + \left( \frac{\sigma}{\omega\epsilon_0} \right)^2} + \sqrt{2} \sqrt{\sqrt{1 + \left( \frac{\sigma}{\omega\epsilon_0} \right)^2} - 1} + 1 \right]^2} \quad (3.111)$$

It is obvious that, since iron or steel have large conductivities, if we take the limit as  $\sigma \rightarrow \infty$  the emissivity will tend to zero since the reflectivity approaches one. So we expect very small emissivities for clean steel surfaces. This is indeed the case as shown in industry. Now since  $\omega = 2\pi c/\lambda$  expressing the function above in orders of  $\lambda$  we find

$$\epsilon = O\left(\frac{1}{\lambda^{1/2}}\right) + O\left(\frac{1}{\lambda}\right) + O\left(\frac{1}{\lambda^2}\right) \quad (3.112)$$

so we expect the emissivity to vary with  $\epsilon \sim O(\lambda^{-1/2})$  for  $\lambda \gg 1$  otherwise the extra terms present in each denominator of each of the terms in (3.112) must be taken into account. Similarly, if we choose terms for which  $\lambda \ll 1$  then the emissivity is approximately equal to 1,  $\epsilon \sim O(1)$ . It is possible to get a description for limited cases but the full expression must be used for the general behaviour in between these two.

We also know that the conductivity of iron decreases with increase in temperature to a first approximation as

$$\sigma \sim \frac{1}{T} \quad (3.113)$$

then we again expect an increase in emissivity with temperature of the order  $\epsilon \sim O(T^{1/2})$ . This holds for temperatures approaching 1000°C beyond which the increase is considerably smaller, in most cases levelling out at some constant.

### 3.3.2 Oxidised Surfaces

Making the same assumptions as for the unoxidised case except,  $d \neq 0$ , then the reflection coefficient for a single film of oxide on top of iron, is

$$R = \frac{r_1 + r_2 e^{2i\delta}}{1 + r_1 r_2 e^{2i\delta}} \quad (3.114)$$

where  $r_{1,2}$  are as before

$$r_1^\perp = \frac{N_2 - 1}{N_2 + 1} \quad (3.115)$$

$$r_1^\parallel = \frac{1 - N_2}{1 + N_2} \quad (3.116)$$

$$r_2^\perp = \frac{N_3 - N_2}{N_3 + N_2} \quad (3.117)$$

$$r_2^\parallel = \frac{N_2 - N_3}{N_2 + N_3} \quad (3.118)$$

with  $\delta$

$$\delta = kN_2d = \frac{2\pi N_2d}{\lambda} \quad (3.119)$$



so  $R$  becomes

$$R^\perp = \frac{(N_2 - 1)(N_3 + N_2) + (N_3 - N_2)(N_2 + 1)e^{\frac{2iN_2d\pi}{\lambda}}}{(N_2 + 1)(N_3 + N_2) + (N_2 - 1)(N_3 - N_2)e^{\frac{2iN_2d\pi}{\lambda}}} \quad (3.120)$$

$$R^\parallel = \frac{(1 - N_2)(N_3 + N_2) + (N_2 - N_3)(N_2 + 1)e^{\frac{2iN_2d\pi}{\lambda}}}{(N_2 + 1)(N_3 + N_2) + (1 - N_2)(N_2 - N_3)e^{\frac{2iN_2d\pi}{\lambda}}} = -R^\perp \quad (3.121)$$

Three important cases must be considered. The refractive index of the oxide can be written

$$N_2 = n_2 + i\eta_2 \quad (3.122)$$

then the exponential term becomes

$$e^{\frac{2iN_2d\pi}{\lambda}} = e^{\frac{-2\eta_2d\pi}{\lambda}} \left[ \cos\left(\frac{2n_2d\pi}{\lambda}\right) + i \sin\left(\frac{2n_2d\pi}{\lambda}\right) \right] \quad (3.123)$$

Three consequences arise from this term

1. If the ratio  $\frac{\eta_2d\pi}{\lambda} \rightarrow \infty$  which can happen if either  $\lambda$  is very small or  $d$  is very large (since  $n_2$  is always  $O(\sqrt{\lambda})$ , therefore not changing this result). Then the second lot of terms in the reflection coefficients above reduce to zero and the Fresnel coefficients become

$$R^\perp = \frac{(N_2 - 1)(N_3 + N_2)}{(N_2 + 1)(N_3 + N_2)} \quad (3.124)$$

$$R^\parallel = \frac{(1 - N_2)(N_3 + N_2)}{(N_2 + 1)(N_3 + N_2)} \quad (3.125)$$

The case for iron gave us the two reflection coefficients

$$R = \pm \frac{N_3 - 1}{N_3 + 1} \quad (3.126)$$

if we take the limit as  $N_3 \rightarrow \infty$  which would happen for perfect conductivity then  $R \rightarrow \pm 1$ , producing a reflectivity close to one giving a very small emissivity close to zero. Now adopt the same procedure for the oxidised case above

$$\lim_{N_3 \rightarrow \infty} R = \lim_{N_3 \rightarrow \infty} \pm \frac{(N_2 - 1)(N_3 + N_2)}{(N_2 + 1)(N_3 + N_2)} \quad (3.127)$$

$$= \pm \frac{N_2 - 1}{N_2 + 1} \quad (3.128)$$

a reflection coefficient not equal to one, in fact always being less than one in size, unless  $N_2 \rightarrow \infty$  as well. In fact, this is the reflection coefficient of pure iron-oxide demonstrating that we will mainly observe Scale rather than iron in thermometry experiments. This indicates the emissivity of oxidised surfaces will always be larger than unoxidised ones. This is valid as long as either  $\lambda$  is small compared to  $d$  or  $d$  is large compared to  $\lambda$  so we expect a large emissivity for small wavelengths which will decrease as soon as this is no longer true. If, for example, the thickness and wavelength become comparable to each other. Note that the wavelength dependence is of the same form as the steel case ie  $\epsilon \propto \lambda^{-1/2}$ , the temperature dependence now relies on how the conductivity of  $FeO$  varies with temperature. It is known that the conductivity of Wustite actually increases with temperature so the emissivity should decrease with temperature in a similar manner to that of steel  $\epsilon \propto O(T^{-1/2})$ , if the temperature increase is linear.

2. If the ratio  $d/\lambda \sim 0$  which can happen if  $d$  is very small or  $\lambda$  is very large. Then the reflection coefficient acts like that of clean steel which was discussed in the previous section. So an oxidised surface ‘ looks ’ like an unoxidised one at long wavelengths or very small oxide thicknesses.
3. The case where  $d/\lambda \sim O(1)$ . This is the most interesting case and gives rise to the interference characteristics of layered media. The crucial term will be one of the form

$$\sin\left(\frac{4n_2d\pi}{\lambda}\right) e^{-\frac{4\eta_2d\pi}{\lambda}} \quad (3.129)$$

this being a result of the oscillatory term and the decaying term in the exponential. The sinusoidal part will tend to produce oscillations inside the oxide film as long as  $d/\lambda$  is not too small. The decaying exponential will try to reduce these oscillations. Since the sine term will always lie in the range  $\pm 1$ , the decay term will be of great importance. If the absorption properties of the oxide layer, governed by  $\eta_2$ , are

small then many oscillations can take place. If the absorption is large however the oscillations quickly die off.

When does this decay reduce the oscillations close to zero ? This is determined by the term  $\frac{2\eta_2 d\pi}{\lambda}$ . Let us arbitrarily assign a size to this oscillation reduction. Let us say that the oscillations are eliminated when

$$e^{-\frac{4\eta_2 d\pi}{\lambda}} \simeq 0.01 \quad (3.130)$$

this occurs when

$$d = \frac{-\lambda \ln(0.01)}{4\eta_2 \pi} \quad (3.131)$$

For some other choice instead of 0.01 say some small constant  $C = \log_e(const)$ , then oscillations cease at

$$d_{critical} = \frac{\lambda C}{4\eta_2 \pi} \quad (3.132)$$

this is the critical thickness at which oscillations cease. It may be compared to the skin depth of the film or the depth to which a wave penetrates into the medium. If we suggest that the number of skin depths required for oscillations to cease be

$$s\Delta = \frac{2sN_2}{c\mu_0\sigma_2} \quad (3.133)$$

where  $s$  is some real number and we have used the fact  $\alpha/\omega = N_2/c$ ,  $\mu_2 = \mu_0$ . Then

$$d_{critical} \simeq s\Delta \quad (3.134)$$

then the constant can be calculated as

$$C = \frac{8s\pi}{c\mu_0} \left( \frac{n_2\eta_2}{\lambda\sigma_2} \right) \quad (3.135)$$

this constant then depends on the temperature via  $\sigma_2$  which has a significant temperature dependence and through the individual real and imaginary parts of the refractive index which can eliminate the wavelength since according to (2.27) and (2.28) both  $n_2$  and  $\eta_2$  are proportional (approximately) to  $\sqrt{\lambda}$  this is also true to some degree of conductivity. This constant  $C$  is mostly dependent on the simple constants  $s, \pi, c, \mu_0$ . A comparison will be made when numerical solutions are produced.

### 3.3.3 Instability of Emissivity at low thickness of Scale

It has already been pointed out that for small oxide thicknesses (cf  $d$ ) the emissivity is very small (that of steel) and depends on  $N_3$ . Now the growth of oxide layers takes place over time via the equation

$$d = K\sqrt{te^{-\frac{40500}{RT}}} \quad (3.136)$$

where  $K$  is a constant, then as the thickness of oxide increases the emissivity must be less under the control of  $N_3$  and come more under the influence of both  $N_2$  and the decaying oscillations produced by the ratio  $d/\lambda$ . This means that the emissivity must be determined more and more by the ratio  $\frac{N_2-1}{N_2+1}$  this has the effect of a sudden increase in emissivity from that of steel to that of the oxide (dependent on  $N_2$ ). Similarly the ratio  $d/\lambda$  is no longer so small since as  $d$  increases the ratio tends more to one. Then oscillations take place which decay away to a relatively constant value determined by the critical thickness

$$d_{critical} = \frac{\lambda C}{4\eta_2\pi} \quad (3.137)$$

we may then calculate approximately the time taken for this critical thickness to be reached, as the oxide grows, with the use of equation (3.136) above. The time is given by

$$t_{critical} = \left(\frac{d_{critical}}{K}\right)^2 e^{\frac{40500}{RT}} \quad (3.138)$$

$$= \left(\frac{C'\lambda}{4\pi\eta_2}\right)^2 e^{\frac{40500}{RT}} \quad (3.139)$$

( $C' = C/K$ ). So the time at which oscillations cease is determined by the temperature of the steel/oxide, the wavelength the measurement (of emissivity) is taken at, and some basic constants.

### Emissivity Trends

In industry measurements are often made after the interference oscillations cease, a clear reading can then be made since the emissivity remains relatively stable after these oscillations. It should be noted that as the thickness of the oxide increases further from zero then

as a consequence so does the emissivity, becoming more that of oxide than steel. Once this value is reached it remains constant (for constant  $\lambda$ ) since  $d/\lambda$  is large and  $R$  depends only on the ratio  $\frac{N_2-1}{N_2+1}$  which is only a function of the electrical properties of oxide.

Alternatively if we keep the oxide thickness constant, this is possible when little growth occurs after an initial spurt, the oxide slows its own growth to some extent, [78]. Then if we increase the wavelength slowly from very small (cf  $d$ ) the emissivity will at first be very large due to the size of  $d/\lambda$  which implies  $\epsilon = \epsilon(N_2)$ . As the wavelength increases small oscillations take place until the wavelength increases beyond  $O(d)$ ,  $d/\lambda \sim 1$  and the emissivity must decrease until it comes into line with the emissivity of steel which decreases as  $\lambda^{-1/2}$ ,  $\lambda$  large.



## Chapter 4

# Numerical Solutions for Smooth Surfaces

### 4.1 The Numerical Scheme

The relatively simple problem is to obtain data relating the emissivity  $\epsilon$  to the variables : temperature  $T$ , thickness of oxide layer  $d$  and wavelength of incident radiation  $\lambda$ . The process is to first obtain the reflection coefficient, both parallel and perpendicular polarisation, as a function of  $\lambda, d, T$ . This is achieved with use of the equations

$$R_{\perp} = \frac{\gamma_1 m_{11} + \gamma_1 \gamma_5 m_{12} - m_{21} - \gamma_5 m_{22}}{\gamma_1 m_{11} + \gamma_1 \gamma_5 m_{12} + m_{21} + \gamma_5 m_{22}} \quad (4.1)$$

$$R_{\parallel} = - \left( \frac{\gamma_1 m_{11} + \gamma_1 \gamma_5 m_{12} - m_{21} - \gamma_5 m_{22}}{\gamma_1 m_{11} + \gamma_1 \gamma_5 m_{12} + m_{21} + \gamma_5 m_{22}} \right) \quad (4.2)$$

where in each case the  $\gamma_j$ 's are calculated by

$$\gamma_j^{\perp} = \frac{N_j}{c\mu_j \cos \theta_{Tj}} \quad (4.3)$$

$$\gamma_j^{\parallel} = \frac{N_j \cos \theta_{Tj}}{c\mu_j} \quad (4.4)$$

for each case of polarisation. The electrical properties  $\mu_j = \mu_0, \varepsilon_j = \varepsilon_0$  with the refractive indices calculated with use of the equations

$$Re(N) = \frac{c\alpha}{\omega} = c\sqrt{\frac{\mu\varepsilon}{2}} \sqrt{\sqrt{1 + \left(\frac{\sigma}{\omega\varepsilon}\right)^2} + 1} \quad (4.5)$$

$$Im(N) = \frac{c\beta}{\omega} = c\sqrt{\frac{\mu\varepsilon}{2}} \sqrt{\sqrt{1 + \left(\frac{\sigma}{\omega\varepsilon}\right)^2} - 1} \quad (4.6)$$

for each oxide, differing through the conductivities which are constructed from the graphical data of Adler, [2], and Davis, [26]. The  $m_{ij}$ 's are calculated as cosine and sine functions of the phase difference calculated via

$$kh = 2kN_2d \cos \theta_{T1} \quad (4.7)$$

all angles computed with Snell's law

$$\sin \theta_{Tj} = \frac{N_1}{N_{j+1}} \sin \theta_{I1} \quad (4.8)$$

The reflectivity is then calculated by multiplication of its own complex conjugate after which an average of both kinds of polarisation is taken and then subtracted from 1 to obtain the emissivity as a function of

$$\epsilon = \epsilon(\lambda, T, d) \quad (4.9)$$

various graphical results can then be obtained for study under specific conditions.

The solutions written in FORTRAN are run on a VAX mainframe computer using NCAR graphing routines.

## 4.2 Multi-Layer Oxide Films

The treatment of multilayer oxide films, that is, all three layers of iron-oxide on top of steel will be along similar lines to that of the one layer case. For the solution for the multilayer case one could, in principle, adopt a similar methodology to the one-layer case



studied previously. However this is not straightforward and closed form solutions are not easily simplified, as such the analysis of this case will be done with the use of a numerical solution whose character is already typified in the one-layer case. We should expect the following characteristic phenomena :

1. Depending on the electrical properties of the various oxides, as the film grows on smooth steel, the first layer will be wustite, its effects have already been described. We expect very low emissivities, that of steel, at first, then, an increase to that of wustite and a period of oscillation which decays away over a critical time calculated previously. The emissivity should now stay constant. If we increase the wavelength it will start to penetrate the wustite layer provided the ratio  $d/\lambda$  becomes small. The emissivity of steel is now approximated by an inverse square root law.
2. As the layers continue to grow the thickness of magnetite increases slowly in the ratios 1 : 0.04, compared to wustite. As soon as the thickness of magnetite approaches that of the measurement wavelength we get interference and oscillations are produced in a manner akin to that for wustite. The critical time for cessation of oscillations now depends on the refractive index of magnetite rather than wustite. The emissivity will now be read as that of magnetite plus some influence from the next layer down, wustite. Again  $\epsilon$  will remain constant unless the wavelength is increased and it penetrates the two layers producing low emissivities of steel. This wavelength may depend on not just the combined thickness of the two layers but also each of their refractive indices (electrical properties).
3. Similarly, as the films continue to grow, eventually, the topmost, thinnest layer, haematite, will start to influence the emissivity. As its thickness approaches the incident wavelength the familiar oscillations will take place as well as the rise to the emissivity of haematite (a combination with wustite and magnetite). Again, the EM wave will be able to penetrate given a long enough wavelength. Note that for each film, its conductivity, which depends on temperature, can effect the results in a

complicated way. Generally however, we expect behaviour like that of the single layer of wustite studied in section (3.3.2). This is true since it is typical of the behaviour of the emissivity, given a layer of oxide, and because it is the major contributor to the final emissivity, solely by the fact that it is the dominant layer present.

### 4.3 Interpretation and Discussion of Results

The graphical results of the numerical solutions will be now be analysed.

#### 4.3.1 Comparison to Experimental Data

Figure 4.3.1 is a comparison of the experimentally obtained graphs of Tanaka & DeWitt, [82], and the numerical simulation of one layer of wustite ( $FeO$ ) on top of an iron substrate at two wavelengths of emitted radiation :  $1.6\mu m$  and  $3.0\mu m$ . The numerical graph was constructed on the basis of equation (3.136) to obtain a time axis by use of

$$t(sec) = \frac{d^2(mm)}{575} e^{\frac{40500}{RT(^{\circ}C)}}$$

For one layer of  $FeO$ ,  $K = 575$ ,  $R = 2.87$  then 300 seconds at a temperature of  $627^{\circ}C$  ( $900^{\circ}K$ ) to a thickness of about

$$d = \sqrt{300 \times 575 \times e^{\frac{-40500}{2.87 \times 627}}} = 0.005mm = 5.38 \times 10^{-6}m$$

notice that this time scale is not linearly related to the thickness and as such any direct comparison must be taken as an approximation. The time scale so created allows a crude comparison of layer growth over time with the experimental results. So a graph of emissivity verses  $FeO$  thickness ranging from  $5 \times 10^{-8} - 5 \times 10^{-6}$  was compared to an experimental graph of emissivity verses time 0-300 seconds. The thicknesses corresponded approximately to the times according to equation (4.3.1).

Note that for this comparison several sources of error exist :

1. The growth of iron-oxide is theoretically governed, on the average, by the exponential rate law (3.136), this is of course a simplification and can only represent the basics

of layer growth. Similarly, the accuracy of this law is based on the measurements of the rate constants. Any deviation in accuracy can markedly effect results. Finally the law is non-linear and so does not fit easily onto a linear graph over time as in the experimental results. Since the time varies as the square of thickness earlier calculated time values increase faster than later ones this gives rise to a distinctly non-linear appearance to the graph and we expect the later stages of the graph to change at a slower rate than the earlier stages.

2. Tanaka & DeWitt's results are for carbon steel, the numerical ones are those of iron. Unfortunately data relating to electrical properties of carbon steel were not available. The comparison must be approximate at best.
3. The numerical solution was most suited to higher temperature ranges where the magnetic properties of iron were negligible. The experimental temperatures are below the Curie point and permeability effects may not be ignorable.

However upon comparison of both graphs we see :

- Strikingly similar behaviour of the two graphs as a whole. They follow the same trend of a steep rise and then a region of oscillation due to interference in the iron-oxide layer. Then there is the drop off and rise in the latter part of both graphs.
- Note that the emissivities at time zero (thickness =  $5 \times 10^{-8}$  m) are lower for the iron graphs, this is to be expected since with the presence of carbon in the steel we may expect a slightly higher emissivity since this acts as a dielectric and changes the conductive properties so the refractive index is smaller.
- At both wavelengths the two graphs combine almost as an average of the experimental results.

So, generally speaking, given the possible errors, the numerical solution gives a reliable estimate of emissivity behaviour over varying oxide-layer thickness. We may feel confident the model results will be relevant and accurate for use in further emissivity investigations.

### 4.3.2 Comparison of One-Layer and Three-Layer Models

It was stated at the outset that the treatment of theoretical emissivity studies must be constructed on the basis of the full three-layer (wustite, magnetite, haematite) model rather than the more limited use of one of these as the basic oxide on steel. How do these two models compare ?

Figure 4.3.2 shows the calculated emissivity graphs of the two models varying with wavelength at a temperature of  $800^{\circ}\text{C}$  and a thickness of  $FeO$  of  $0.2\text{ mm}$ . Wustite was chosen as the thickness scale since it is the thickest of the oxides which form in the ratios  $1 : 0.04 : 0.009$  (wustite : magnetite : haematite). This implies that as the thickness of wustite increases beyond the range of interference for its own thickness then the next thickest layer, magnetite, must increase in thickness until it too reaches a point where its thickness is comparable to the wavelength at which point we expect interference phenomena to show up. Then for a wavelength of  $2\mu\text{m}$  a thickness of haematite of about  $2\mu\text{m}$  should produce oscillations in the graph. This occurs at  $1/0.009 \times 2\mu\text{m}$  of wustite  $\sim 0.22\text{mm}$ . The variation of emissivity with wavelength is clearly seen occurring at  $d_{FeO} = 0.2\text{mm}$  at a wavelength of about  $2\mu\text{m}$ . We notice that

- As the wavelength is increased beyond this interference region, and the oscillations die out, the emissivity decreases with wavelength in much the same way as the one-layer model except that it is larger. This is due to the fact that the refractive index of haematite, magnetite and wustite combine to decrease the conductivities which increases the corresponding emissivity. Compare this with section (3.3.2) where it was shown that the emissivity observed at smaller wavelengths (IR) is that of the oxide not of steel. This increase is due to the refractive index of the oxide. This is a similar result except the the higher emissivity is due to the combined effects of all layers, not the least of which is haematite which is responsible for interference effects.
- Note that, as the wavelength is increased, the two models converge. This happens

as the wavelength starts to penetrate the outer two oxides and eventually ‘sees’ only wustite.

As a conclusion we have

1. The highest contribution to emissivity arises from the particular layer whose thickness is comparable to the wavelength used in the measurement.
2. The three-layer model ( $FeO : Fe_3O_4 : Fe_2O_3$ ) may be reduced to a one-layer model of  $FeO$  only provided that the measurement wavelength is much longer than the thickness of both magnetite and haematite.
3. For temperatures greater than  $570^\circ\text{C}$  all three layers of oxide exist. Therefore in general we must use the three-layer model rather than just a one-layer model. However below this temperature the prevalent oxide is magnetite and we may use it as a single-layer model.

### 4.3.3 Emissivity Change with Thickness

Observe Figures 4.3.5-4.3.8 and Figures 4.3.11 and 4.3.12. These graphs display the change of emissivity with thickness of (equivalent) wustite at  $1000^\circ\text{C}$  for

1. different wavelengths Fig 4.3.5, 4.3.6, 4.3.11, 4.3.12
2. different temperatures Fig 4.3.7, 4.3.8

In each case the left most graphs are the single-layer model of wustite only and the corresponding three-layer model is on the right hand side.

**Figures 4.3.5, 4.3.6,  $T = 1000^\circ\text{C}$ ,  $\lambda : 0.1 - 0.8\mu\text{m}$ ,  $d : 0 - 1\mu\text{m}$**

We see immediately that

- For the wavelengths and ranges of thicknesses chosen in either model little differences are obvious. Careful observation reveals slightly larger emissivity values for

the three-layer case. This is expected because of the extra addition of the other oxides, magnetite and haematite. For interference phenomena to show up we must consider much larger thickness ranges. We do see interference effects present as oscillations about a mean curve for a wavelength of  $0.1\mu\text{m}$ . Notice the similarity to Figures 2.2.1-2.2.4 as typical experimental results. Interference also occurs for the larger wavelengths  $0.2\text{-}0.6\mu\text{m}$  at a thickness of about  $0.5\mu\text{m}$ . The difference is that the interference is of a much larger variation than that of the case for  $\lambda = 0.1\mu\text{m}$ . The amplitudes of oscillation are very small for  $\lambda = 0.1\mu\text{m}$  whereas for  $\lambda = 0.2$  and  $0.6\mu\text{m}$  they are quite prolonged and larger in height. This must be so because of the small wavelength involved. The amplitude is then governed mainly by the refractive index so that oscillations must occur about the mean emissivity curve rather than causing large fluctuations which occur at longer wavelengths.

- Notice that the longer wavelengths,  $6$  and  $8\mu\text{m}$  do not oscillate as much as the smaller ones. This is expected as soon as the wavelength range starts to exceed the interference region where both thickness and wavelength must be of the same order. We wish to avoid this interference region in measurement so that a reliable measurement may be made.
- The emissivities of each curve decreases as the wavelength is increased, eg for  $\lambda = 0.1\mu\text{m}$  the emissivity is close to one whereas for  $\lambda = 0.8\mu\text{m}$  it is closer to  $0.7$ . Once again this implies longer wavelengths may ‘see’ through layers of Scale.

**Figures 4.3.7, 4.3.8,  $\lambda = 0.4\mu\text{m}$ ,  $T : 800 - 1200^\circ\text{C}$ ,  $d : 0 - 10\mu\text{m}$**

For both single and multi-layer models the usual interference oscillations are noticed. Similarly, the increase from the emissivity of iron at zero thickness is rapid reaching the emissivity of iron-oxide, which is close to  $1$ . However, there is a marked difference between the two models as we vary the temperatures from  $800\text{-}1200^\circ\text{C}$ . Now, since the conductivity

of the oxides increases with increase in temperature so does the reflectivity which means the emissivity must decrease. This is observed in the three-layer case but not for the one-layer model. This reduction in emissivity is most prominent at the highest temperature 1200°C. The decrease as a comparison with the highest and lowest emissivities in Figure 4.3.8 is a jump in emissivity of  $\Delta\epsilon \simeq 0.1$ . This difference between the two models must be due to either magnetite or haematite since the influence of wustite is recorded in Figure 4.3.7, with no such a jump occurring. Most likely this is due to haematite since its conductivity increases at a much faster rate than does magnetite. At a thickness of 10 $\mu\text{m}$  haematite has a thickness of 0.09 $\mu\text{m}$  but a conductivity of close to  $10^7\Omega^{-1}\text{m}^{-1}$  which is 100 times that of either wustite or magnetite.

**Figures 4.3.11, 4.3.12,  $T = 1000^\circ\text{C}$ ,  $\lambda : 0.2 - 16\mu\text{m}$ ,  $d : 0 - 20\mu\text{m}$**

These two diagrams represent the large Scale thickness variation. The one-layer case reaches the emissivity of wustite and stays constant over the whole thickness range at each wavelength. The longer the wavelength the smaller the emissivity of course. However, the three-layer model deviates from the one-layer case by a significant reduction in emissivities as the wavelength is increased. At small wavelengths  $\epsilon$  remains constant close to one. But at wavelengths  $> 4\mu\text{m}$  there is gradual decrease in emissivity as thickness is increased. This decrease takes place immediately after the oscillations cease. Since the temperature is constant this decrease is due to the ratio  $d/\lambda$  where the thickness  $d$  represents the thickness not only of wustite but magnetite and haematite. Now, since this ratio is present in the term  $e^{-\frac{4\eta d\pi}{\lambda}}$  for wustite this term has already acted over the thickness range above, and is no longer influential in changing the emissivity, it has already reached zero for smaller thicknesses. For the other oxides this term diminishes the emissivity as the ratio  $d/\lambda$  increases until it too no longer effects proceedings. This is the cause of the decrease in emissivity. Notice too, the levelling off occurring in Figure 4.3.12 at longer thicknesses.

#### 4.3.4 Emissivity Change with Wavelength

This area of investigation includes Figures 4.3.3, 4.3.4 and Figures 4.2.9 and 4.2.10. The first group contain graphs for different oxide thicknesses and the second graphs of varying temperature. Both single and multi-layer models are involved.

**Figures 4.3.3, 4.3.4,  $T = 1000^\circ\text{C}$ ,  $d = 0 - 0.8\mu\text{m}$ ,  $\lambda : 0.1 - 10\mu\text{m}$**

Each graph contains the numerical solution for thicknesses  $d = 0, d = 0.4\mu\text{m}$  and  $0.8\mu\text{m}$ . A careful study of each graph shows the inevitable slightly larger emissivity values for the three-layer model over the one-layer case. Oscillations occur at small wavelengths and comparable thicknesses, notably the graph of  $d = 0.8\mu\text{m}$  at a thickness of about  $\lambda \simeq 0.6\mu\text{m}$ . The oscillations almost disappear at  $d = 1.0\mu\text{m}$ . The  $d = 0$  or unoxidised case is included as a comparison.

We notice the following :

- The most striking feature is that, given a long enough wavelength, each of the graphs asymptotes to the flat case. This is especially noticeable for the  $d = 0.8\mu\text{m}$  graph. This effect for long wavelengths shows that radiometers whose wavelength lies in the millimetre and centimetre range can approximately measure the temperature of clean steel even if it has been oxidised. The longer wavelengths penetrate straight through the outer oxide layers and reproduce the emissivity of clean steel at that wavelength. Notice however that these readings are very low, of the order 0.02. This implies the radiometer needs to be very sensitive in order to obtain a reliable measurement and not be drowned out by environmental noise.
- We also see that the clean steel case,  $d = 0$ , is only reached at very long wavelengths whereas a wide separation is noticed for the larger thicknesses. This again demonstrates the large difference in emissivity for Scaled and clean steel. This implies pyrometers must measure the emissivity of oxide, not steel.



- We also recognise the fact that wavelength variation occurs via the rule

$$\epsilon \propto \frac{1}{\sqrt{\lambda}}$$

**Figures 4.3.9, 4.3.10,  $d = 0.4\mu\text{m}$ ,  $T : 800 - 1200^\circ\text{C}$ ,  $\lambda : 0.1 - 10\mu\text{m}$**

Other than previously mentioned results, the only notable exception in these graphs is that the emissivity increases with temperature slightly. For the three-layer model the variation between each reading is spread over a wider emissivity range. No doubt this is due to the influence of other oxide layers as already discussed.

Compare these results with those of Figures 2.2.5, 2.2.8 and 2.2.10. The experimental trends agree well with the numerical simulation.

#### 4.3.5 Emissivity Variation with Temperature

These diagrams include Figures 4.3.13-4.3.16. Again both models are represented. In each case the emissivity variation with temperature is described for both different wavelengths and thicknesses.

**Figures 4.3.13, 4.3.14,  $\lambda = 0.4\mu\text{m}$ ,  $d : 0 - 0.8\mu\text{m}$ ,  $T : 800 - 1300^\circ\text{C}$**

We obtain two basic results :

- For the one-layer model there is a slight increase in emissivity with temperature. For the clean steel case this is expected from theory, see section (3.3.1) for a discussion. The conductivity of iron decreases with temperature increase therefore decreasing the reflectivity and thus increasing the emissivity, if only slightly. This gradual increase is expected since at these temperature ranges conductivity decrease is only very slight. Of course, the thicker the oxide the higher the emissivity. This trend in temperature increase seems to be maintained for the one-layer model even in the presence of wustite. This may be explained by the fact that wustite's conductivity changes little (over this temperature range) as does that of magnetite.

- Comparison of the two models shows the drastic change in the graphical results as we reach temperatures in excess of  $1100^{\circ}\text{C}$ . Beyond this point the emissivity sharply declines for thicknesses  $> 0.2\mu\text{m}$ . This result must be due to the very high conductivity of haematite at higher temperatures. As the thickness increases and the temperatures reach large values the conductivity of haematite increases as high as  $10^6$  or  $10^7\Omega^{-1}\text{m}^{-1}$ . We expect a sharp decline at such temperatures. Below these thicknesses there is not enough haematite present to effect any noticeable change.

**Figures 4.3.15, 4.3.16,  $d = 0.4\mu\text{m}$ ,  $\lambda : 2 - 10\mu\text{m}$ ,  $T : 800 - 1300^{\circ}\text{C}$**

As for the previous data the one-layer case has a gradual increase with temperature at different wavelengths. However the three-layer model shows most unusual behaviour. First, there is an increase in emissivity followed by a levelling out and a decrease. A comparison with Figures 2.2.6, 2.2.7 and 2.2.9 shows both of these trends. They show the emissivity increase for clean metal surfaces, as expected, and the emissivity decrease for oxidised ones. As well, they show this rise and fall behaviour, see Figure 2.2.7. Once again, this variation must be due to the extra oxide layers magnetite and haematite. It is also seen that smaller wavelengths do not possess this behaviour, but only seem to remain steady and then start to decrease at higher temperatures as expected. The larger wavelengths give rise to this extra increase. Certainly, the decrease is due to haematite conductivity. The initial increase must arise from the larger wavelengths. This effect must be due to a combination of both temperature and wavelength. It may be a complicated interaction with temperature and wavelength, possibly a kind of interference due to both of them.

### 4.3.6 Final Conclusions for the Smooth Case

#### General Conclusions

1. If the measurement wavelength is larger than the thickness of wustite, that is, larger than all oxides, then the three-layer model approximates to the one-layer case.

2. If the wavelength of measurement is much larger than the combined thicknesses of all oxides then the emissivity will be nearly that of pure steel.
3. If either of the above two conditions are not satisfied the complete three-layer model must be used.

In the introduction the additional variables : absorption, three layers of oxide and semi-conducting properties of each oxide were discussed. It is found that each of these three additions is a worthwhile extension of previous investigations, with absorption properties accounting for extra features such as decrease in emissivity oscillations and decrease in emissivity for multi-layer models. The three-layer model presents us with extra behaviour such as unusual temperature variation, interference at large oxide thicknesses and emissivity decrease with temperature. The semiconducting properties of the oxides induced the sharp temperature decreases and the interaction phenomena between temperature and wavelength.



## Part III

# The Optical Problem-Irregular Surfaces



## Chapter 5

# Rough Surfaces

### 5.1 Introduction

There are several important areas of consideration when discussing rough surfaces. The first section of this chapter discusses what surfaces are rough, what makes them rough, and why is this an important contributor in temperature measurement in industry. Next, we consider what sort of rough surfaces are possible and how to characterise them. All of these sections are necessary for an understanding of the industrial problem.

We next analyse the techniques that have been used to study rough surface scattering and where they are applicable. Also included, is a section on two areas of scattering not often considered : multiple scattering and surface shadowing. A most important area of consideration is : which parts of a rough surface contribute the most to the scattered field. It is shown that only a small section of the illuminated area of the surface needs to be considered.

We also give a detailed review of theoretical and experimental research to highlight the main emissivity characteristics and those areas not yet explained by theory. The theories used in research are mentioned with detailed reviews already available elsewhere, these are given where appropriate.

## 5.2 The Nature of Rough Surfaces

Previously we were concerned with the scattering of radiation off plane or optically smooth surfaces. As is well known, all of the incident radiation is scattered in the specular direction. However, real surfaces are never smooth and flat, but are, what is generally called ‘rough’.

If this is the case why does one study the plane case at all? The answer to this question lies in the fact that not only are some surfaces flat in the usual sense, for example polished metal, but a surface ‘looks’ smooth when observed at certain frequencies of light. For example, unpolished sheet metal is smooth with regard to radio waves but rough in the case of ordinary visible light, [8]. Similarly, the glare perceived from a road surface may be observed at sunset but not at noon. So, in some cases a surface can be regarded as smooth and essentially flat. If this is the case then the investigation of plane surface scattering is of great importance.

For our present case we are given steel sheets that are hot rolled, and as such, we are presented with several different types of surface roughness :

- (i) The induced roughness due to the shape of the roller itself, this imbues the surface with large scale undulations.
- (ii) Small scale roughness due to the steel surface crystalline structure and environmental conditions at the time of cooling, that is, all surfaces are rough unless polished or smoothed in some way.
- (iii) Lastly, small scale roughness present on either smooth or rough steel surfaces due to the processes of oxidation, sulphurisation or other reaction mechanisms occurring in industry. This type of roughness may be of a different scale to that of (ii).

A more accurate definition of surface roughness will now be considered.



### 5.3 The Rayleigh Criterion

We are interested in the question of when is a seemingly smooth surface rough ? The simplest approach to this problem was studied by Rayleigh in 1877 and is still used today because of its relative simplicity.

Consider a plane monochromatic electromagnetic wave incident upon a rough surface at an incident angle  $\theta_1$  and scattered at an angle  $\theta_2$  from two points on the surface in the  $(x, z)$  plane of incidence as shown in Figure 5.3.1

Figure 5.3.1 Phase changes for a wave incident upon a rough surface, [57]

The phase difference between the two scattered rays is given by, [57] :

$$\Delta\phi = k[(h_1 - h_2)(\cos\theta_1 + \cos\theta_2) + (x_2 - x_1)(\sin\theta_1 - \sin\theta_2)] \quad (5.1)$$

where  $k_1 = k_2 = |\mathbf{k}| = k$ , the wavenumber of the incident and scattered waves,  $x_1$  and  $x_2$  are the  $x$ -coordinates of the scattering points of height  $h_1 = h(x_1)$  and  $h_2 = h(x_2)$

respectively, where the surface is represented by the function  $h = h(x)$  measured from the mean plane defined by  $z = 0$ .

For specular scattering,  $\theta_1 = \theta_2$ , the phase difference becomes

$$\Delta\phi = \frac{4\pi}{\lambda} \Delta h \cos \theta_1 \quad (5.2)$$

where  $\Delta h = h_1 - h_2$ . Two obvious cases for the phase difference exist

- $\Delta\phi = \pi$  or  $\Delta\phi \sim \pi$
- $\Delta\phi \ll \pi$  or  $\Delta\phi \sim 0$

The first case is when the two waves are  $\pi$  out of phase and interfere destructively thereby producing no energy flow in the specular direction, instead it is redistributed into other directions. Therefore the surface is rough for  $\Delta\phi \sim \pi$ . For the second case, if the phase difference between the waves is negligible then they will constructively interfere directing most of the scattered energy in the specular direction. Therefore when  $\Delta\phi \sim 0$  the surface can be considered smooth as in the flat case.

We observe that a surface is smooth only when either

- $\frac{\Delta h}{\lambda} \sim 0$
- $\theta_1 \sim \frac{\pi}{2}$

So a surface is smooth for either very large wavelengths, eg. radio waves on a rough steel surface, or small surface undulations, eg. polished steel surface. It is also smooth if the angle of incidence is close to  $\pi/2$  or the wave impinges at grazing incidence, eg road glare. Similarly a surface is considered rough if

$$\frac{4}{\lambda} \Delta h \cos \theta_1 \simeq 1 \quad (5.3)$$

that is, if the incident wavelength is small or the angle of incidence is close to the surface normal, [57]. Therefore, one cannot state the degree of roughness without reference to the radiation being scattered, [57]. So the scale of roughness is then determined, in the main,

by a ratio of the form  $\Delta h/\lambda$ . This ratio is often replaced by  $\sigma/\lambda$  where  $\sigma$  is the root mean square deviation of the surface height from the smooth. The importance of this parameter will be made clear, presently.

Note that the dividing line between rough and smooth surfaces is often stated as  $\Delta\phi < \pi/2$  which is chosen somewhat arbitrarily, the above approach is certainly clearer.

## 5.4 Scattering Characteristics of Rough Surfaces

Consider the two cases

- (i) Smooth surface having  $\Delta h = 0$  everywhere
- (ii) Non-smooth surface with  $\Delta h \neq 0$  generally

For (i) we find from (5.1), above, that the phase becomes

$$\Delta\phi = \frac{2\pi}{\lambda}(x_2 - x_1)(\sin\theta_1 - \sin\theta_2) \quad (5.4)$$

smooth surfaces in the specular direction produce  $\Delta\phi = 0$  giving a strong specularly scattered field. However for  $\theta_1 \neq \theta_2$  we find the phase difference is large since the surface dimensions are large and generally  $x_1 - x_2 \gg \lambda/2$  producing destructive interference and no scattered energy. This implies that an infinite smooth surface scatters energy only in the specular direction.

If the maximum size of the surface is restricted to a length of  $2L$  then the largest separation in scattering points gives a phase difference of

$$\Delta\phi = \frac{4\pi L}{\lambda}(\sin\theta_1 - \sin\theta_2) \quad (5.5)$$

then strong scattering can occur depending on the dimensions of the surface and the incident wavelength. This scattering will of course occur mainly about the specular direction since the dimensions of scatterers are often much larger than the incident wavelength.

Now for (ii), in the specular direction, the phase difference is given by (5.1) if this is much less than  $\pi$  then the surface appears smooth. If however the phase becomes comparable to  $\pi$ , cancellation and much less incident radiation is scattered in the specular direction and more is directed in the remaining directions.

For non-specular scattering of (ii) we no longer have a smooth surface, ( $h_1 = h_2$ ), and the phase is generally determined by the height undulations across the surface.

Figure 5.4.1 Polar plots showing the scattered intensity of the incident field for : (a) A plane surface, strong coherent field, (b) Slightly rough surface, some diffuse scattering,

(c) Very rough surface, strong diffuse scattering, [57].

Generally the energy scattered in the specular direction as mentioned above, in (i), has a strong ‘lobe’ (of energy) in this direction, it is often called the coherent wave as shown in Figure 5.4.1. This field is usually calculated as an average over the phase of the scattered wave. Similarly, the strongly scattered wave having almost no direct phase relationship to the incident wave is called the incoherent or diffuse wave. This field must be calculated by averaging the intensity, [57].

The different cases of scattered energy distribution over scattering angles  $\theta_S$  is shown, Figure 5.4.1. For further analysis of the coherent and diffuse fields and their phases refer to Beckmann & Spizzichino, [8] or Bass & Fuks, [6].

## 5.5 Rough Surface Types

Rough surfaces, that is, surfaces which deviate in their height from a mean plane can usually be classified into three separate cases :

- (i) Those surfaces whose height distribution from the mean is known, for example surfaces whose height is a known function of the variables,  $\zeta = \zeta(x, y)$ , where  $\zeta$  is a function representing the surface in the usual  $(x, y, z)$  coordinate system. Note that many coordinate systems are possible including cylindrical coordinates and coordinates fitted to the surface. A typical example would be a periodic function or one generated as a Fourier series of periodic functions.
- (ii) Random rough surfaces, meaning those surfaces where the height distribution (from the mean plane)  $\zeta = \zeta(x, y)$  is an unknown function of the random variable  $\zeta(x, y)$  at each point  $(x, y)$ . The distribution of surface heights is then given in terms of a height probability distribution (often assumed Gaussian). Note that several types of these surfaces exist including those generated by stochastic processes and those made up of a planar array of objects. the random process may be continuous or

discrete. For a fuller discussion see, [8].

- (iii) Surfaces whose structure is described in terms of Fractals, or surfaces having structure on all scales, and whose dimension is not necessarily an integer. For example fractal surfaces may have a dimensionality between 1 and 2. These surfaces cannot be described statistically as those in (ii). Many natural surfaces may be considered fractal for example the growth of oxidation films on metals, [53].

## 5.6 Rough Surface Statistics

Rough surfaces are often described in terms of the deviation of the surface heights from some mean plane or reference surface. As already mentioned the height variations from the mean are expressed as a height probability distribution  $p(\zeta)$  where this is the probability of any point of the surface being located at some height  $\zeta$  away from the mean surface. Generally the average height is then zero.

An important parameter derived from the above definition is that of root mean square height of the surface which is the standard deviation usually written  $\sigma$ .

Many other parameters exist to define the roughness characteristics, but probably the most important of them is the surface correlation function. This is required to assist in describing the change of a random function over different length scales, [57]. It is often assumed Gaussian as follows :

$$C(R) = e^{-\frac{R^2}{\lambda_0}} \quad (5.6)$$

where  $\lambda_0$  is the well known correlation length relating the rate of change of surface height with distance along the surface, [57].

For a full discussion of rough surface statistics refer to Ogilvy, [57], Bass & Fuks, [8] or Beckmann & Spizzichino, [6].

In this thesis we will only consider periodic surfaces, that is, surfaces of the type where

the surface undulation,  $\zeta$ , away from the the mean is described by

$$\zeta = A \sin Kx \quad (5.7)$$

where  $A$  is the amplitude, related to  $\sigma$  and  $K = 2\pi/T$ ,  $T$  the period of surface peaks or troughs, with  $A/T$  being related to  $\lambda_0$ . These two parameters  $A$  and  $A/T$  describe the roughness of a sinusoidal surface. The amplitude is the maximum variation away from the mean and  $A/T$  the gradient of surface slopes.

## 5.7 Physical and Geometrical Optics

We are interested in solving the problem of the scattering of electromagnetic waves from a rough surface. This is an optical problem and can be attacked in two fundamental ways via Geometrical Optics or as a problem in Physical Optics.

### 5.7.1 Geometrical Optics

When studying the interaction of electromagnetic radiation with objects or surfaces it is often valid to neglect the wave nature of light and deal with the propagation of the radiation in terms of light rays. This is known as geometrical optics and corresponds to the limiting case of  $\lambda \rightarrow 0$  (wavelength of light). Obviously then optical laws may be constructed via the laws of geometry, [13].

This is only possible if the dimensions of the scatterer are much larger than the wavelength of light used in the scattering experiment. This may at first seem irrelevant to our problem, but if, in fact, the ratio  $\sigma/\lambda$ , the RMS surface height, compared with the wavelength of incident radiation is large enough, geometrical optics can be applied. This ratio is analogous to our  $A/\lambda$  which will be the critical parameter for rough surfaces in this thesis. Additionally, even though most scattering problems are analysed using the theory of diffraction, in some cases certain approximations from geometrical optics are used, eg Kirchhoff boundary conditions on a rough surface. This last point forms the starting point

for the solution of the scattering problem in this thesis.

Note that it is possible to extend the theory of geometrical optics to include the effects of diffraction and this is called the Geometrical Theory of Diffraction, [45].

### 5.7.2 Physical Optics and Diffraction

A more precise treatment of the optical problem when the dimensions of the scatterer become comparable to the wavelength of light is that of physical optics, [40]. In this case the wave nature of light is the dominant characteristic guiding the solution of the problem. The laws of geometrical optics are no longer valid because they ignore the significance of the wave nature of electromagnetic radiation.

So, the case where the ratio  $\sigma/\lambda \sim 1$  or  $\sigma/\lambda < 1$  is of concern in the present problem. Note that physical optics is not specifically restricted to small ratios of  $\sigma/\lambda$  but in fact covers the spectrum from large values to fairly small. We will refer to the ratio  $\sigma/\lambda$  as the optical roughness of the surface from now on. Generally the case where the optical roughness of an object approaches one, deals with the area of physics known as the diffraction of light. This treatment requires analysis of Maxwell's equations in detail and usually leads to the solution of the problem at hand in terms of some wave equation. Generally the equations of electromagnetics are vector equations relating the electric and magnetic fields to each other in some region of interest. As such, two theories of diffraction exist, one is the Vector Theory of Diffraction which is a rigorous theory treating the problem as a boundary value problem of electromagnetic field scattering. Difficulties in the solution in this manner usually lead to the simplified treatment of the general problem in terms of the Scalar Theory of Diffraction, the use of which is made in this thesis. It is important to note that this theory ignores the vector nature of electromagnetic fields and so neglects the effects of polarisation which can be significant.



## 5.8 Fresnel and Fraunhofer Diffraction

When an object scatters (diffracts) EM waves, we are interested in the scattered image either close to the object, which allows us to observe how the wave scatters near the scattering point, or far from the object, essentially at an infinite distance (as compared to the dimension of the scattering obstacles). The first case is called Fresnel diffraction and the second is Fraunhofer diffraction. To make this distinction more precise consider that the object under consideration is illuminated by a EM wave emitted from some point source  $S$  considered to be very far from the object. Similarly the point of observation of the scattered radiation,  $P$  is also very distant so that the wave at the points  $S$  and  $P$  ‘approach being planar over the extent of the diffracting obstacles’, [40]. The dividing line between Fresnel and Fraunhofer diffraction is given by the phase

$$\frac{kL^2}{R} \lessgtr \frac{\pi}{4} \quad (5.8)$$

Where Fresnel diffraction is the greater than case and Fraunhofer the less than one, [45], and  $k = 2\pi/\lambda$  is the wavenumber of the incident wave,  $L$  the maximum dimension of the scatterer, and  $R$ , the distance of the scatterer to the observation point  $P$ . A closer analysis of this condition will be given when required.

## 5.9 Multiple Scattering and Surface Shadowing

Two effects not often considered in most scattering theories are the phenomena of multiple scattering and surface self-shadowing. The first of these simply refers to the possibility that for relatively deep surface cavities radiation can reflect more than once. For small irregularity heights relative to the wavelength only small distortions are noticed in the scattered field, [6]. If however, the surface gradients are no longer small, which may happen if either  $\sigma$  increases or  $\lambda_0$  decreases, [57], the incident radiation may be momentarily ‘trapped’ inside the cavity and thus considerably alter the final scattered field. First, by

extra absorption at each scattering point, and second, by a further randomisation of the scattered field. This may also happen when the angles of incidence increase away from the normal.

Surface self shadowing is caused by the surface itself shading other parts of itself. This can happen in three ways : either parts of the surface will be in total shadow others will be illuminated fully or with the inclusion of diffraction effects, regions of semi-shadow can exist, [57]. Obviously, those parts in shadow will not give rise to a reflected field and will not contribute to the overall scattered field, [8]. It is known that the scattered field is drastically altered for large angles of incidence, [8]. It is standard practice to modify the various theories by the inclusion of a shadowing function based on the assertion of Brekhovskikh, [17], that the integration over the surface be carried over the entire illuminated surface removing the shadowed parts. This has, to some degree, been successful, except when dealing with semi-shadowing encountered when  $\sigma/\lambda \sim 1$ , in which case it is very difficult to construct such functions, [57].

These effects are complicated but may be of consequence especially near grazing incidence. Since we are restricted to mainly normal incidence in industry we will not consider these two phenomena in this thesis. Generally they may not be ignored however.

## 5.10 Influence of Scattering Regions

In order to analyse the scattering of EM radiation from rough surfaces we are also interested in which region of the surface contributes the most to the scattered field at some point of observation  $B$ . An analysis of this problem is carried out by Beckmann & Spizzichino, [8]. Consider the following diagram, Figure 5.10.1, where a scattering object with mean plane  $z = 0$  is illuminated by a source located at  $A(0, 0, h_1)$ . The surface generates scattered radiation which arrives at the observation point  $B(x, 0, h_2)$ . Those points whose contribution produce scattered radiation of constant phase difference  $\delta$  at  $B$  are the ones

which make the most significant contribution to the scattered field. Following Beckmann & Spizzichino, [8], this occurs when

$$\delta = R_1 + R_2 - R \quad (5.9)$$

is a constant. If now we increase the phase in steps of  $\lambda/2$  ie

$$\delta = \frac{n\lambda}{2} \quad (5.10)$$

Figure 5.10.1 Fresnel zones producing radiation of constant phase at the observation point  $B(x, 0, h_2)$  [8]

then we produce a series of zones in the  $(x, y)$  plane each bounded by an ellipse determined by (5.9). We find that for each successive zone its contribution is reduced away from the scattering point. Therefore the region contributing the most to the scattered field at  $B$  are the first few Fresnel zones defined by (5.10) above.

This means that the region of interest in scattering lies within a small distance of the scattering point (usually the first Fresnel zone,  $n = 1$ ) and that when considering the

solution to the scattering problem, which is often carried out by integration of a scattering integral, only a small range of integration limits are required for an accurate solution. For example, a scatterer of maximum dimensions,  $L - (-L)$ , does not require an integration over the whole domain  $[-L, L]$  but simply over the distances  $[-l, l]$ ,  $l$  being a fraction of  $L$  determined by the first Fresnel zone (5.10). This simplification aids in the computation time of the integral without significantly reducing the accuracy of the result. This is an important point and will be implemented in the solution of the problem at hand later on. N.B. for cases where only parts of the surface are rough or where the surface does not enclose the first Fresnel zone the entire domain of integration is required in the solution, [8].

## 5.11 The Emissivity of Rough Surfaces - A Review to Date

The problem of this thesis is that of determining the influence of several parameters deemed to be of importance in the study of the surface emissivity of steel surfaces in industry in order to accurately measure the temperature of steel. As has already been stated, they are : the wavelength of EM radiation used in the measurement, the thickness and roughness of oxide layers on the steel and the influence of temperature on the emissivity. This means that we must deal with two problems, the first, that of scattering of radiation from rough unoxidised steel surfaces, and the second, that of rough oxidised steel surfaces. In the first case we are restricted to testing the influence of roughness, wavelength and temperature, whereas in the second case we test the influence of roughness, film thickness, wavelength and temperature. It is important to stress that both problems are worth study since both may be treated in isolation. For a concrete understanding of surface scattering the first must be comprehended before the second may be properly understood.

Similarly, for each problem, previous research to date can be categorised into work dealing with experimental (industrial, empirical results) and theoretical work attempting to verify, and, most importantly, get a physical ‘feel’ for the problem considered. In most cases

little direct research exists into the emissivity problem, both experimental and theoretical, as such most research material looks at the rough surface scattering problem for which a good deal of experimental work and a vast quantity of theoretical research exists.

As already expounded in the introduction to the first part of this thesis three types of surface characteristics influence the emissivity of metallic surfaces. We are presently interested in the Topographical characteristics.

It is considered that the most important influence on the emissivity is the surface roughness and the growth of oxide films on the surface, especially when the surface profile variations and film thickness are of the same order as the wavelength of measurement radiation, [89]. It is also apparent that film thickness has a greater influence on spectral radiative properties than does surface roughness of the same dimension [89], this is unexpected since one would assume surface roughness would overwhelm any film interference effects given a large enough optical roughness.

In order to clarify the aspects of scattering theory we will qualify the various kinds of surfaces into two types. Making use of the optical roughness ratio, [68].

- when  $\sigma/\lambda > 1$  then the reflective behaviour is determined by geometrical optics
- when  $\sigma/\lambda \ll 1$  the reflective properties are governed by diffraction

In fact, other researchers give an approximate upper limit to the diffraction range as  $\sigma/\lambda \simeq 0.15$ , [89], beyond this limit surface topography must be considered, [65].

### 5.11.1 Optical Roughness ratios $\sigma/\lambda > 1$

In this case, geometrical optics reigns and each of the rough surface facets act as small mirrors reflecting light in various directions. When a ray strikes one of the pits of the surface it may reflect more than once leading to multiple scattering of light. It is obvious that each time the ray hits the surface it is partially absorbed, and since Kirchhoff's law states  $\epsilon = a$ , then the surface emissivity of a rough surface must be greater than that of a smooth one [72]. Occasionally it is possible to solve the problem for surfaces of a given

profile, for example, the work of Popova, [64], Zipin, [98] and Barrick, [5], produce results in good agreement with experiment. But generally some statistical description must be given, [89], for instance Spetner, [76].

### 5.11.2 Optical Roughness ratios $\sigma/\lambda \ll 1$

For small optical roughness, multiple reflection effects become negligible and diffraction effects dominate. Even though the surface would appear optically smooth, diffraction effects still operate. As such, due to scattering (single scatter), a significant portion of radiation is scattered away from the specular, thereby reducing the reflectivity and thus increasing the emissivity.

Note that, no mention of surface absorption is made which would only add to the increase in emissivity. It should be noted that almost all theoretical research either requires or uses the assumption of perfect conductivity, that is, zero absorption. This is done for simplification of the theory and as a means of extracting closed form solutions rather than just numerical results. All such work must be considered somewhat restricted in nature. So, generally, we expect an increase in emissivity no matter which theory is used to analyse the diffraction problem.

N.B. the use of the roughness ratio as a measure of the influence of the roughness of the surface on the scattering of radiation seems to be the most useful parameter, however it should be noted that it is only one of many such parameters and is by no means the only necessary parameter for such a description. For example, Smith & Hering, [74], note that the optical roughness parameter is inadequate to describe all surface roughness effects and the additional variable of RMS roughness element slope is needed.

Relatively few experimental investigations exist into the problem of rough steel surface emissivity. However, Saint-Jacques et al, [70], conducted experiments on etched steel to study the effect of surface roughness on radiative properties. Their etched surfaces varied approximately periodically with height up to  $1 \mu\text{m}$  and periods of the order of  $0.7 \mu\text{m}$ . It

is found that a rough surface behaves partially like a double layer or thin film on top of a steel substrate. This is supported by other authors who state that a rough surface may be replaced by an equivalent film with plane-parallel boundaries whose thickness is equal to  $\sigma$ , the RMS roughness of the surface, and whose optical characteristics can be obtained from Maxwell Garnett, [50]. It is also found that the emissivity increases with the depth of surface undulations. Typical graphs of reflectance versus wavelength are shown in Figure 5.11.1 and 5.11.2.

Von Esser, [92], notes that the effect of surface roughness is to increase the emissivity greatly as compared to the specular case (also, [86]). As noted already, he states that the effect of roughness and oxide film thickness is far greater than the optical absorption properties of the steel under consideration. He further states that in some cases the error introduced in the determination of surface temperatures is so great that no simple corrective procedures are adequate. Birkebak & Eckart, [11], conducted experimental research into the effects of surface roughness on the reflectivity of metal surfaces, in their case mainly aluminium surfaces. Their surfaces were roughened by using ground glass as a substrate and evaporating the metal (aluminium & nickel). Their results support those of Von Esser and produce graphs akin to those of Saint-Jacques et al, [70]. These are shown in Figure 5.11.3. These results were confirmed in the research of Smith & Hering, [74], with similar graphical data, Figure 5.11.4, which also included comparisons to theoretical models. Good agreement is obtained over a fairly large wavelength range. It is found, as expected from earlier research, that as wavelength increases the rough surface scattering characteristics approach that of a smooth surface. Similarly, as roughness height is decreased the trend is to reflect specularly. Similar trends were noticed in earlier research, [10] or [11].

Often the change in surface emissivity is studied as a sample is slowly oxidised over time at some temperature. Apart from effects generated by oxide film growth, already mentioned in chapter 3, it was found that as the sample oxidises at a given temperature and oxide film thickness increases, so does roughness. Or as Hill et al, [41], puts it ‘ optical

roughness values show the .. trend of increased (emissivity) values with increased time-at-temperature for the samples'. Additionally the radiative characteristics of the surface go from specular to diffuse as the roughness is increased. It is of fundamental importance that the authors state that some of the samples were too rough for the application of scalar diffraction theory. Stressing again that maybe some effects of surface roughness depend on the polarisation changes upon scattering from the surface, [79]. Recent research of Chen, [20], into hot rolled steel point to similar consequences, such as emissivity increase over temperature and roughness. Browne, [19], and Chen, [20], also noticed oscillations in the emissivity at certain wavelengths.

The theoretical analysis of the diffraction problem was studied early on by Rice, [67], Davies, [24], and further modified by, Bennet & Bennet, [9], they obtained an analytic result relating the scattering coefficient or relative reflectance ratio to the surface roughness ratio as follows :

$$\frac{\mathcal{R}_S}{\mathcal{R}_0} = e^{-\left(\frac{4\pi\sigma}{\lambda}\right)^2} + \frac{32\pi^4}{m} \left(\frac{\sigma}{\lambda}\right)^4 (\Delta\theta)^2 \quad (5.11)$$

where  $\mathcal{R}_S$  and  $\mathcal{R}_0$  represent the reflectance, for normal incidence angle, of rough and smooth surfaces respectively,  $\Delta\theta$  is the half angle of the field of view and  $m$  the RMS slope of the surface undulations. The first term is the coherent component of the scattered radiation and the second the diffuse component. Specular reflection dominates at long wavelengths ie  $\sigma/\lambda \sim 0$  (geometrical optics region) since the second term decreases at a faster rate than the coherent term, [10]. When the optical roughness is of the order of one (diffraction region) both terms contribute and it is found that a statistical description of the surface topography is required rather than the simplified treatment of roughness via  $\sigma/\lambda$ . Note, that the surfaces in the above representation were at all times considered to be perfectly conducting, thereby ignoring absorption effects of real materials. Similarly, the effects of shadowing and multiple scattering were not included. As stated earlier, [72], some success in comparison with experimental results was had, although some cases of surface roughness led to poor agreement. The theory also used Gaussian roughness as an approximate representation of rough surfaces and it is known that some surfaces cannot



be estimated in this way at all, eg fractal surfaces, [57].

Beckmann & Spizzichino, [8], have extended the consideration of statistical roughness properties with the use of the correlation length mentioned in section (5.6). Their results produced a more favourable comparison with experiment reproducing emissivity increase at small wavelengths and specular scattering characteristic at long wavelengths.

For cases where geometrical optics is dominant, Zipin, [98], studied the optics of V-grooved surfaces of  $\sigma : 0.05\text{-}5 \mu\text{m}$  in the visible region, including the effects of multiple scattering. He found good agreement with experiment except near grazing incidence, finding the results independent of groove height. Other authors, [64], used an analogous model which also included the effects of surface self shadowing which were absent from all of the theories so far mentioned and concluded that 'the characteristics obtained were in good agreement with existing experimental data'. Torrance & Sparrow, [88], confirmed the results of experimental data, their graphs relating emissivity to angles of incidence at an optical roughness of 2.6 are shown in Figure 5.11.6.

In industry it should be noted that the effects of surface roughness are often treated in an ad hoc manner by assuming the emissivity is higher than that of the specular case and using an approximate value such as  $\epsilon = 0.8$ .

### Summary

Let us summarise the results of experimental and theoretical research, for unoxidised surfaces, so far.

#### (a) Experimental Research

- (i) Roughness is known to significantly raise the emissivity of metal surfaces when compared to a polished or smooth one. The emissivity of rough surfaces is always higher than the equivalent smooth one.

- (ii) Roughness effects are known to be most important when they are comparable to the wavelength of the measurement radiation.
- (iii) A rough surface behaves like an extra layer of material on top of the substrate.
- (iv) A rough surface appears smooth if the wavelength of incident radiation is much greater than the typical dimensions of the scattering elements. Similarly, even for relatively small wavelengths, if the roughness height is very small, the surface has the characteristics of a specularly reflecting one.
- (v) Some evidence of emissivity oscillations exist without requiring an oxide layer.

(b) Theoretical Research

Theoretical research is usually restricted to perfectly conducting surfaces ignoring absorption effects for the sake of simplicity and analytic solubility. This hampers their usefulness, although results in agreement with experiment can still be found.

- (i) Agreement with experiment was confirmed with results (i), (ii) and (iv) above.
- (ii) To the authors knowledge no results indicated the presence of emissivity oscillations on unoxidised surfaces. A result that needs to be demonstrated.
- (iii) Some theoretical results confirm that a rough surface acts much like an extra layer of material on top of the metal substrate.

### 5.11.3 Rough Filmed Surfaces

Steel surfaces are subject to oxidation at high temperatures. This process may alter the shape of the original steel surface as well as adding one or more layers of iron-oxide. These layers are themselves rough, usually to a higher degree than the original unoxidised metal surface. This roughness may be caused by a multitude of factors such as crystal grain boundaries, cavity formation in the oxide layers, contraction and buckling of Scale on cooling, spalling of Scale and surface roughness see Stott, [78], and section (1.4.3) for further information.

Generally, the layers of oxide possess a resistivity (cf conductivity) higher (lower) than iron and so act to some degree as dielectrics even though section (1.4.3) demonstrates their high conductivities at elevated temperatures. This results in them having relatively high emissivities, [72]. Two factors are working to alter the emissivity both the electrical properties of the films themselves which tend to increase the emissivity and the rough surface of the films which has a similar effect. This effect is demonstrated in Figure 5.11.5 and 5.11.7. The increase in emissivity, known to be quite large for the transition from smooth to rough steel, is not as pronounced in the case of dielectrics. Siegel & Howell, [72], state that the increase in emissivity for dielectrics is only slight. This behaviour is noticed for dielectrics and so may be applicable to many oxides. This is certainly the case at low temperatures, below say  $600^{\circ}\text{C}$ . Above this, the conductivity of the iron-oxides increase especially that of  $\text{Fe}_2\text{O}_3$ . Nonetheless, most of the oxides act as semiconducting ceramics. It has been shown that, [48], semiconductors behave as metals with a high resistivity so their behaviour is analogous to the metal case already discussed.

There is not a great deal of theoretical work involving both surface roughness and oxide film thickness. There are however a considerable number analysing the characteristics of rough surface films in different contexts. One of the earliest attacks on the problem of rough surface film optical characteristics was carried out by Eastman, [30], who approximated the film roughness with the use of Beckmann's theory and then used an Airy summation to solve for the scattered field. He also used the scattering matrix approach already employed in section (3.2). He found that the scattering properties of a rough film having identically shaped boundaries, with regard to the substrate and the ambient medium, is determined solely by surface roughness of the substrate and the optical properties of the covering film. For the case of a nonidentical film the spatial separation of the two boundaries determine the scattering characteristics in the main. His results were confirmed experimentally in 'most cases', [30], and any deviations were assumed due to bulk scattering inside the layer. In a series of articles, Ohlidal et al, [58], [59], [60], investigated the problem with the use of Beckmann's formalism in a completely different way to that of Eastman, [30]. He showed

that a relatively small change in optical thickness of the rough film can markedly alter the reflectance. The coherent component of the scattered reflectance (rough case) is always less than that of the reflectance of the smooth case, and for some wavelength regions close to zero. For maximum values of the flat surface reflectance the scattered case is identical. Lutter & Ferencz, [49], using perturbation theory, found that scattering away from the specular could be increased by increasing the substrate temperature which could be identified with an increase in surface roughness. Also, the greatest light intensity near normal incidence was a result not only of volume or rough surface characteristics but also due to interference from ‘cross-correlation’ of the interfaces. In other words the relationship between the shapes of the substrate and ambient boundaries. This is supported by the work of, [31]. In line with previously mentioned results, section (5.11.2), it was shown by other authors, [81], using a Beckmann method with  $\lambda_0 \gg \lambda$ , that a rough surface may be considered smooth but optically inhomogeneous having an effective refractive index depending on a parameter linking both the amplitude and density of the surface roughness. For other techniques where  $\lambda_0 \ll \lambda$  see [91] and [14]. Using second order perturbation theory, Fung, [34], noticed a direct relationship between radiation scattered in non-specular directions and the Fourier spectra of the boundary surfaces of the layer. Multiple scattering was noticed even for small roughness as well as wave depolarisation.

### Summary

In summary the characteristics of rough oxidised surfaces

- (i) Depends only on the optical properties of the film and roughness of the substrate, for identical film/substrate boundary profiles. Whereas for non-identical boundaries the roughness of both boundaries plays a part because of cross-correlation.
- (ii) As for the flat case we expect a rise in emissivity and possibly oscillations due both to interference and roughness.

- (iii) The electrical properties of the film are important, more so than for the unlayered case.
- (iv) Wave depolarisation and multiple scattering occur.

## 5.12 Review of Electromagnetic Scattering Approaches

The solution of the scattering problem above may be achieved with a host of techniques. They are basically divided into integral methods and differential methods. For a derivation of the general scattering problem refer Cho, [21].

### 5.12.1 Differential Methods

In this case we solve the exterior Dirichlet problem directly with the use of Numerical methods such as finite differences or finite element techniques. Currently, numerical methods which solve the Dirichlet problem directly are not used to a great extent in rough surface scattering. Exceptions include the problems dealing with specific shapes such as sphere, cylinders, flat planes and parabolas all of which can be approached with the use of special coordinate systems and often special functions. For a detailed study see, [15]. Other approaches are those of Petit, [62], and Maystre, [51], all of which deal with the scalar diffraction problem for periodic gratings.

### 5.12.2 Integral Methods

These are used extensively for the solution of most rough surface scattering problems. The process is usually to reduce the exterior Dirichlet problem above to either an integral equation problem or an integral representing the problem at hand. Direct solution methods such as the Galerkin method are possible although substitution of approximate solutions are common.

### 5.12.3 Rayleigh Method

The basic principle of the method is to write the scattered field as a sum of outgoing plane waves and then determine the unknown coefficients in the sum with the use of the boundary conditions on the rough surface. For use of the method refer to, [8],[57], [62] for periodically rough surfaces or [47] for a general periodic surface and, [67] for random rough surfaces.

### 5.12.4 Perturbation Theory

Perturbation theory may be invoked when the surface corrugation height function given by  $\zeta(x, y)$  is restricted by the following inequalities,  $k|\zeta(x, y)| \ll 1$  and  $|\nabla\zeta(x, y)| \ll 1$ , in other words the surface undulations at any point are always smaller than the incident wavelength and its surface gradients are small. For a comparison to other theories such as the Rayleigh method see, [23]. For a review refer to, Ogilvy, [57], and Thorsos & Jackson, [85].

### 5.12.5 Integral Equation Methods

Integral equations (IE) which are equivalent to the original diffraction problem, may be constructed for electromagnetic theory and then solved subject to certain boundary conditions. For the scattering problem they are defined as the electric field integral equation (EFIE) and the magnetic field integral equation (MFIE) over the surface,  $S$ , of the scatterer. There are a great many research articles on the use of either of EFIE or MFIE, above, for scattering such as, [57], [22] and for solution methods, [69], [62] and for an in depth analysis of their use, [96]. Most IE methods deal with perfect conductors, [97]. The solution techniques vary widely from iterative methods (eg, [54]), Galerkin methods (eg, [69], [36] also known as the method of moments), Quadrature methods (eg, [85]), Green's function methods (eg, [28]) and Fourier Transform methods (eg, [18]).

### 5.12.6 Variational Methods

It is often possible to replace the problem of integrating a differential equation with the equivalent one of finding a minimum (maximum, saddle point) of some integral, these are called variational methods or the construction of a variational principle. The solution often involves the use of trial fields which are optimised by the stationary principle, or they are substituted into the integral, which is solved up to first-order errors in the trial fields, [57].

### 5.12.7 Other Methods

Various other methods exist to solve both the original exterior Dirichlet problem and facilitate the construction of some integral or integral equation. The most popular of which is the Kirchhoff method which is to be discussed in the next chapter. Other methods relating to the direct solution of the Helmholtz equation include the finite element method and Monte Carlo methods.

For integral-like techniques there exist Spectral methods these types include the methods of, [28], the full-wave method, [4], and the stochastic functional method, [56].

## 5.13 The Purpose of Further Research

We know from the review and the theories above, that further research is required in the explanation of certain physical results such as oscillations in emissivity for unoxidised rough surfaces and a more complete understanding of the role of profile parameters such as average amplitude of corrugations and period of the profile. In addition, virtually all theories address the problem with the assumption of perfect conductivity an assumption certainly not representing the real situation.

We also wish to avoid as much as we can the restrictions imposed by other theories such as small roughness (perturbation theory), convergence problems (Rayleigh theory), long

correlation lengths (IE methods) and poor accuracy (Variational methods).



# Chapter 6

## Kirchhoff Theory

### 6.1 Introduction

The final method dealt with is surely the most popular one in the literature, [57]. The work of Beckmann & Spizzichino, [8], is referred to more than any other. It is this method which will be used in this thesis to construct a solution to the scalar scattering problem. The theory is also known by the terms Physical Optics Theory, Kirchhoff Theory, Tangent Plane Method and occasionally the Helmholtz Representation. Why is Kirchhoff theory so well used, the reasons are many, let us first summarise the assumptions (or simplifications) made in most scattering theories, [8]. :

1. The dimensions of the scattering elements of the rough surface are considered either much smaller or much greater than the wavelength of the incident radiation.
2. The radius of curvature of the scattering elements is much larger than the wavelength of the incident radiation.
3. Surface self-shadowing is neglected.
4. The scattered field is assumed to be in the Fraunhofer zone.
5. Multiple scattering effects are mainly ignored.

6. The theories treat either random rough surfaces or special surfaces, not considering fractal surfaces or investigating each roughness aspect in depth.
7. The density of scattering elements per unit length of surface are not considered.
8. The scatterer is often assumed to be perfectly conducting.
9. The depolarisation of the electromagnetic field upon scattering is not considered.
10. The incident wave is taken as monochromatic and planar.

The most general Kirchhoff theory developed so far makes the simplifications 2, 4, 5, 8 and 9. Kirchhoff theory is mainly used because it has a relatively limited number of assumptions, it has a straightforward physical basis, and it allows, in some cases, analytic solutions to the scattering problem. Most of the previous theories relied on numerical solutions, the analysis of which is difficult. For example, differentiating the effects of multiple scattering on the one hand and the surface roughness in a solution is not easily achieved, when the results, often in graphical form, contain both effects.

This chapter will consider Kirchhoff theory in some detail, its derivation in a rigorous form and the assumptions and criticisms levelled at it. The first section deals with the formulation of the scattering integral. The basis of the method including its satisfaction of the Helmholtz equation and the far-field radiation condition, these making up the fundamental Dirichlet problem. There is a section dealing with the theory's existence and uniqueness which appeals to the physical justification of the theory's basis.

Finally the full theory comprising the formulation of Beckmann, [8], is presented and arrives at the scattering integral which forms the basis for all solutions of the scattering problem both theoretical and numerical. There is also the inclusion of the technique used to determine the emissivity for a rough rather than a smooth surface. This definition is not that used previously, [8], but is closely related.

## 6.2 The Helmholtz Representation

### 6.2.1 The Interior Problem in $R^3$

Before applying the theory directly to the scattering problem let us construct the basis of the theory itself. We will follow the construction of Cho, [21], in the subsequent analysis. First, consider the interior problem in a homogeneous medium  $D_i \subset R^3$  which is enclosed by a smooth surface  $S$ . In  $D_i$  the scalar field  $\phi(\mathbf{r})$ ,  $\mathbf{r} \in D_i$  is assumed to obey the Helmholtz equation

$$\nabla^2 \phi(\mathbf{r}) + k^2 \phi(\mathbf{r}) = 0 \quad (6.1)$$

Similarly, define a Green's function such that it satisfies the differential equation

$$\nabla^2 G(\mathbf{r}, \mathbf{r}_0) + k^2 G(\mathbf{r}, \mathbf{r}_0) = -\delta(\mathbf{r} - \mathbf{r}_0) \quad (6.2)$$

where  $G(\mathbf{r}, \mathbf{r}_0)$  is called the free space Green's function depending on the distance  $\mathbf{r} - \mathbf{r}_0$  as follows

$$G(\mathbf{r}, \mathbf{r}_0) = \frac{e^{ik|\mathbf{r}-\mathbf{r}_0|}}{4\pi|\mathbf{r}-\mathbf{r}_0|} \quad (6.3)$$

where  $\delta(\mathbf{r} - \mathbf{r}_0)$  is the Dirac delta function such that

$$\delta(\mathbf{r} - \mathbf{r}_0) = \begin{cases} 1 & \text{if } \mathbf{r} = \mathbf{r}_0 \\ 0 & \text{if } \mathbf{r} \neq \mathbf{r}_0 \end{cases} \quad (6.4)$$

Now, postulate a vector defined by

$$\mathbf{w}(\mathbf{r}, \mathbf{r}_0) = G(\mathbf{r}, \mathbf{r}_0) \nabla_0 \phi(\mathbf{r}_0) - \phi(\mathbf{r}_0) \nabla_0 G(\mathbf{r}, \mathbf{r}_0) \quad (6.5)$$

Where  $\nabla_0$  refers to  $\nabla(\mathbf{r}_0)$ . Taking the divergence of  $\mathbf{w}(\mathbf{r}, \mathbf{r}_0)$  at  $\mathbf{r}_0$  we get

$$\nabla_0 \cdot \mathbf{w}(\mathbf{r}, \mathbf{r}_0) = \phi(\mathbf{r}_0) \delta(\mathbf{r} - \mathbf{r}_0) \quad (6.6)$$

now, integrate over the region  $D_i$  using the divergence theorem

$$\int_{D_i} \nabla_0 \cdot \mathbf{w} dV = \int_S \mathbf{w} \cdot \hat{\mathbf{n}}_0 dS_0 \quad (6.7)$$

therefore

$$\int_{D_i} \phi(\mathbf{r}_0) \delta(\mathbf{r} - \mathbf{r}_0) dV = \int_S G(\mathbf{r}, \mathbf{r}_0) \nabla_0 \phi(\mathbf{r}_0) - \phi(\mathbf{r}_0) \nabla_0 G(\mathbf{r}, \mathbf{r}_0) \cdot \hat{\mathbf{n}}_0 dS_0 \quad (6.8)$$

where  $\hat{\mathbf{n}}_0$  is the unit vector normal to  $S$  drawn into  $D_i$ , so

$$\phi(\mathbf{r}) = \int_S \phi(\mathbf{r}_0) \frac{\partial G(\mathbf{r}, \mathbf{r}_0)}{\partial n_0} - G(\mathbf{r}, \mathbf{r}_0) \frac{\partial \phi(\mathbf{r}_0)}{\partial n_0} dS_0 \quad (6.9)$$

where  $\partial/\partial n_0 \equiv \hat{\mathbf{n}}_0 \cdot \nabla_0$ . This is of course Green's second theorem also called the Kirchhoff integral.

### 6.2.2 The Exterior Problem in $R^3$

Now construct the exterior problem with the use of the results from (6.2.1). The scalar scattering problem in an exterior region of free space in which a monochromatic plane wave  $E_I(\mathbf{r})$  is incident upon a scatterer with smooth surface  $S$  produces a scattered wave  $E_S(\mathbf{r})$  in the exterior region  $D_e \subset R^3$ . The scattered wave, as well as the incident wave, is assumed to satisfy the scalar Helmholtz equation, ie

$$\nabla^2 E_I(\mathbf{r}) + k^2 E_I(\mathbf{r}) = 0 \quad (6.10)$$

$$\nabla^2 E_S(\mathbf{r}) + k^2 E_S(\mathbf{r}) = 0 \quad (6.11)$$

and the scattered field satisfies the Sommerfeld radiation condition

$$\lim_{r \rightarrow \infty} r \left( \frac{\partial E_S(\mathbf{r})}{\partial r} - ik E_S(\mathbf{r}) \right) = 0 \quad (6.12)$$

To relate this problem to the interior one, enclose the unbounded region  $D_e$  with a spherical surface  $A_s$  having infinite radius, thus presenting us with an interior problem enclosed by the surface  $S$  of the scatterer and  $A_s$ . Note that the surfaces  $S$  and  $A_s$  must both be closed in order to use the divergence theorem, there must be no 'holes' or discontinuities in  $S$  or  $A_s$ . This implies of course that the given formulation does not strictly apply to

scatterers having non-continuous surfaces, for these cases see, [29]. Define  $E(\mathbf{r})$  as the total field in  $D_e$  so that

$$E(\mathbf{r}) = E_I(\mathbf{r}) + E_S(\mathbf{r}) \quad (6.13)$$

We then find that the Kirchhoff integral, (6.9), becomes

$$E(\mathbf{r}) = \int_{S \cup A_s} E(\mathbf{r}_0) \frac{\partial G(\mathbf{r}, \mathbf{r}_0)}{\partial n_0} - G(\mathbf{r}, \mathbf{r}_0) \frac{\partial E(\mathbf{r}_0)}{\partial n_0} dS_0 \quad (6.14)$$

This becomes

$$E(\mathbf{r}) = \int_S E(\mathbf{r}_0) \frac{\partial G(\mathbf{r}, \mathbf{r}_0)}{\partial n_0} - G(\mathbf{r}, \mathbf{r}_0) \frac{\partial E(\mathbf{r}_0)}{\partial n_0} dS_0 + \int_{A_s} E(\mathbf{r}_0) \frac{\partial G(\mathbf{r}, \mathbf{r}_0)}{\partial n_0} - G(\mathbf{r}, \mathbf{r}_0) \frac{\partial E(\mathbf{r}_0)}{\partial n_0} dS_0 \quad (6.15)$$

the second integral can be divided into one for the incident field  $E_I(\mathbf{r})$  and one for the scattered field  $E_S(\mathbf{r})$ , that is

$$\mathcal{I}_I = \int_{A_s} \left[ E_I(\mathbf{r}_0) \frac{\partial G(\mathbf{r}, \mathbf{r}_0)}{\partial n_0} - G(\mathbf{r}, \mathbf{r}_0) \frac{\partial E_I(\mathbf{r}_0)}{\partial n_0} \right] dS_0 \quad (6.16)$$

and

$$\mathcal{I}_S = \int_{A_s} \left[ E_S(\mathbf{r}_0) \frac{\partial G(\mathbf{r}, \mathbf{r}_0)}{\partial n_0} - G(\mathbf{r}, \mathbf{r}_0) \frac{\partial E_S(\mathbf{r}_0)}{\partial n_0} \right] dS_0 \quad (6.17)$$

since the RHS of (6.16) is just an integral representation of the function  $E_I(\mathbf{r})$  at  $\mathbf{r} \in D_e$ , and since the second integral is zero by the radiation condition then

$$\mathcal{I}_I = E_I(\mathbf{r}), \quad \mathcal{I}_S = 0 \quad (6.18)$$

therefore the final integral solution for the scattered field is

$$E_I(\mathbf{r}) + E_S(\mathbf{r}) = E_I(\mathbf{r}) + \int_S E(\mathbf{r}_0) \frac{\partial G(\mathbf{r}, \mathbf{r}_0)}{\partial n_0} - G(\mathbf{r}, \mathbf{r}_0) \frac{\partial E(\mathbf{r}_0)}{\partial n_0} dS_0 \quad (6.19)$$

or

$$E_S(\mathbf{r}) = \int_S E(\mathbf{r}_0) \frac{\partial G(\mathbf{r}, \mathbf{r}_0)}{\partial n_0} - G(\mathbf{r}, \mathbf{r}_0) \frac{\partial E(\mathbf{r}_0)}{\partial n_0} dS_0 \quad (6.20)$$

where  $E(\mathbf{r}_0)$  represents the total field at  $\mathbf{r}_0 \in S$  of the surface of the scatterer. It is straightforward to prove that the above, well known Kirchhoff integral for the scattered field, satisfies the Helmholtz equation and the radiation condition. Satisfying the Helmholtz

equation is easily shown, see, [21] and will not be shown here. The radiation condition is also satisfied. Consider the asymptotic form of (6.12) for  $kr \gg 1$  or  $k|\mathbf{r} - \mathbf{r}_0| \gg 1$ , first the Green's function is expressed in terms of the difference  $|\mathbf{r} - \mathbf{r}_0|$  ie

$$k|\mathbf{r} - \mathbf{r}_0| = k\sqrt{(\mathbf{r} - \mathbf{r}_0) \cdot (\mathbf{r} - \mathbf{r}_0)} \quad (6.21)$$

$$= k\sqrt{r^2 - 2\mathbf{r} \cdot \mathbf{r}_0 + r_0^2} \quad (6.22)$$

$$= k\sqrt{r^2 \left\{ 1 - 2 \left[ \frac{(\hat{\mathbf{r}} \cdot \mathbf{r}_0)}{r} - \frac{1}{2} \left( \frac{r_0}{r} \right)^2 \right] \right\}} \quad (6.23)$$

expanding the square root as a binomial series we get

$$k|\mathbf{r} - \mathbf{r}_0| \sim r - \hat{\mathbf{r}} \cdot \mathbf{r}_0 \quad (6.24)$$

for the asymptotic Green's function when  $r \gg r_0$

$$\lim_{r \rightarrow \infty} G(\mathbf{r}, \mathbf{r}_0) \sim \frac{e^{ikr}}{r} \frac{e^{-ik\hat{\mathbf{r}} \cdot \mathbf{r}_0}}{4\pi} \quad (6.25)$$

and similarly for  $\partial G(\mathbf{r}, \mathbf{r}_0)/\partial n$  we get

$$\lim_{r \rightarrow \infty} \frac{\partial G(\mathbf{r}, \mathbf{r}_0)}{\partial n} \sim \frac{-e^{ikr}}{4\pi} [ik(\hat{\mathbf{r}} \cdot \hat{\mathbf{n}}_0)] e^{-ik\hat{\mathbf{r}} \cdot \mathbf{r}_0} \quad (6.26)$$

since in the Fraunhofer zone  $\hat{\mathbf{r}} \cdot \hat{\mathbf{n}}_0 \approx -1$  then

$$\lim_{r \rightarrow \infty} E_S(\mathbf{r}) \sim -\frac{e^{ikr}}{4\pi r} \int_S \left[ ikE(\mathbf{r}_0) + \frac{\partial E(\mathbf{r}_0)}{\partial n_0} \right] e^{-ik\hat{\mathbf{r}} \cdot \mathbf{r}_0} dS_0 \quad (6.27)$$

and

$$\lim_{r \rightarrow \infty} \frac{\partial E(\mathbf{r}_0)}{\partial n_0} \sim -\frac{e^{ikr}}{4\pi r} ik \int_S \left[ ikE(\mathbf{r}_0) + \frac{\partial E(\mathbf{r}_0)}{\partial n_0} \right] e^{-ik\hat{\mathbf{r}} \cdot \mathbf{r}_0} dS_0 \quad (6.28)$$

finally giving

$$\lim_{r \rightarrow \infty} r \left( \frac{\partial}{\partial r} - ik \right) E_S(\mathbf{r}) = 0 \quad (6.29)$$

which is the Sommerfeld radiation condition. So the above Helmholtz representation for the scattered electric field is a general solution which satisfies both the Helmholtz equation, (6.10), and the radiation condition, (6.12). However as Cho, [21], states with some emphasis there is no assurance that the solution, (6.20), will produce a solution of a specific scattering problem with prescribed boundary conditions.

### 6.2.3 Existence and Uniqueness

The existence and uniqueness of the solution to the exterior scattering problem with Dirichlet or Neumann conditions has been considered for some time. As regards the existence of the solution to the general problem no theorems exist presently which prove this to be the case. However under certain stringent requirements on the boundary conditions existence may be proved, refer, for example to, [3]. It will be assumed forthwith that existence of solution is verified on physical grounds, [51].

Uniqueness on the other hand has been proven under much less severe conditions. It was shown, [66], that for a scattered field in an unbounded, homogeneous medium the Dirichlet or Neumann problem in an exterior region  $D_e \subset R^3$  for the scalar Helmholtz equation, with the Sommerfeld radiation condition and a complex wavenumber  $k$  having  $Im(k) \geq 0$ , there exists at most one scattered field  $E_S(\mathbf{r})$  in  $D_e$ . One consequence of the theorem is that the scattered field (from either the Dirichlet or Neumann problem) decay with distance from the scatterer (ie  $r$ ) inversely at most (ie  $1/r$ ). Any solution decaying faster than this is not a scattered field. Once again this brings to light the possibility that the formulation above will not represent a scattered field. Additionally if the wavenumber  $k$  has components such that  $Im(k) < 0$  then we find that the complex eigenvalues of the Laplacian,  $\nabla^2$ , give rise to a set of complex poles in the wave number intrinsic to the features of the scatterer, [21]. This situation will not be considered here as all wavenumbers are taken as real.

Let us now state the general assumptions made so far in the formulation of the scattering problem

- The Helmholtz integral representation features the so-called Huygens vector  $\mathbf{w}(\mathbf{r}, \mathbf{r}_0)$  this relies on the validity of Huygens principle on the surface of the scatterer.
- The formulation uses the free-space Green's function in  $R^3$  and the fundamental solution of the scalar Helmholtz equation which is not directly related to the actual boundary value problem.

- The solution is formulated without due regard to any boundary conditions that exist on the scatterer, it is only a general solution.

Notice that the incident field is defined everywhere ignoring the presence of the scatterer. It exists on the shadowed side of the scatterer as well as inside it, [21]. Therefore, it is quite reasonable to state that the Kirchhoff formulation may produce results not directly representative of the actual scattered field. In fact, this anomaly in the representation relies very much on the boundary conditions imposed on the problem. Since the formulation was constructed without reliance on some boundary condition (BC), the BC's applied in whatever situation will determine whether the solution represents a 'real' scattered field or not. This reliance on the BC's will be considered again in section (6.3.1). The above mentioned worries are mathematical in nature, however, our problem is a physical one. So, it is important to note that the integral representation, (6.20), and the differential formulation, (6.10), (eg Leontovich BC) be constructed strictly on physical grounds, not mathematical ones, unless they have good physical support. This suggestion is supported by Stamnes, [77], who notes that it is not the choice of the boundary conditions that is worrisome but whether the result at the end is a reasonable one from a physical point of view.

## 6.3 Beckmann's Theory

### 6.3.1 Preliminary Problem Construction

The definition of the scattering problem may be set up using the so called tangent plane approximation, [8]. A plane monochromatic wave travelling in free space (linear, homogeneous, isotropic, sourceless) is incident upon a scattering object (also linear, homogeneous, isotropic, sourceless) having as mean surface the plane  $z = 0$  in an  $(x, y, z)$  coordinate system with origin  $O$ . The scatterer  $S$ , is assumed to be 'rough' in the sense of possessing a



surface irregularity (deviating from the mean plane) defined by the function

$$\zeta = \zeta(x, y) \quad (6.30)$$

As usual, the incident field will be denoted by  $\mathbf{E}_I$  and the scattered field by  $\mathbf{E}_S$ . So, the 'upper' medium, above the scatterer, is defined by  $z > \zeta$ , this being free space with electrical properties as defined in section (1.4). The scattering medium occupies the lower region defined by  $z < \zeta$  and has electrical properties  $\mu, \varepsilon, \sigma$ .

Figure 6.3.1 Geometric construction for the incident and scattered waves at a rough surface.

### Polarisation Characteristics

At all times the incident field will be considered linearly polarised in either the perpendicular (horizontal) or parallel (vertical) direction with regard to the plane of incidence which will be arbitrarily defined as the  $(x, z)$  plane, that is, the plane defined by  $(\mathbf{k}_I, \hat{\mathbf{k}})$  where  $\mathbf{k}_I$  is the wave vector of the incident wave. In other words if  $\mathbf{E}_I$  lies in the plane of incidence,  $(\mathbf{k}_I, \hat{\mathbf{k}})$ , its polarisation will be called parallel ( $\parallel$ ); also if  $\mathbf{E}_S$  lies in the scattering plane  $(\mathbf{k}_S, \hat{\mathbf{k}})$ . Similarly the fields will be called perpendicularly polarised if  $\mathbf{E}_I$  and

$\mathbf{E}_S$  are normal to the incidence and scattering plane respectively. If such is the case we may neglect the polarisation effects by dealing only with each separate polarisation and so consider only the scalar scattering problem.

The scalar scattering problem for the total field  $E(\mathbf{r})$  is then

$$\nabla^2 E(\mathbf{r}) + k^2 E(\mathbf{r}) = 0 \quad (6.31)$$

$$\lim_{r \rightarrow \infty} r \left( \frac{\partial}{\partial r} - ik \right) E_S(\mathbf{r}) = 0 \quad (6.32)$$

plus a Dirichlet or Neumann BC. Note, only one such condition is required for a unique solution.

The incident field is given by the monochromatic plane wave

$$E_I = e^{i(\mathbf{k}_I \cdot \mathbf{r} - \omega t)} \quad (6.33)$$

with

$$\mathbf{k}_I = k_I \hat{\mathbf{k}}_I = \frac{2\pi}{\lambda} \hat{\mathbf{k}}_I \quad (6.34)$$

where  $\lambda$  is the wavelength of the incident radiation,  $\omega$  the frequency and  $\mathbf{r}$  the position vector in the space  $(x, y, z)$

$$\mathbf{r} = x\hat{\mathbf{i}} + y\hat{\mathbf{j}} + z\hat{\mathbf{k}} \quad (6.35)$$

as usual, the basis vectors are the unit vectors in Euclidean space. For points on  $S$ ,  $\mathbf{r}$  becomes

$$\mathbf{r}_0 = x\hat{\mathbf{i}} + y\hat{\mathbf{j}} + \zeta(x, y)\hat{\mathbf{k}} \quad (6.36)$$

Note that any electric field may be expanded as a series of plane waves, [77]. This being the case it explains the use of the plane wave approximation, apart from its obvious simplicity. In addition it should be stated that the plane wave is a solution of the scattering problem provided that it satisfies the dispersion relation

$$k^2 = k_x^2 + k_y^2 + k_z^2 = \left( \frac{\omega}{c} \right)^2 \quad (6.37)$$

as required by the scalar Helmholtz equation, (6.10).

### Geometric Considerations

As shown in Figure 6.3.1, an EM wave is incident at the global angle of incidence defined with respect to the  $z$ -axis as  $\theta_I$  measured anti-clockwise from  $\hat{\mathbf{k}}$  to  $\mathbf{k}_I$ . This is a global rather than local angle of incidence since it is not defined wrt to the rough surface itself, as such it is always constant and may also be termed the mean plane incidence angle. Similarly the scattering angle is defined by  $\theta_S$  and is measured clockwise from the  $z$ -axis to the scattered field with wave vector  $\mathbf{k}_S$  lying in the  $(\mathbf{k}_S, \hat{\mathbf{k}})$  plane.

Figure 6.3.2 Local Scattering Geometry at the rough surface  $\zeta(x)$

It is the angle at which scattering observations are made at some observation point  $P$ , see Figure 6.3.2, it may be termed the observation angle, it is also a constant depending on which angle you wish to observe from. As above

$$\mathbf{k}_S = k_S \hat{\mathbf{k}}_S = \frac{2\pi}{\lambda} \hat{\mathbf{k}}_S \quad (6.38)$$

so that

$$|\mathbf{k}_I| = |\mathbf{k}_S| = k = \frac{2\pi}{\lambda} \quad (6.39)$$

For scattering away from the plane of incidence we define the extra angle  $\phi$ , all scattering will be confined to the  $(x, z)$  plane so that  $\phi = 0$  at all times. This will be shown presently. The total field  $E(\mathbf{r})$  in the presence of a scattering object can be decomposed into the incident and the scattered field ie

$$E(\mathbf{r}) = E_I(\mathbf{r}) + E_S(\mathbf{r}) \quad (6.40)$$

Then the scattered field  $E_S$  at an observation point  $P$  is given by the Kirchhoff integral

$$E_S(\mathbf{r}) = \int_S E(\mathbf{r}_0) \frac{\partial G(\mathbf{r}, \mathbf{r}_0)}{\partial n_0} - G(\mathbf{r}, \mathbf{r}_0) \frac{\partial E(\mathbf{r}_0)}{\partial n_0} dS_0 \quad (6.41)$$

Then the scattered field is defined in terms of the total field on the scatterer.

### Aside

N.B. it should be stressed that from the above integral relation it would seem that the values taken by  $E$  on the surface of the scatterer  $S$ , that is, the BC's  $E(\mathbf{r}_0)$  and  $\partial E(\mathbf{r}_0)/\partial n$  may be assigned arbitrarily, and, most importantly, independent of one another. In fact it is possible to express  $E(\mathbf{r})$  uniquely in terms of  $E(\mathbf{r}_0)$  alone or  $\partial E(\mathbf{r}_0)/\partial n$  alone. Following Sneddon, [73], if the Green's function  $G(\mathbf{r}, \mathbf{r}_0)$  satisfies the Helmholtz equation

$$\nabla_0^2 G(\mathbf{r}, \mathbf{r}_0) + k^2 G(\mathbf{r}, \mathbf{r}_0) = 0 \quad (6.42)$$

is finite, continuous wrt to the all points  $\mathbf{r}$  and  $\mathbf{r} = \mathbf{r}_0$  in a region  $V$  bounded by a closed surface  $S$  except at a singularity at the point  $\mathbf{r}$ , as  $\mathbf{r} \rightarrow \mathbf{r}_0$ , of the same type as (6.3). Then it follows that if  $G_1(\mathbf{r}, \mathbf{r}_0)$  is such a function and that

$$G_1(\mathbf{r}, \mathbf{r}_0) = 0 \quad (6.43)$$

for all points  $\mathbf{r}_0$  on  $S$  then

$$E_S(\mathbf{r}) = \int_S E(\mathbf{r}_0) \frac{\partial G_1(\mathbf{r}, \mathbf{r}_0)}{\partial n_0} dS_0 \quad (6.44)$$

Similarly if  $G_2(\mathbf{r}, \mathbf{r}_0)$  is such a function satisfying the BC

$$\frac{G_2(\mathbf{r}, \mathbf{r}_0)}{\partial n} = 0 \text{ for } \mathbf{r}_0 \text{ on } S \quad (6.45)$$

then

$$E_S(\mathbf{r}) = \int_S \frac{\partial E(\mathbf{r}_0)}{\partial n_0} G(\mathbf{r}, \mathbf{r}_0) dS_0 \quad (6.46)$$

So, the actual Kirchhoff integral is overdetermined and this means the two conditions  $E$  and  $\partial E/\partial n$  must be related. Usually only one need be chosen and the other can be derived from the first.

### The Tangent Plane Approximation

We are given the value of  $G(\mathbf{r}, \mathbf{r}_0)$ , ie (6.3), we also require the values  $E$  and  $\partial E/\partial n$  on  $S$ . The precise nature of these expressions originates from geometrical optics theory, [17], which states that the field at any point of the surface  $S$  is the field that would be present on the tangent plane at that point, [8]. The validity of these BC's will be discussed under the section entitled 'The Tangent Plane Criterion' to be found in the appendix. This approximation can obviously be considered accurate if the surface undulations possess a large radius of curvature,  $r_c$ , compared to the wavelength  $\lambda$  of incident radiation, since then the tangent plane is a good approximation to the surface at that particular point, [17]. This can be stated mathematically, [8], as

$$4\pi r_c \cos \vartheta \gg \lambda \quad (6.47)$$

If however, the surface contains any sharp points or edges this construction breaks down and the theory will be more inaccurate as this problem is exacerbated. In fact, the theory is exact only for surfaces that are infinite smooth and planar, [57]. (Note surfaces with discontinuities are also discounted from the earlier formulation of the Kirchhoff integral, section (6.2.1)).

Then the reflection coefficient at any point where the tangent plane approximation is valid

will be the coefficient of a smooth plane at that point. This of course varies as the surface changes, since the reflection coefficient must a function of the local angle of incidence,  $\vartheta$ , on the surface. Therefore, the scattered field on  $S$  can be represented by

$$E_S(\mathbf{r}_0) = R(\mathbf{r}_0)E_I(\mathbf{r}_0) \quad (6.48)$$

so the total field becomes

$$E(\mathbf{r}_0) = E_I(\mathbf{r}_0) + E_S(\mathbf{r}_0) \quad (6.49)$$

$$E(\mathbf{r}_0) = [1 + R(\mathbf{r}_0)]E_I(\mathbf{r}_0) \quad (6.50)$$

then the other condition on  $S$ ,  $\partial E/\partial n_0$  will be determined by

$$\frac{\partial E(\mathbf{r}_0)}{\partial n_0} = \frac{\partial E_I(\mathbf{r}_0)}{\partial n_0} + \frac{\partial E_S(\mathbf{r}_0)}{\partial n_0} \quad (6.51)$$

it is straightforward to determine the first term in (6.51)

$$\frac{\partial E_I(\mathbf{r}_0)}{\partial n_0} = i[\hat{\mathbf{n}}_0 \cdot \mathbf{k}_I]E_I(\mathbf{r}_0) \quad (6.52)$$

now Brekhovskikh, [17], assumes that  $\hat{\mathbf{n}}_0 \cdot \mathbf{k}_S = -\hat{\mathbf{n}}_0 \cdot \mathbf{k}_I$  therefore the second term in (6.51) becomes

$$\frac{\partial E_S(\mathbf{r}_0)}{\partial n_0} = -i[\hat{\mathbf{n}}_0 \cdot \mathbf{k}_I]E_S(\mathbf{r}_0) \quad (6.53)$$

$$= -i[\hat{\mathbf{n}}_0 \cdot \mathbf{k}_I]R(\mathbf{r}_0)E_I(\mathbf{r}_0) \quad (6.54)$$

finally we get

$$\frac{\partial E(\mathbf{r}_0)}{\partial n_0} = i[(1 - R(\mathbf{r}_0))(\hat{\mathbf{n}}_0 \cdot \mathbf{k}_I)]E_I(\mathbf{r}_0) \quad (6.55)$$

An alternative derivation is possible via Maxwell's equations, [8].

### Fresnel Reflection Coefficients

As can be seen in Figure 6.3.2 the Reflection coefficients for both parallel and perpendicular polarisation depend on the local angle of incidence thereby they are also dependent on the

surface slopes at every point  $\mathbf{r}_0$ . They are determined by the usual Fresnel, plane surface reflection, coefficients, as

$$R^{\parallel}(\mathbf{r}_0) = \frac{N_2 \cos \vartheta - \cos \theta_t}{N_2 \cos \vartheta + \cos \theta_t} \quad (6.56)$$

$$R^{\perp}(\mathbf{r}_0) = \frac{\cos \vartheta - N_2 \cos \theta_t}{\cos \vartheta + N_2 \cos \theta_t} \quad (6.57)$$

since the refractive index of air is assumed,  $N_1 = 1$ , then the refractive index of the metal is given by  $N_2$ . The angle of refraction is given by Snells law as

$$\sin \theta_t = \frac{1}{N_2} \sin \vartheta \quad (6.58)$$

so

$$\cos \theta_t = \frac{1}{N_2} \sqrt{N_2^2 - \sin^2 \vartheta} \quad (6.59)$$

then the reflection coefficients become

$$R^{\parallel}(\mathbf{r}_0) = \frac{N_2^2 \cos \vartheta - \sqrt{N_2^2 - \sin^2 \vartheta}}{N_2^2 \cos \vartheta + \sqrt{N_2^2 - \sin^2 \vartheta}} \quad (6.60)$$

$$R^{\perp}(\mathbf{r}_0) = \frac{\cos \vartheta - \sqrt{N_2^2 - \sin^2 \vartheta}}{\cos \vartheta + \sqrt{N_2^2 - \sin^2 \vartheta}} \quad (6.61)$$

from Fig 6.3.2 it is also possible to see that the local angle of incidence is given by

$$\vartheta = \theta_I - \beta \quad (6.62)$$

where of course  $\beta$  is given by

$$\beta = \tan^{-1} \left( \frac{d\zeta(x)}{dx} \right) \quad (6.63)$$

where we will be assuming the surface to be rough in only one dimension, ie

$$\frac{\partial \zeta}{\partial y} = 0 \quad (6.64)$$

if this is the case, it may be shown, [51], that the scattered field will be confined to the  $(x, z)$  plane only, implying that the extra scattering angle,  $\phi = 0$ , at all times for one-dimensionally rough surfaces. Making use of (6.62) and (6.63), above, we find

$$\cos \vartheta = \cos(\theta_I - \beta) = \cos \theta_I \cos \beta + \sin \theta_I \sin \beta \quad (6.65)$$

$$\sin \vartheta = \sin(\theta_I - \beta) = \sin \theta_I \cos \beta - \cos \theta_I \sin \beta \quad (6.66)$$

we have that

$$\tan \beta = \zeta' \quad (6.67)$$

(“ ’ ” refers to differentiation wrt  $x$ ). Then from simple trigonometric identities we find

$$\cos \beta = (1 + \tan^2 \beta)^{-1} = \frac{1}{\sqrt{1 + \zeta'^2}} \quad (6.68)$$

$$\sin \beta = \sqrt{1 - \cos^2 \beta} = \frac{\zeta'}{\sqrt{1 + \zeta'^2}} \quad (6.69)$$

upon substitution into (6.65) and (6.66) we get

$$\cos \vartheta = \frac{\cos \theta_I + \zeta' \sin \theta_I}{\sqrt{1 + \zeta'^2}} \quad (6.70)$$

$$\sin \vartheta = \frac{\zeta' \cos \theta_I - \sin \theta_I}{\sqrt{1 + \zeta'^2}} \quad (6.71)$$

finally substituting these results into (6.60) and (6.61) for the reflection coefficients we find

$$R^{\parallel}(\mathbf{r}_0) = \frac{N_2^2(\cos \theta_I + \zeta'^2 \sin \theta_I) - \sqrt{(N_2^2 - \cos^2 \theta_I)\zeta'^2 + \sin 2\theta_I \zeta' + (N_2^2 - \sin^2 \theta_I)}}{N_2^2(\cos \theta_I + \zeta'^2 \sin \theta_I) + \sqrt{(N_2^2 - \cos^2 \theta_I)\zeta'^2 + \sin 2\theta_I \zeta' + (N_2^2 - \sin^2 \theta_I)}} \quad (6.72)$$

$$R^{\perp}(\mathbf{r}_0) = \frac{\cos \theta_I + \zeta'^2 \sin \theta_I - \sqrt{(N_2^2 - \cos^2 \theta_I)\zeta'^2 + \sin 2\theta_I \zeta' + (N_2^2 - \sin^2 \theta_I)}}{\cos \theta_I + \zeta'^2 \sin \theta_I + \sqrt{(N_2^2 - \cos^2 \theta_I)\zeta'^2 + \sin 2\theta_I \zeta' + (N_2^2 - \sin^2 \theta_I)}} \quad (6.73)$$

for the two special cases  $\zeta' = 0$  (flat plane) and  $\theta_I = 0$  (normal incidence) we find

$$R_0^{\parallel}(\mathbf{r}_0) = \frac{N_2^2 \cos \theta_I - \sqrt{N_2^2 - \sin^2 \theta_I}}{N_2^2 \cos \theta_I + \sqrt{N_2^2 - \sin^2 \theta_I}} \quad (6.74)$$

$$R_0^{\perp}(\mathbf{r}_0) = \frac{\cos \theta_I - \sqrt{N_2^2 - \sin^2 \theta_I}}{\cos \theta_I + \sqrt{N_2^2 - \sin^2 \theta_I}} \quad (6.75)$$

for  $\zeta' = 0$ , the  $_0$  subscript indicating the flat case, and

$$R^{\parallel}(\mathbf{r}_0) = \frac{N_2^2 - \sqrt{(N_2^2 - 1)\zeta'^2 + N_2^2}}{N_2^2 + \sqrt{(N_2^2 - 1)\zeta'^2 + N_2^2}} \quad (6.76)$$



$$R^\perp(\mathbf{r}_0) = \frac{1 - \sqrt{(N_2^2 - 1)\zeta'^2 + N_2^2}}{1 + \sqrt{(N_2^2 - 1)\zeta'^2 + N_2^2}} \quad (6.77)$$

for  $\theta_I = 0$ .

## 6.4 The Scattering Integral

The scattering integral (6.20) may now be evaluated using the above constructions. Consider the scattered field to be evaluated in the Fraunhofer zone so that we make the approximation  $r \gg r_0$ ,  $kr \gg 1$ . The Green's function (6.3) and its derivative, become

$$G(\mathbf{r}, \mathbf{r}_0) \sim \frac{e^{i(kr - \mathbf{k}_S \cdot \mathbf{r}_0)}}{4\pi(r - \hat{\mathbf{r}} \cdot \mathbf{r}_0)} \quad (6.78)$$

$$\frac{\partial G(\mathbf{r}, \mathbf{r}_0)}{\partial n_0} \sim \frac{-ie^{ikr}}{4\pi r} (\hat{\mathbf{n}}_0 \cdot \mathbf{k}_S) e^{-i\mathbf{k}_S \cdot \mathbf{r}_0} \quad (6.79)$$

substituting the various terms (6.50), (6.55), (6.3) and (6.79) into the Kirchhoff integral (6.20) we get

$$E_S(\mathbf{r}) = \frac{ie^{ikr}}{4\pi r} \int_{S_0} [(R(\mathbf{r}_0)\mathbf{k}^- - \mathbf{k}^+) \cdot \hat{\mathbf{n}}_0] e^{i\mathbf{k}^- \cdot \mathbf{r}_0} dS_0 \quad (6.80)$$

using the notation, [57]

$$\mathbf{k}^- = \mathbf{k}_I - \mathbf{k}_S \quad (6.81)$$

$$\mathbf{k}^+ = \mathbf{k}_I + \mathbf{k}_S \quad (6.82)$$

Note, that the far field approximation above must equally be true for the dimensions of the scattering object itself, referring to section (5.8) we see this is true when, [6]

$$\frac{L}{r} \ll 1, \quad \frac{kL^2}{r} \ll 1 \quad (6.83)$$

### Mean Plane Integration

As is correctly pointed out by Ogilvy, [57], it is possible to integrate over the surface  $S_0$ , as above, by projecting a differential area element  $dS_0$  onto the mean plane ( $x$ -axis)

producing a mean plane area element  $dS_M$ , see Figure 6.4.1. If this is permitted by the surface and the size of the area element then we find

$$dS_0 = \frac{dx_0}{|\mathbf{n}_0 \cdot \hat{\mathbf{k}}|} = \sqrt{1 + \left(\frac{d\zeta(x_0)}{dx_0}\right)^2} dx_0 \quad (6.84)$$

If  $\mathbf{n}_0 \cdot \hat{\mathbf{k}} = 0$  at any point then the integral is not well defined. We have

$$\mathbf{n}_0 \cdot \hat{\mathbf{k}} = \frac{1}{\sqrt{1 + (\zeta'(x))^2}} \quad (6.85)$$

since

$$\mathbf{n}_0 = \frac{-\zeta'(x_0)\hat{\mathbf{i}} + \hat{\mathbf{k}}}{\sqrt{1 + (\zeta'(x_0))^2}} \quad (6.86)$$

so

$$\mathbf{n}_0 dS_0 = \left(-\zeta'(x_0)\hat{\mathbf{i}} + \hat{\mathbf{k}}\right) dx_0 \quad (6.87)$$

Figure 6.4.1 The projection of an area element  $dS_0$  onto the mean plane  $dS_M$  provided the area element  $dS_0$  is small enough, [57].

The integration is always performed over small planar elements which are parallel to the local surface tangent. It is vital that these planar elements be made as small as possible in order to increase the accuracy of the solution. Therefore, the solution (6.80) is accurate provided the surface has no infinite gradients and one takes a small step size  $dx_0$  along the mean plane.

### 6.4.1 The Kirchhoff Solution in the Fraunhofer Zone

Figure 6.3.1 shows that the incident and reflected wave vectors are given by

$$\mathbf{k}_I = k(\sin \theta_I \hat{\mathbf{i}} - \cos \theta_I \hat{\mathbf{k}}) \quad (6.88)$$

$$\mathbf{k}_S = k(\sin \theta_S \hat{\mathbf{i}} + \cos \theta_S \hat{\mathbf{k}}) \quad (6.89)$$

then

$$\mathbf{k}^- = k[(\sin \theta_I - \sin \theta_S) \hat{\mathbf{i}} - (\cos \theta_I + \cos \theta_S) \hat{\mathbf{k}}] \quad (6.90)$$

$$\mathbf{k}^+ = k[(\sin \theta_I + \sin \theta_S) \hat{\mathbf{i}} - (\cos \theta_I - \cos \theta_S) \hat{\mathbf{k}}] \quad (6.91)$$

$$\mathbf{k}^- \cdot \mathbf{r}_0 = k[(\sin \theta_I - \sin \theta_S)x_0 - (\cos \theta_I + \cos \theta_S)\zeta(x_0)] \quad (6.92)$$

$$\mathbf{k}^- \cdot \mathbf{n}_0 = -k[(\sin \theta_I - \sin \theta_S)\zeta' + (\cos \theta_I + \cos \theta_S)] \quad (6.93)$$

$$\mathbf{k}^+ \cdot \mathbf{n}_0 = -k[(\sin \theta_I + \sin \theta_S)\zeta' + (\cos \theta_I - \cos \theta_S)] \quad (6.94)$$

substitute these terms into the integral

$$E_S(\mathbf{r}) = \frac{ie^{ikr}}{4\pi r} \int_{S_{MP}} (a\zeta' - b)e^{i(k_x^- x_0 + k_z^- \zeta(x_0))} dS_{MP} \quad (6.95)$$

where

$$a = (\sin \theta_I + \sin \theta_S) + (\sin \theta_S - \sin \theta_I)R \quad (6.96)$$

$$b = (\cos \theta_S - \cos \theta_I) + (\cos \theta_I + \cos \theta_S)R \quad (6.97)$$

which are constant only when  $R$  is independent of position ie when  $\zeta' = \text{constant}$ .

For a finite surface defined over the interval  $-L \leq x \leq L$  we get

$$E_S(\mathbf{r}) = \frac{ie^{ikr}}{4\pi r} \int_{-L}^L (a\zeta' - b)e^{i(k_x^- x_0 + k_z^- \zeta(x_0))} dx_0 \quad (6.98)$$

Let us now generate the solution specific to a flat surface,  $\zeta = \zeta' = 0$ , when all the energy is in the specular direction ( $\theta_S = \theta_I$ ). This implies  $k_x^- = 0$ ,  $b = 2 \cos \theta_I R$

$$E_{SF}(\mathbf{r}) = \frac{ib e^{ikr}}{4\pi r} \int_{-L}^L -2 \cos \theta_I R_0 dx_0 \quad (6.99)$$

$$= \frac{-2 \cos \theta_I R_0 i b e^{i k r}}{4 \pi r} \int_{-L}^L dx_0 \quad (6.100)$$

$$= -\frac{i b e^{i k r} L R_0 \cos \theta_I}{\pi r} \quad (6.101)$$

(the  $_{SF}$  subscript standing for a field scattered ( $S$ ) from a flat surface ( $F$ )). This is the field reflected in the specular direction by a flat, finitely conducting surface ( $\partial R_0 / \partial \sigma_c \neq 0$ ), of the same dimensions, at the same distance as the rough surface. We may then normalise the general scattered field, (6.98)

$$\rho_S = \frac{E_S}{E_{SF}} \quad (6.102)$$

where  $\rho_S$  is the scattering coefficient of the rough surface

$$\rho_S = -\frac{1}{4 L R_0 \cos \theta_I} \int_{-L}^L (a \zeta' - b) e^{i(k_x^- x_0 + k_z^- \zeta(x_0))} dx_0 \quad (6.103)$$

Notice the dependence on the flat surface reflection coefficient. The scattering coefficient must, as is the case for the reflection coefficient, lie in the interval,  $|\rho_S| \leq 1$ , where the modulus refers to complex modulus since  $\rho_S$  is complex due to the presence of a complex refractive index  $n$ . The medium, be it a metal or an iron-oxide, will be lossy due to the conductivity with the real and imaginary parts given by (2.19) and (2.20) of section (2.4.2). It is also complex because of the second term in the integral  $e^{i \mathbf{k}^- \cdot \mathbf{r}_0} = \cos(\mathbf{k}^- \cdot \mathbf{r}_0) + i \sin(\mathbf{k}^- \cdot \mathbf{r}_0)$ , although it will be possible to eliminate this aspect of complexity later on.

### 6.4.2 The Determination of Rough Surface Emissivity

As has already been demonstrated in section (1.2.4) the emissivity will be obtained by use of equation (1.9), where the reflectivity is calculated from the reflection coefficients obtained from the scattering problem. The solution to the scattering problem will be in the form of the scattered electric field  $\mathbf{E}_S$ . The reflection coefficient will be defined in terms of the amplitudes of the incident,  $E_I$ , and scattered (reflected) fields,  $E_S$  :

$$R = \frac{E_S}{E_I} \quad (6.104)$$

Defining the field  $E_{SF}$  as the field scattered by a perfectly smooth surface,  $\zeta = 0$ , under the same conditions as the field  $E_S$ . The reflection coefficient becomes :

$$R = \frac{E_S}{E_{SF}} \frac{E_{SF}}{E_I} \quad (6.105)$$

or

$$R_S = \rho_S R_0 \quad (6.106)$$

where  $R_0 = E_{SF}/E_I$  is the smooth surface reflection coefficient and  $\rho_S = E_S/E_{SF}$  the scattering coefficient. This merely states that the reflection coefficient for rough surface,  $R_S$ , is just the smooth surface coefficient weighted with respect to a function  $\rho_S$ .

Notice that the value of  $R_S$  is now determined by the scattering coefficient only since

$$R_S = \rho_S R_0 = -\frac{1}{4L \cos \theta_I} \int_{-L}^L (a\zeta' - b) e^{i(k_x^- x_0 + k_z^- \zeta(x_0))} dx_0 \quad (6.107)$$

where the coefficient  $R_0$  is cancelled out,  $R$  dependence is however still included through the coefficients  $a$  and  $b$ .



# Chapter 7

## Unoxidised Rough Steel Surfaces

### 7.1 Introduction

This chapter comprises one of two chapters reserved for the authors contribution to research in periodic and non-periodic rough surface scattering. First let us mention previous research in this field.

#### 7.1.1 Non-Periodic Surfaces

Our approach is based on that of Beckmann, [8], and so previous work will consider mainly his contributions as most others either use his results or extend the basis of validity of his theory. The research of does not deal with analytic solutions to the complete integral, instead, he makes certain simplifications in order to allow closed form solutions to be possible. He assumes either that the surface is smooth,  $\zeta = 0$ , is perfectly conducting, or has a specific profile.

1. For the smooth case he obtains an analytic solution and can explain certain scattering characteristics, such as, scattering only in the specular direction.
2. He also analyses the problem of perfect conductivity, that is, when metals are assumed perfect conductors. This removes the extra complication of the reflection coefficient

terms inside the integral which depend on surface profile gradients. The amplitude of the scattered wave is then constant and determined only by the angles  $\theta_I, \theta_S$ . This is not a realistic assumption since absorption characteristics are not considered nor the effect of position dependent reflection coefficients. Are their contributions significant ?

3. He also makes the wide ranging conclusion that the solution of the integral at its edges, when  $x = \pm L$ , is not of a significant contribution in scattering. Since these terms are results of edge diffraction which is certainly not irrelevant from a heuristic point of view, they must be considered. In fact Ogilvy, [57], states categorically that their inclusion is vital for the determination of the correct solution to scattering problems, such as the smooth case.

### 7.1.2 Periodic Surfaces

1. Beckmann also analyses surfaces possessing a periodic profile,  $\zeta(x + T) = \zeta(x)$ . Two types may be considered, one : where the integral is made periodic by use of grating theory and, two : where the general non-periodic integral is considered giving rise to a generalised grating equation. Since Beckmann erroneously assumed the edge effects may be ignored, he did not consider their contribution. This must lead to incorrect results. Nevertheless, the original theory, which is based again on perfect conductivity produces Bessel function solutions. A solution which is physically acceptable on the grounds that many diffraction problems have similar solutions, [13].
2. He finds for periodic integrals obeying the grating equation that if
  - $\lambda/T \ll 1$  then the incident wave is scattered widely breaking up into many scattered waves, giving rise to many different directions of scatter.
  - $\lambda/T \gg 1$  then the scattering will be specular in nature and any wave will be specularly reflected regardless of the amplitude,  $A$ , of the surface. These results



agree well with experimental facts, especially the second of these, this result is also to be expected on grounds of common sense.

3. He does make certain assumptions in order to arrive at these results, such as forcing his surface to be an even function with perfect conductivity. His research is extended to scattering integrals not necessarily periodic, giving rise to a generalised grating equation with the addition of a sinusoidal expression in the amplitude representing the non-integer aspects of the generalised grating equation; compare this with the periodic integral case whose amplitude is only related to the angles  $\theta_I, \theta_S$ .
4. He briefly extends his periodic analysis both to rectangular and sawtooth profiles. The interested reader is referred to [8] and, [27]. These types of surfaces will not be considered here. He also barely mentions sinusoidal periodic profiles with more than one scale of roughness by adding an extra harmonic to the original profile. This interesting research is no doubt important in investigating the effect these extra scales of roughness have on scattering, surely a topic for further research.

Lastly, he discusses what happens if finite conductivity is used rather than perfect conductivity. His conclusion is that finite conductivity can only ever effect the scattering behaviour if the local reflection coefficients  $R(\vartheta)$  ( $\vartheta$  the local angle of incidence), are determined by the local angle of incidence rather than by the electrical properties of the scattering material. He states that the scattering characteristics are essentially determined only by the roughness and not the electrical properties.

Beckmann also only ever investigates surfaces of finite extent not considering any surface that may be considered infinite in certain circumstances. In this case and only this case the edge effects are non-existent since there is of course no edge to the surface.

There are then, several avenues left open for consideration in this work. These have been expanded upon in this chapter. The following research has not previously been carried out and is a new contribution to both analytic scattering theory and the investigation of rough surface emissivity.

1. Surfaces of infinite extent are considered, it is found the extension to infinite surfaces is a straightforward process using the finite surface results.
2. Finite conductivity is considered by the inclusion in the scattering integral of the reflection coefficients varying both with local surface gradients and electrical properties.
3. The edge terms neglected by Beckmann are comprehensively included in the analysis.
4. Instead of only considering surfaces whose dimensions are integer multiples of the period we extend the analysis to deal with irregular surfaces.
5. Each surface profile is analysed either as an even or odd function of dimension, not a restriction to one type.
6. The consequences of the above extensions to rough surface emissivity calculations are considered as well as the conclusions drawn in previous work on rough scattering.

Generally, the rough steel surface will be characterised by the reflection coefficient and the surface roughness expressed by the function  $\zeta(x)$ . We should note that the final scattering coefficient will depend on several parameters. These are : the electrical properties of the scatterer, its angles of incidence and reflection, the wavelength of the incident radiation and the temperature of the steel surface. From (6.103) we see that

$$\rho_S = \rho_S(\theta_I, \theta_S; \sigma_c, \mu, \varepsilon, \lambda; \sigma, \lambda_0) \quad (7.1)$$

where the temperature dependence enters through the conductivity  $\sigma_c = \sigma_c(T)$ . Are there any simplifications possible over this range of variables ? As in section (3.2) we will only consider dependence on  $T$ ,  $\lambda$ ,  $\theta_I$ ,  $\theta_S$  and the roughness factors  $\sigma$  (RMS surface height) and  $\lambda_0$  (correlation length). This is true since we will assume the other electrical properties to be those of free space a not unreasonable assumption, except in special circumstances, ie  $\mu = \mu_0$ ,  $\varepsilon = \varepsilon_0$ . When considering the emissivity we will be most interested in the normal incidence case since this is the preferred measurement made in industry. Similarly the

scattering angle  $\theta_S$  will be most often confined to the specular case since this is the region of interest when comparing the smooth and the rough case. So eventually we will assess

$$\rho_S = \rho_S(\lambda, T, \sigma, \lambda_0) \quad (7.2)$$

## 7.2 The Extension to Infinite Surfaces

If we wish to extend the scattering integral to surfaces having dimensions  $L \rightarrow \infty$  then we must consider the limit defined by

$$- \lim_{L \rightarrow \infty} \left\{ \frac{1}{4LR_0 \cos \theta_I} \int_{-L}^L (a\zeta' - b) e^{i(k_x^- x_0 + k_z^- \zeta(x_0))} dx_0 \right\} \quad (7.3)$$

It is possible to do a simple analysis of this limit. With the inclusion of the infinite limit it may be possible for the integral to become unbounded. Now, if it stays finite and is a function of  $L$  then the integral must be computed by some method, analytical or numerical, and the limit applied. If however the limit of the integral is infinite, then, we are presented with the situation

$$\lim_{L \rightarrow \infty} \mathcal{I}(L) = \infty \quad (7.4)$$

where

$$\mathcal{I}(L) = \int_{-L}^L (a\zeta' - b) e^{i(k_x^- x_0 + k_z^- \zeta(x_0))} dx_0 \quad (7.5)$$

the limit may be written

$$\lim_{L \rightarrow \infty} \rho_S = \frac{-1}{4R_0 \cos \theta_I} \lim_{L \rightarrow \infty} \frac{\mathcal{I}(L)}{L} \quad (7.6)$$

since we are given that

$$\lim_{L \rightarrow \infty} \mathcal{I}(L) = \infty \quad (7.7)$$

and

$$\lim_{L \rightarrow \infty} L = \infty \quad (7.8)$$

and both  $\mathcal{I}(L)$  and  $L$  are analytic in  $(-\infty, \infty)$  we may use L'Hospital's rule to get

$$\lim_{L \rightarrow \infty} \frac{\mathcal{I}(L)}{L} = \lim_{L \rightarrow \infty} \frac{\mathcal{I}'(L)}{L'} \quad (7.9)$$

where " ' " refers to differentiation wrt  $L$

$$= \lim_{L \rightarrow \infty} \frac{d\mathcal{I}(L)}{dL} \quad (7.10)$$

now

$$\frac{d\mathcal{I}(L)}{dL} = \frac{d}{dL} \int_{-L}^L (a\zeta' - b) e^{i(k_x^- x_0 + k_z^- \zeta(x_0))} dx_0 \quad (7.11)$$

change variable  $X = x + L$  then we get

$$\frac{d}{dL} \int_0^{2L} [a(X-L)\zeta'(X-L) - b(X-L)] e^{i[k_x^- (X-L) + k_z^- \zeta(X-L)]} dX \quad (7.12)$$

$$2 \frac{d}{d(2L)} \int_0^{2L} [a(X-L)\zeta'(X-L) - b(X-L)] e^{i[k_x^- (X-L) + k_z^- \zeta(X-L)]} dX \quad (7.13)$$

then by the Fundamental Theorem of Calculus this can be evaluated as

$$2[a(L)\zeta'(L) - b(L)] e^{i[k_x^- L + k_z^- \zeta(L)]} \quad (7.14)$$

so the limit becomes

$$\lim_{L \rightarrow \infty} \frac{d\mathcal{I}(L)}{dL} = \lim_{L \rightarrow \infty} 2[a(L)\zeta'(L) - b(L)] e^{i[k_x^- L + k_z^- \zeta(L)]} \quad (7.15)$$

So the general result is

$$\lim_{L \rightarrow \infty} \rho_S = \frac{-1}{4R_0 \cos \theta_I} \begin{cases} \lim_{L \rightarrow \infty} \frac{1}{L} \int_{-L}^L (a\zeta' - b) e^{i(k_x^- x_0 + k_z^- \zeta(x_0))} dx_0 & \text{if } \lim_{L \rightarrow \infty} \mathcal{I}(L) \text{ finite} \\ \lim_{L \rightarrow \infty} 2[a(L)\zeta'(L) - b(L)] e^{i[k_x^- L + k_z^- \zeta(L)]} & \text{if } \lim_{L \rightarrow \infty} \mathcal{I}(L) \text{ infinite} \end{cases} \quad (7.16)$$

Each theoretical result, could, if necessary, be extended in this fashion. We will find in the last section that this leads to a simple conclusion.

### 7.3 Non-Periodically Rough Surfaces

Our region of investigation will be an analysis of rough surface scattering when the surface is periodically rough, the simplest possible case of a rough surface. It also allows us to analyse in some detail the effects of the roughness parameters  $\sigma$  and  $\lambda_0$ . As a comparison, surfaces which are not periodic will also be briefly investigated.

### 7.3.1 Smooth Surface $\zeta' = 0$

It is instructive to examine the case when the surface is that of a flat plane  $\zeta = \zeta' = 0$  then the scattering coefficient, (6.103), becomes

$$\rho_S = -\frac{1}{4LR_0 \cos \theta_I} \int_{-L}^L -be^{ik_x^- x_0} dx_0 \quad (7.17)$$

since  $R_0$  is no longer a function of  $x_0$

$$= \frac{(\cos \theta_S - \cos \theta_I) + (\cos \theta_I + \cos \theta_S)R_0}{4LR_0 \cos \theta_I} \int_{-L}^L e^{ik_x^- x_0} dx_0 \quad (7.18)$$

$$= \frac{(\cos \theta_S - \cos \theta_I) + (\cos \theta_I + \cos \theta_S)R_0}{4LR_0 \cos \theta_I ik_x^-} (e^{ik_x^- L} - e^{-ik_x^- L}) \quad (7.19)$$

then since  $\sin k_x^- L = \frac{e^{ik_x^- L} - e^{-ik_x^- L}}{2i}$

$$= \frac{(\cos \theta_S - \cos \theta_I) + (\cos \theta_I + \cos \theta_S)R_0}{2R_0 \cos \theta_I} \left( \frac{\sin k_x^- L}{k_x^- L} \right) \quad (7.20)$$

for specular reflection  $\theta_S = \theta_I$ , and using the fact that  $k_x^- = k(\sin \theta_I - \sin \theta_S)$ , it reduces to the simple expression (applying the limit  $k_x^- \rightarrow 0$ )

$$\lim_{k_x^- \rightarrow 0} \rho_{S_{spec}} = \lim_{k_x^- \rightarrow 0} \frac{\sin k_x^- L}{k_x^- L} \quad (7.21)$$

$$\rho_{S_{spec}} = 1 \quad (7.22)$$

indicating all the energy is directed into the specular direction and none in any other as would be expected for the smooth surface case. Note, this does not depend on  $R_0$ . The actual reflection coefficient for a rough surface is calculated via (6.106), section (6.4.2), as

$$R_S = \rho_S R_0 \quad (7.23)$$

so we get

$$R_{S_{spec}} = \rho_{S_{spec}} R_0 = R_0 \quad (7.24)$$

as expected. Other specific cases is that of perfect conductivity, ie  $\sigma_c, n \rightarrow \infty$ , giving  $R^{\parallel} = 1$ ,  $R^{\perp} = -1$  and a scattering coefficient of

$$\rho_{S_{metallic}}^{\parallel} = \left( \frac{\cos \theta_S}{\cos \theta_I} \right) \frac{\sin k_x^- L}{k_x^- L} \quad (7.25)$$

$$\rho_{S_{metallic}}^{\perp} = \frac{\sin k_x^- L}{k_x^- L} \quad (7.26)$$

once again the energy is concentrated into the specular direction only for both cases of polarisation. This is the solution for a highly conducting metal, in fact any material having a high conductivity would be expected to behave in the above manner. It is a simple matter to calculate the rough surface reflection coefficient as

$$R_{S_{metallic}} = \rho_{S_{metallic}} R_0 \quad (7.27)$$

$$R_{S_{metallic}}^{\parallel} = \left( \frac{\cos \theta_S}{\cos \theta_I} \right) \frac{\sin k_x^- L}{k_x^- L} R_0^{\parallel} \quad (7.28)$$

$$R_{S_{metallic}}^{\perp} = -\frac{\sin k_x^- L}{k_x^- L} R_0^{\perp} \quad (7.29)$$

so the reflectivity becomes

$$R_y = \frac{R_{S_{metallic}}^{\parallel} R_{S_{metallic}}^{\parallel*} + R_{S_{metallic}}^{\perp} R_{S_{metallic}}^{\perp*}}{2} \quad (7.30)$$

For the specular case we find

$$R_{y_0} = \frac{R_0^{\parallel} R_0^{\parallel*} + R_0^{\perp} R_0^{\perp*}}{2} \quad (7.31)$$

giving

$$\epsilon = 1 - R_{y_0} \quad (7.32)$$

as for the smooth case. This then confirms the previous analysis of section (3.2) for the flat case.

### 7.3.2 Non-Periodic, Perfectly Conducting Surface

This case has already been studied, [8], with the assumption of perfect conductivity,  $R^{\parallel, \perp} = \pm 1$  then the values  $a$  and  $b$  are constants. Taking them out of the integral we get

$$\rho_S = \frac{\pm 1}{4L \cos \theta_I} \left\{ a \int_{-L}^L \zeta^t e^{ik_z^- \zeta} e^{ik_x^- x_0} dx_0 - b \int_{-L}^L e^{i\mathbf{k}^- \cdot \mathbf{r}_0} dx_0 \right\} \quad (7.33)$$

replacing  $R_0 = \pm 1$ , integrating the first term by parts

$$\frac{\pm 1}{4L \cos \theta_I} \left\{ \frac{ae^{i\mathbf{k}^- \cdot \mathbf{r}_0}}{ik_z^-} \Big|_{-L}^L - \frac{ak_x^-}{k_z^-} \int_{-L}^L e^{i\mathbf{k}^- \cdot \mathbf{r}_0} dx_0 - b \int_{-L}^L e^{i\mathbf{k}^- \cdot \mathbf{r}_0} dx_0 \right\} \quad (7.34)$$

$$= \frac{\mp 1}{4L \cos \theta_I} \left\{ \left( \frac{ak_x^-}{k_z^-} + b \right) \int_{-L}^L e^{i\mathbf{k}^- \cdot \mathbf{r}_0} dx_0 - \frac{ae^{i\mathbf{k}^- \cdot \mathbf{r}_0}}{ik_z^-} \Big|_{-L}^L \right\} \quad (7.35)$$

so

$$\rho_S = \frac{\mp 1}{4L \cos \theta_I} \left( \frac{ak_x^-}{k_z^-} + b \right) \int_{-L}^L e^{i\mathbf{k}^- \cdot \mathbf{r}_0} dx_0 + E(L) \quad (7.36)$$

where  $E(L)$  is the edge term

$$E(L) = \frac{\pm 1}{4L \cos \theta_I} \frac{ae^{i\mathbf{k}^- \cdot \mathbf{r}_0}}{ik_z^-} \Big|_{-L}^L \quad (7.37)$$

this is the edge term since it is the evaluation of the wave  $e^{i\mathbf{k}^- \cdot \mathbf{r}_0}$  at the endpoints of the rough surface ie

$$E(L) = \frac{\pm 1}{4L \cos \theta_I} \left( \frac{a}{ik_z^-} \right) \left[ e^{i(k_x^- L + k_z^- \zeta(L))} - e^{i(-k_x^- L + k_z^- \zeta(-L))} \right] \quad (7.38)$$

note that if the endpoints are fixed such that  $\zeta(L) = \zeta(-L) = 0$  then we find

$$E(L) = \frac{\pm 1}{4L \cos \theta_I} \left( \frac{a}{ik_z^-} \right) \left[ e^{ik_x^- L} - e^{-ik_x^- L} \right] \quad (7.39)$$

$$= \frac{\mp a \sin(k_x^- L)}{2L k_z^- \cos \theta_I} \quad (7.40)$$

If for example we let  $\zeta = 0$  then we get for the scattering solution

$$\rho_S = \frac{\mp 1}{4L \cos \theta_I} \left( \frac{ak_x^-}{k_z^-} + b \right) \int_{-L}^L e^{ik_x^- x_0} dx_0 + \frac{\pm 1}{2L \cos \theta_I} \frac{a \sin k_x^- L}{k_z^-} \quad (7.41)$$

the integral is easily evaluated giving

$$= \frac{\mp 1}{2L \cos \theta_I} \left( \frac{ak_x^-}{k_z^-} + b \right) \frac{\sin k_x^- L}{k_x^-} \pm \frac{1}{2L \cos \theta_I} \frac{a \sin k_x^- L}{k_z^-} \quad (7.42)$$

$$= \frac{\mp \sin k_x^- L}{2L \cos \theta_I} \left[ \left( \frac{ak_x^-}{k_z^-} + b \right) \frac{1}{k_x^-} - \frac{a}{k_z^-} \right] \quad (7.43)$$

cancelling leaves us with

$$\rho_S = \frac{\mp b}{2 \cos \theta_I} \left( \frac{\sin k_x^- L}{k_x^- L} \right) \quad (7.44)$$

then we find as in the flat case

$$\rho_S = \left\{ \begin{array}{ll} \frac{\sin k_x^- L}{k_x^- L} & \text{for perpendicular polarisation and } \theta_S = \theta_I \\ \left( \frac{\cos \theta_S}{\cos \theta_I} \right) \frac{\sin k_x^- L}{k_x^- L} & \text{for parallel polarisation and } \theta_S = \theta_I \end{array} \right\} \quad (7.45)$$

Confirming the result in section (7.3.1) above.

### Even and Odd Functions

If  $\zeta$  is even  $\zeta(-x) = \zeta(x)$  then the the integral and edge terms each become

$$\frac{\mp i}{2L \cos \theta_I} \left( \frac{ak_x^-}{k_z^-} + b \right) \int_0^L e^{ik_z^- \zeta(x_0)} \sin k_x^- L dx_0 + E(L) \quad (7.46)$$

and

$$E(L) = \frac{\pm 1}{2L \cos \theta_I} \left( \frac{a}{k_z^-} \right) e^{ik_z^- \zeta(L)} \sin(k_x^- L) \quad (7.47)$$

then for  $\zeta(L) = 0$

$$E(L) = \left( \frac{\pm a \sin(k_x^- L)}{2L k_z^- \cos \theta_I} \right) \quad (7.48)$$

If  $\zeta$  is odd  $\zeta(-x) = -\zeta(x)$  we get

$$\frac{\mp i}{2L \cos \theta_I} \left( \frac{ak_x^-}{k_z^-} + b \right) \int_0^L \sin(k_x^- L + k_z^- \zeta(x_0)) dx_0 + E(L) \quad (7.49)$$

where

$$E(L) = \frac{\pm 1}{2L \cos \theta_I} \left( \frac{a}{k_z^-} \right) \sin(k_x^- L + k_z^- \zeta(L)) \quad (7.50)$$

and for  $\zeta(L) = 0$

$$E(L) = \left( \frac{\pm a \sin(k_x^- L)}{2L k_z^- \cos \theta_I} \right) \quad (7.51)$$

as for (7.48) above



N.B. It is obvious from (7.48) that we cannot at any stage ignore the endpoint contributions since it is they that add the correct factor in order to produce the smooth case scattering solution (7.45) above.

Also, in the extension to infinite surfaces applying the limit as  $L \rightarrow \infty$  guarantees the elimination of the edge effects ie

$$\lim_{L \rightarrow \infty} \frac{\pm 1}{4L \cos \theta_I} \left( \frac{a}{ik_z^-} \right) \left[ e^{ik_x^- L} - e^{-ik_x^- L} \right] = 0 \quad (7.52)$$

## 7.4 Rough Periodic Functions

The surface  $S$  will be assumed rough in the following manner

$$\zeta(x) = \zeta(x + T) \quad (7.53)$$

that is, the surface is periodic with period  $T$ . Notice also that the same applies for an integer multiple of the period. That is (refer to appendix for justification)

$$\zeta(x + nT) = \zeta(x) \quad (7.54)$$

similarly for the derivative of a periodic function we find

$$\zeta'(x + T) = \zeta'(x) \quad (7.55)$$

the same is true for the integer multiple case. In fact generally

$$\zeta^{(m)}(x + nT) = \zeta^{(m)}(x) \quad (7.56)$$

These results will shortly be required.

## 7.5 Simplifications of the Kirchhoff Integral

The integral (6.103) is difficult to solve except for the simple case  $\zeta = 0$ , however other simplifications are possible. Using the fact that the surface is periodically rough as defined above, then there are several possible simplifications to the solution of the scattering

integral.

### 7.5.1 Periodicity of $\zeta(x)$

The original scattering integral is given by

$$\rho_S = -\frac{1}{4LR_0 \cos \theta_I} \int_{-L}^L (a\zeta' - b) e^{i(k_x^- x_0 + k_z^- \zeta(x_0))} dx_0 \quad (7.57)$$

we will assume that the dimensions of the scatterer,  $L$ , may be made up of an integer multiple of periods of the surface,  $nT$ , and a small fractional addition,  $\eta T$ , ie

$$\frac{L}{T} = n + \eta \quad (7.58)$$

or

$$L = nT + \eta T \quad (7.59)$$

where  $n$  is an integer and  $0 \leq \eta < 1$ . Then the integral becomes

$$\rho_S = -\frac{1}{4LR_0 \cos \theta_I} \int_{-(nT+\eta T)}^{nT+\eta T} (a\zeta' - b) e^{i(k_x^- x_0 + k_z^- \zeta(x_0))} dx_0 \quad (7.60)$$

$$= -\frac{1}{4LR_0 \cos \theta_I} \left\{ \int_{-nT}^{nT} (a\zeta' - b) e^{i\mathbf{k}^- \cdot \mathbf{r}_0} dx_0 + \int_{nT}^{nT+\eta T} (a\zeta' - b) e^{i\mathbf{k}^- \cdot \mathbf{r}_0} dx_0 + \int_{-(nT+\eta T)}^{-nT} (a\zeta' - b) e^{i\mathbf{k}^- \cdot \mathbf{r}_0} dx_0 \right\} \quad (7.61)$$

### 7.5.2 Main Integral (non-edge terms)

Dividing the length  $nT$  into strips so that each strip extends from  $x_0 = jT$  to  $x_0 = (j+1)T$  where  $j$  is an integer with  $-n \leq j \leq n-1$  then we get for the first integral

$$= -\frac{1}{4LR_0 \cos \theta_I} \sum_{j=-n}^{n-1} \int_{-jT}^{(j+1)T} (a\zeta' - b) e^{i(k_x^- x_0 + k_z^- \zeta(x_0))} dx_0 \quad (7.62)$$

changing variable such that  $x_0 = X_0 + jT$ ,  $dx_0 = dX_0$

$$= -\frac{1}{4LR_0 \cos \theta_I} \sum_{j=-n}^{n-1} e^{ik_x^- jT} \int_0^T (a\zeta'(X_0 + jT) - b) e^{i(k_x^- X_0 + k_z^- \zeta(X_0 + jT))} dX_0 \quad (7.63)$$

similarly the reflection coefficients involved in the  $a$  and  $b$  terms become

$$R(\zeta'(X_0 + jT)) = R(\zeta'(X_0)) \quad (7.64)$$

by periodicity ( $j$  an integer), we get

$$= -\frac{1}{4LR_0 \cos \theta_I} \sum_{j=-n}^{n-1} e^{ik_x^- jT} \int_0^T (a\zeta' - b) e^{i(k_x^- X_0 + k_z^- \zeta(X_0))} dX_0 \quad (7.65)$$

we will rename the dummy variable back to  $X_0 \rightarrow x_0$  again, now let

$$k_x^- T = 2\pi p \quad (7.66)$$

where  $p$  is some real number, then we have

$$p = \frac{T}{\lambda} (\sin \theta_I - \sin \theta_S) \quad (7.67)$$

or

$$\sin \theta_S = \sin \theta_I - \frac{p\lambda}{T} \quad (7.68)$$

which is the grating equation if  $p$  is an integer, generally it is the generalised grating equation having real modes. The integral becomes

$$-\frac{1}{4(n + \eta)R_0 \cos \theta_I} \sum_{j=-n}^{n-1} e^{ik_x^- jT} \cdot \frac{1}{T} \int_0^T (a\zeta' - b) e^{i(k_x^- x_0 + k_z^- \zeta)} dx_0 \quad (7.69)$$

the sum in front of the integral may be calculated, provided it is finite, as

$$W = \frac{1}{2n} \sum_{j=-n}^{n-1} e^{2i\pi p j}, \quad |W| \leq 1 \quad (7.70)$$

we get

$$W = \frac{\sin 2np\pi}{2n \sin p\pi} e^{-ip\pi} \quad (7.71)$$

(If  $p$  is an integer  $W = 1$  as required, [8]). Then the first integral becomes

$$\rho_S = -\frac{Wn}{2(n + \eta)R_0 \cos \theta_I} \frac{1}{T} \int_0^T (a\zeta' - b) e^{i\mathbf{k}^- \cdot \mathbf{r}_0} dx_0 \quad (7.72)$$

### 7.5.3 Edge Terms

The second set of integrals have two parts to them both of which are tractable upon change of variable  $x_0 \rightarrow x_0 \pm nT$ . The limits become  $x_0 : 0 \rightarrow nT$  and  $-nT \rightarrow 0$ . The first of the two can then be written

$$\int_0^{\eta T} (a\zeta'(x_0 - nT) - b)e^{i(k_x^-(x_0 - nT) + k_z^-\zeta(x_0 - nT))} dx_0 \quad (7.73)$$

with periodicity  $\zeta(x_0 \pm nT) = \zeta(x_0)$ ,  $\zeta'(x_0 \pm nT) = \zeta'(x_0)$  we get

$$\int_{nT}^{nT + \eta T} (a\zeta' - b)e^{i\mathbf{k}^- \cdot \mathbf{r}_0} dx_0 = e^{-ik_x^- nT} \int_0^{\eta T} (a\zeta' - b)e^{i\mathbf{k}^- \cdot \mathbf{r}_0} dx_0 \quad (7.74)$$

note,  $a$  and  $b$  are also functions of  $\zeta'$  which of course are similarly periodic. Also, the second of the two integrals above becomes after the change  $x_0 \rightarrow x_0 + nT$

$$\int_{-\eta T}^0 (a\zeta'(x_0 + nT) - b)e^{i(k_x^-(x_0 + nT) + k_z^-\zeta(x_0 + nT))} dx_0 \quad (7.75)$$

again finally giving

$$\int_{-(nT + \eta T)}^{-nT} (a\zeta' - b)e^{i\mathbf{k}^- \cdot \mathbf{r}_0} dx_0 = e^{ik_x^- nT} \int_{-\eta T}^0 (a\zeta' - b)e^{i\mathbf{k}^- \cdot \mathbf{r}_0} dx_0 \quad (7.76)$$

### 7.5.4 Complete Solution

The final general result for periodically rough surfaces becomes

$$\rho_S = -\frac{1}{4LR_0 \cos \theta_I} \left\{ 2Wn \int_0^T (a\zeta' - b)e^{i\mathbf{k}^- \cdot \mathbf{r}_0} dx_0 + e^{-2in\pi p} \int_0^{\eta T} (a\zeta' - b)e^{i\mathbf{k}^- \cdot \mathbf{r}_0} dx_0 + \right. \quad (7.77)$$

$$\left. e^{2in\pi p} \int_{-\eta T}^0 (a\zeta' - b)e^{i\mathbf{k}^- \cdot \mathbf{r}_0} dx_0 \right\} \quad (7.78)$$

We stress that the edge effects ignored as being irrelevant by Beckmann, [8], (if  $L \gg T$ ) were found not to be by Ogilvy, [57], who states that they cannot be neglected (unless  $\eta = 0$ ) as the correct result is found only when they are included.

Notice again that if we take the limit up to infinite surfaces the edge terms disappear

through division by  $L$ , we may ignore the actual integration because it is up to  $\eta T$  at most, this is much smaller than  $L$  of course. If this is the case the integral becomes

$$\rho_S = - \lim_{L \rightarrow \infty} \left\{ \frac{Wn}{2LR_0 \cos \theta_I} \int_0^T (a\zeta' - b) e^{i\mathbf{k}^- \cdot \mathbf{r}_0} dx_0 \right\} \quad (7.79)$$

Note that for this limit to be taken the infinite extension,  $n \rightarrow \infty$  of the sum  $W$ , must be considered. We will now consider the simplifications possible to this integral.

## 7.6 Perfect Conductivity

The case of perfect conductivity has already been considered for the smooth surface case, now consider the case where  $\zeta' \neq 0$  and  $R = \pm 1, R_0 = \pm 1$  for each case of polarisation. Then the amplitude term  $a\zeta' - b$  has no  $x$  dependence except through  $\zeta'$ ,  $a$  and  $b$  are now constant.

### 7.6.1 Main Integral

Taking these values outside the integral (7.79), excluding the edge terms momentarily

$$\rho_S = \frac{\mp Wn}{2(n + \eta) \cos \theta_I T} \left\{ a \int_0^T \zeta' e^{i\mathbf{k}^- \cdot \mathbf{r}_0} dx_0 - b \int_0^T e^{i\mathbf{k}^- \cdot \mathbf{r}_0} dx_0 \right\} \quad (7.80)$$

We can integrate the first of these integrals using integration by parts, it becomes

$$a \int_0^T \zeta' e^{i\mathbf{k}^- \cdot \mathbf{r}_0} dx_0 = \frac{ae^{i\mathbf{k}^- \cdot \mathbf{r}_0}}{ik_z^-} \Big|_0^T - \frac{ak_x^-}{k_z^-} \int_0^T e^{i\mathbf{k}^- \cdot \mathbf{r}_0} dx_0 \quad (7.81)$$

we get

$$\rho_S = \frac{\mp Wn}{2(n + \eta) \cos \theta_I T} \left\{ \frac{ae^{i\mathbf{k}^- \cdot \mathbf{r}_0}}{ik_z^-} \Big|_0^T - \left( \frac{ak_x^-}{k_z^-} + b \right) \int_0^T e^{i\mathbf{k}^- \cdot \mathbf{r}_0} dx_0 \right\} \quad (7.82)$$

$$= \frac{\pm Wn}{2(n + \eta) \cos \theta_I T} \left\{ \left( \frac{ak_x^-}{k_z^-} + b \right) \int_0^T e^{i\mathbf{k}^- \cdot \mathbf{r}_0} dx_0 - \frac{ae^{i\mathbf{k}^- \cdot \mathbf{r}_0}}{ik_z^-} \Big|_0^T \right\} \quad (7.83)$$

### 7.6.2 Edge Terms

The two other integrals form the solutions to the edge of the surface, ie the edge contributions, they are given by (using  $k_x^- T = 2\pi p$ )

$$\mp \frac{1}{4L \cos \theta_I} \left\{ e^{-2in\pi p} \int_0^{\eta T} (a\zeta' - b)e^{i\mathbf{k}^- \cdot \mathbf{r}_0} dx_0 + e^{2in\pi p} \int_{-\eta T}^0 (a\zeta' - b)e^{i\mathbf{k}^- \cdot \mathbf{r}_0} dx_0 \right\} \quad (7.84)$$

following the same procedure as for the main integral, the two integrals become

$$e^{-2in\pi p} \left[ a \int_0^{\eta T} \zeta' e^{i\mathbf{k}^- \cdot \mathbf{r}_0} dx_0 - b \int_0^{\eta T} e^{i\mathbf{k}^- \cdot \mathbf{r}_0} dx_0 \right] + e^{2in\pi p} \left[ a \int_{-\eta T}^0 \zeta' e^{i\mathbf{k}^- \cdot \mathbf{r}_0} dx_0 - b \int_{-\eta T}^0 e^{i\mathbf{k}^- \cdot \mathbf{r}_0} dx_0 \right] \quad (7.85)$$

as above the integrals containing  $\zeta'$  become using integration by parts

$$\int_0^{\eta T} \zeta' e^{ik_z^- \zeta} e^{ik_x^- x_0} dx_0 = \frac{e^{i\mathbf{k}^- \cdot \mathbf{r}_0}}{ik_z^-} \Big|_0^{\eta T} - \frac{k_x^-}{k_z^-} \int_0^{\eta T} e^{i\mathbf{k}^- \cdot \mathbf{r}_0} dx_0 \quad (7.86)$$

$$\int_{-\eta T}^0 \zeta' e^{ik_z^- \zeta} e^{ik_x^- x_0} dx_0 = \frac{e^{i\mathbf{k}^- \cdot \mathbf{r}_0}}{ik_z^-} \Big|_{-\eta T}^0 - \frac{k_x^-}{k_z^-} \int_{-\eta T}^0 e^{i\mathbf{k}^- \cdot \mathbf{r}_0} dx_0 \quad (7.87)$$

giving finally

$$e^{-2in\pi p} \left\{ \frac{ae^{i\mathbf{k}^- \cdot \mathbf{r}_0}}{ik_z^-} \Big|_0^{\eta T} - \left( \frac{ak_x^-}{k_z^-} + b \right) \int_0^{\eta T} e^{i\mathbf{k}^- \cdot \mathbf{r}_0} dx_0 \right\} \quad (7.88)$$

$$e^{2in\pi p} \left\{ \frac{ae^{i\mathbf{k}^- \cdot \mathbf{r}_0}}{ik_z^-} \Big|_{-\eta T}^0 - \left( \frac{ak_x^-}{k_z^-} + b \right) \int_{-\eta T}^0 e^{i\mathbf{k}^- \cdot \mathbf{r}_0} dx_0 \right\} \quad (7.89)$$

### 7.6.3 Total Solution

The complete solution is then

$$\frac{\pm 2Wn}{4L \cos \theta_I} \left\{ \left( \frac{ak_x^-}{k_z^-} + b \right) \int_0^T e^{i\mathbf{k}^- \cdot \mathbf{r}_0} dx_0 + \frac{ae^{ik_z^- \zeta(0)}}{ik_z^-} \right\} + E(T) \quad (7.90)$$

where the edge terms  $E(T)$  are made up of the terms

$$\frac{\pm 1}{4L \cos \theta_I} \left\{ \left[ e^{2in\pi p} \left( \frac{ak_x^-}{k_z^-} + b \right) \int_{-\eta T}^0 e^{i\mathbf{k}^- \cdot \mathbf{r}_0} dx_0 - \frac{ae^{i\mathbf{k}^- \cdot \mathbf{r}_0}}{ik_z^-} \Big|_{-\eta T}^0 \right] + \right. \quad (7.91)$$

$$e^{-2in\pi p} \left[ \left( \frac{ak_x^-}{k_z^-} + b \right) \int_0^{\eta T} e^{i\mathbf{k}^- \cdot \mathbf{r}_0} dx_0 - \frac{ae^{i\mathbf{k}^- \cdot \mathbf{r}_0} \Big|_0^{\eta T}}{ik_z^-} \right] - 2Wn \left( \frac{ae^{i(k_x^- T + k_z^- \zeta(T))}}{ik_z^-} \right) \quad (7.92)$$

where the last term above is included in the edge terms since it is evaluated at  $x = T$  at the far end of the surface.

#### 7.6.4 Even Functions

This occurs when

$$\zeta(-x) = \zeta(x) \quad (7.93)$$

$$\Rightarrow \zeta'(-x) = -\zeta'(x) \quad (7.94)$$

(refer to appendix) if this is the case we find

$$\int_{-\eta T}^0 e^{i\mathbf{k}^- \cdot \mathbf{r}_0} dx_0 \rightarrow - \int_0^{-\eta T} e^{i\mathbf{k}^- \cdot \mathbf{r}_0} dx_0 \quad (7.95)$$

$$= \int_0^{\eta T} e^{-ik_x^- x_0} e^{ik_z^- \zeta} dx_0 \quad (7.96)$$

Including the extra term in front  $e^{2in\pi p}$  ie

$$e^{2in\pi p} \int_0^{\eta T} e^{-ik_x^- x_0} e^{ik_z^- \zeta} dx_0 \quad (7.97)$$

and the other term for the second of these integrals is

$$e^{-2in\pi p} \int_0^{\eta T} e^{ik_x^- x_0} e^{ik_z^- \zeta} dx_0 \quad (7.98)$$

adding these two terms

$$\int_0^{\eta T} [e^{i(2n\pi p - k_x^- x_0)} + e^{-i(2n\pi p - k_x^- x_0)}] e^{ik_z^- \zeta} dx_0 \quad (7.99)$$

putting the coefficient  $\frac{ak_x^-}{k_z^-} + b$  in front as in (7.79)

$$= \left( \frac{ak_x^-}{k_z^-} + b \right) \int_0^{\eta T} 2 \cos(2n\pi p - k_x^- x_0) e^{ik_z^- \zeta} dx_0 \quad (7.100)$$

Similarly the other terms evaluated between  $[0, \eta T]$ ,  $[-\eta T, 0]$  become

$$e^{-2in\pi p} \left( \frac{ae^{i\mathbf{k}^- \cdot \mathbf{r}_0}}{ik_z^-} \Big|_0^{\eta T} \right) = \frac{a}{ik_z^-} \left( e^{i(k_x^- \eta T + k_z^- \zeta(\eta T))} - e^{ik_z^- \zeta(0)} \right) e^{-2in\pi p} \quad (7.101)$$

$$= \frac{a}{ik_z^-} \left( e^{2i\pi p(\eta-n)} e^{k_z^- \zeta(\eta T)} - e^{ik_z^- \zeta(0)} e^{-2in\pi p} \right) \quad (7.102)$$

and

$$e^{2in\pi p} \left( \frac{ae^{i\mathbf{k}^- \cdot \mathbf{r}_0}}{ik_z^-} \Big|_{-\eta T}^0 \right) = \frac{a}{ik_z^-} \left( e^{ik_z^- \zeta(0)} - e^{i(-k_x^- \eta T + k_z^- \zeta(-\eta T))} \right) e^{2in\pi p} \quad (7.103)$$

$$= \frac{a}{ik_z^-} \left( e^{ik_z^- \zeta(0)} e^{2in\pi p} - e^{-2i\pi p(\eta-n)} e^{k_z^- \zeta(\eta T)} \right) \quad (7.104)$$

since  $\zeta$  is even. Adding these two terms

$$\frac{a}{ik_z^-} \left( 2i \sin(2\pi p(\eta-n)) e^{k_z^- \zeta(\eta T)} + 2i \sin(2n\pi p) e^{ik_z^- \zeta(0)} \right) \quad (7.105)$$

The total expression for the edge terms becomes

$$\begin{aligned} & \frac{\pm 1}{4L \cos \theta_I} \left\{ \left( \frac{ak_x^-}{k_z^-} + b \right) \int_0^{\eta T} 2 \cos(2n\pi p - k_x^- x_0) e^{ik_z^- \zeta} dx_0 - \frac{a}{ik_z^-} \left( 2i \sin(2\pi p(\eta-n)) e^{k_z^- \zeta(\eta T)} \right. \right. \\ & \left. \left. + 2i \sin(2n\pi p) e^{ik_z^- \zeta(0)} \right) - 2Wn \left( \frac{ae^{i(k_x^- T + k_z^- \zeta(T))}}{ik_z^-} \right) \right\} \quad (7.106) \end{aligned}$$

giving

$$\begin{aligned} & \frac{\pm 1}{4L \cos \theta_I} \left\{ \left( \frac{ak_x^-}{k_z^-} + b \right) \int_0^{\eta T} 2 \cos(2n\pi p - k_x^- x_0) e^{ik_z^- \zeta} dx_0 - \frac{a}{ik_z^-} \left( 2[i \sin(2\pi p(\eta-n))] e^{k_z^- \zeta(\eta T)} \right. \right. \\ & \left. \left. + 2[i \sin(2n\pi p)] e^{ik_z^- \zeta(0)} + 2Wn e^{i(k_x^- T + k_z^- \zeta(T))} \right) \right\} \quad (7.107) \end{aligned}$$

### Total Solution

The complete solution for  $\zeta$  even is then

$$\frac{\pm 2Wn}{4L \cos \theta_I} \left\{ \left( \frac{ak_x^-}{k_z^-} + b \right) \int_0^T e^{i\mathbf{k}^- \cdot \mathbf{r}_0} dx_0 + \frac{ae^{ik_z^- \zeta(0)}}{ik_z^-} \right\} + E(T) \quad (7.108)$$

with the edge term given by

$$\begin{aligned} E(T) = & \frac{\pm 1}{4LR_0 \cos \theta_I} \left\{ \left( \frac{ak_x^-}{k_z^-} + b \right) \int_0^{\eta T} 2 \cos(2n\pi p - k_x^- x_0) e^{ik_z^- \zeta} dx_0 - \frac{a}{ik_z^-} \left( 2[i \sin(2\pi p(\eta-n))] e^{k_z^- \zeta(\eta T)} \right. \right. \\ & \left. \left. + 2[i \sin(2n\pi p)] e^{ik_z^- \zeta(0)} + 2Wn e^{i(k_x^- T + k_z^- \zeta(T))} \right) \right\} \quad (7.109) \end{aligned}$$



## 7.6.5 Odd Functions

If on the other hand  $\zeta$  is odd so that

$$\zeta(-x) = -\zeta(x) \quad (7.110)$$

$$\Rightarrow \zeta'(-x) = \zeta'(x) \quad (7.111)$$

we may carry out an analogous procedure to that above and arrive at

$$e^{-2in\pi p} \left( \frac{ae^{i\mathbf{k}^- \cdot \mathbf{r}_0}}{ik_z^-} \Big|_0^{\eta T} \right) = \frac{a}{ik_z^-} \left( e^{i(k_x^- \eta T + k_z^- \zeta(\eta T))} - e^{ik_z^- \zeta(0)} \right) e^{-2in\pi p} \quad (7.112)$$

$$= \frac{a}{ik_z^-} \left( e^{-i(2n\pi p - k_x^- \eta T - k_z^- \zeta(\eta T))} - e^{ik_z^- \zeta(0)} e^{-2in\pi p} \right) \quad (7.113)$$

$$e^{2in\pi p} \left( \frac{ae^{i\mathbf{k}^- \cdot \mathbf{r}_0}}{ik_z^-} \Big|_{-\eta T}^0 \right) = \frac{a}{ik_z^-} \left( e^{ik_z^- \zeta(0)} - e^{-i(k_x^- \eta T + k_z^- \zeta(\eta T))} \right) e^{2in\pi p} \quad (7.114)$$

$$= \frac{a}{ik_z^-} \left( e^{ik_z^- \zeta(0)} e^{2in\pi p} - e^{i(2n\pi p - k_x^- \eta T - k_z^- \zeta(\eta T))} \right) \quad (7.115)$$

adding gives

$$\frac{a}{ik_z^-} \left( 2i \sin(2n\pi p) e^{ik_z^- \zeta(0)} - 2i \sin(2\pi p(n - \eta) - k_z^- \zeta(\eta T)) \right) \quad (7.116)$$

and

$$e^{-2in\pi p} \left( \frac{ak_x^-}{k_z^-} + b \right) \int_0^{\eta T} e^{i\mathbf{k}^- \cdot \mathbf{r}_0} dx_0 = \left( \frac{ak_x^-}{k_z^-} + b \right) \int_0^{\eta T} e^{i(-2n\pi p + k_x^- x_0 + k_z^- \zeta(x_0))} dx_0 \quad (7.117)$$

$$e^{2in\pi p} \left( \frac{ak_x^-}{k_z^-} + b \right) \int_{-\eta T}^0 e^{i\mathbf{k}^- \cdot \mathbf{r}_0} dx_0 = \left( \frac{ak_x^-}{k_z^-} + b \right) \int_0^{\eta T} e^{-i(-2n\pi p + k_x^- x_0 + k_z^- \zeta(x_0))} dx_0 \quad (7.118)$$

adding

$$\left( \frac{ak_x^-}{k_z^-} + b \right) \int_0^{\eta T} 2 \cos(-2n\pi p + k_x^- x_0 + k_z^- \zeta(x_0)) dx_0 \quad (7.119)$$

and the last term

$$\frac{ae^{i\mathbf{k}^- \cdot \mathbf{r}_0}}{ik_z^-} \Big|_0^T = \frac{a}{ik_z^-} \left( e^{i(k_x^- T + k_z^- \zeta(T))} - e^{ik_z^- \zeta(0)} \right) \quad (7.120)$$

$$= \frac{a}{ik_z^-} \left( e^{i(2\pi p + k_z^- \zeta(T))} - e^{ik_z^- \zeta(0)} \right) \quad (7.121)$$

### Complete Solution

Substituting these terms into the final expression we get for  $\zeta$  odd the solution

$$\frac{\pm 2Wn}{4L \cos \theta_I} \left\{ \left( \frac{ak_x^-}{k_z^-} + b \right) \int_0^T e^{i\mathbf{k}^- \cdot \mathbf{r}_0} dx_0 + \frac{ae^{ik_z^- \zeta(0)}}{ik_z^-} \right\} + E(T) \quad (7.122)$$

where the edge term  $E(T)$  is

$$E(T) = \frac{\pm 1}{4L \cos \theta_I} \left\{ \left( \frac{ak_x^-}{k_z^-} + b \right) \int_0^{\eta T} 2 \cos(2n\pi p - k_x^- x_0 - k_z^- \zeta(x_0)) dx_0 - \right. \\ \left. \frac{a}{ik_z^-} \left( 2[i \sin(2\pi p(n - \eta) - k_z^- \zeta(\eta T))] + 2[i \sin(2n\pi p) +] e^{ik_z^- \zeta(0)} + 2Wn e^{i(k_x^- T + k_z^- \zeta(T))} \right) \right\} \quad (7.123)$$

#### 7.6.6 Solution in Terms of $\theta_I, \theta_S$

The expression in front of (7.122) can be expressed in terms of  $\theta_I, \theta_S$  alone since  $R^{\parallel, \perp} = \pm 1$  the terms  $a$  and  $b$  become

$$a^{\parallel} = 2 \sin \theta_S, \quad b^{\parallel} = 2 \cos \theta_S \quad (7.124)$$

$$a^{\perp} = 2 \sin \theta_I, \quad b^{\perp} = -2 \cos \theta_I \quad (7.125)$$

and the ratio  $\frac{k_x^-}{k_z^-}$  is given by

$$\frac{\sin \theta_S - \sin \theta_I}{\cos \theta_S + \cos \theta_I} \quad (7.126)$$

giving  $\frac{ak_x^-}{k_z^-} + b$  as

$$\frac{\pm 1}{4L \cos \theta_I} \left( \frac{ak_x^-}{k_z^-} + b \right) = \pm \frac{1 + \cos(\theta_I + \theta_S)}{2L \cos \theta_I (\cos \theta_S + \cos \theta_I)} \quad (7.127)$$

independent of the polarisation. However the coefficient

$$\frac{\pm a}{4ik_z^- L \cos \theta_I} = \frac{\mp i \sin \theta^{\parallel, \perp}}{2Lk \cos \theta_I (\cos \theta_S + \cos \theta_I)} \quad (7.128)$$

is not, where

$$\sin \theta^{\parallel, \perp} = \begin{cases} \sin \theta_S & \text{for } \parallel \\ \sin \theta_I & \text{for } \perp \end{cases} \quad (7.129)$$

### 7.6.7 Total Solutions : Even and Odd Functions

#### Even Functions

Therefore the expression for the scattering solution for a perfectly conducting substrate, with  $\zeta$  even is

$$\rho^{\parallel,\perp}(\theta_I, \theta_S) = \frac{\pm 1}{L \cos \theta_I (\cos \theta_S + \cos \theta_I)} \left\{ Wn[1 + \cos(\theta_I + \theta_S)] \int_0^T e^{i\mathbf{k}^- \cdot \mathbf{r}_0} dx_0 - \frac{i \sin \theta^{\parallel,\perp} e^{ik_z^- \zeta(0)}}{2k} \right\} + E^{\parallel,\perp}(T) \quad (7.130)$$

where the edge term is

$$E^{\parallel,\perp}(T) = \frac{\pm[1 + \cos(\theta_I + \theta_S)]}{L \cos \theta_I (\cos \theta_S + \cos \theta_I)} \int_0^{\eta T} 2 \cos(2n\pi p - k_x^- x_0) e^{ik_z^- \zeta} dx_0 - \frac{i \sin \theta^{\parallel,\perp}}{2Lk \cos \theta_I (\cos \theta_S + \cos \theta_I)} \left( 2[i \sin(2\pi p(\eta - n))] e^{k_z^- \zeta(\eta T)} + 2[i \sin(2n\pi p)] e^{ik_z^- \zeta(0)} + 2Wn e^{i(k_x^- T + k_z^- \zeta(T))} \right) \quad (7.131)$$

#### Odd Functions

Similarly for  $\zeta$  odd we get

$$\rho^{\parallel,\perp}(\theta_I, \theta_S) = \frac{\pm 1}{L \cos \theta_I (\cos \theta_S + \cos \theta_I)} \left\{ Wn[1 + \cos(\theta_I + \theta_S)] \int_0^T e^{i\mathbf{k}^- \cdot \mathbf{r}_0} dx_0 + \frac{\pm i \sin \theta^{\parallel,\perp} e^{ik_z^- \zeta(0)}}{2k} \right\} + E^{\parallel,\perp}(T) \quad (7.133)$$

where the edge term is

$$E^{\parallel,\perp}(T) = \frac{\pm[1 + \cos(\theta_I + \theta_S)]}{L \cos \theta_I (\cos \theta_S + \cos \theta_I)} \int_0^{\eta T} 2 \cos(2n\pi p - k_x^- x_0 - k_z^- \zeta(x_0)) dx_0 + \frac{i \sin \theta^{\parallel,\perp}}{2Lk \cos \theta_I (\cos \theta_S + \cos \theta_I)} \left( 2[i \sin(2\pi p(n - \eta) - k_z^- \zeta(\eta T))] + 2[i \sin(2n\pi p)] e^{ik_z^- \zeta(0)} + 2Wn e^{i(k_x^- T + k_z^- \zeta(T))} \right) \quad (7.134)$$

## 7.7 Mean Plane Reflection Coefficient

The second possible case for simplification is the approach of Beckmann, [8]. By letting the reflection coefficient  $R(\vartheta)$  be averaged over the mean plane so that

$$R(\vartheta) \simeq R(\theta_I) \quad (7.135)$$

This variation has already been dealt with extensively, [8], and as such will not be looked at here.

## 7.8 Varying Surface Reflection coefficient

If we allow the surface reflection coefficient  $R(\vartheta)$  to vary with  $\zeta'$ , then the scattering integral for periodic surfaces is given by (7.79)

$$\rho_S = -\frac{1}{4LR_0 \cos \theta_I} \left\{ 2Wn \int_0^T (a\zeta' - b)e^{i\mathbf{k}^- \cdot \mathbf{r}_0} dx_0 + e^{-2in\pi p} \int_0^{\eta T} (a\zeta' - b)e^{i\mathbf{k}^- \cdot \mathbf{r}_0} dx_0 + e^{2in\pi p} \int_{-\eta T}^0 (a\zeta' - b)e^{i\mathbf{k}^- \cdot \mathbf{r}_0} dx_0 \right\} \quad (7.136)$$

### 7.8.1 Main Integral

Looking only at the first of these leaving the edge terms for later

$$\rho_S = -\frac{Wn}{2LR_0 \cos \theta_I} \int_0^T (a\zeta' - b)e^{i\mathbf{k}^- \cdot \mathbf{r}_0} dx_0 \quad (7.137)$$

upon substitution of the terms  $a$  and  $b$  from (6.96) and (6.97) section (6.4.1) we get

$$\rho_S = -\frac{Wn}{2LR_0 \cos \theta_I} \int_0^T \left\{ (\sin \theta_I + \sin \theta_S)\zeta' + (\sin \theta_S - \sin \theta_I)R\zeta' + (\cos \theta_I - \cos \theta_S) - R(\cos \theta_I + \cos \theta_S) \right\} e^{i\mathbf{k}^- \cdot \mathbf{r}_0} dx_0 \quad (7.138)$$

$$= -\frac{Wn}{2LR_0 \cos \theta_I} \left\{ (\sin \theta_I + \sin \theta_S) \int_0^T \zeta' e^{i\mathbf{k}^- \cdot \mathbf{r}_0} dx_0 + (\sin \theta_S - \sin \theta_I) \int_0^T R\zeta' e^{i\mathbf{k}^- \cdot \mathbf{r}_0} dx_0 + (\cos \theta_I - \cos \theta_S) \int_0^T e^{i\mathbf{k}^- \cdot \mathbf{r}_0} dx_0 - (\cos \theta_I + \cos \theta_S) \int_0^T R e^{i\mathbf{k}^- \cdot \mathbf{r}_0} dx_0 \right\} \quad (7.139)$$

$$\left. \right\} \quad (7.140)$$

where the constant terms involving  $\theta_I, \theta_S$  were taken out of the front of each particular integral. Integrals of the form  $\int \zeta' e^{i\mathbf{k}^- \cdot \mathbf{r}_0} dx_0$  have already been considered. The remaining integrals having the reflection coefficient represented explicitly will now be considered. We will adopt the technique of Parkins, [61], who represented the reflection coefficient  $R(\zeta')$  as a Taylor series expansion about the mean slope, or equivalently about the smooth surface reflection coefficient  $R_0$ , which of course is not a function of  $\zeta'$ . This method did not consider the convergence of this series and so only considered the first term of the series, as an approximation for  $R$ .

We will extend his method with the convergence of the series studied specifically.

That is

$$R(\zeta') = R_0 + \left. \frac{dR(\zeta')}{d\zeta'} \right|_{\zeta'=0} \zeta' + \left. \frac{d^2R(\zeta')}{d\zeta'^2} \right|_{\zeta'=0} \frac{\zeta'^2}{2!} + \left. \frac{d^3R(\zeta')}{d\zeta'^3} \right|_{\zeta'=0} \frac{\zeta'^3}{3!} + \dots + O(\zeta'^m) + \dots \quad (7.141)$$

here  $R(0) \equiv R_0$ . The coefficients,  $R_0$ , are given by

$$R_0^{\parallel}(\mathbf{r}_0) = \frac{N_2^2 \cos \theta_I - \sqrt{N_2^2 - \sin^2 \theta_I}}{N_2^2 \cos \theta_I + \sqrt{N_2^2 - \sin^2 \theta_I}} \quad (7.142)$$

$$R_0^{\perp}(\mathbf{r}_0) = \frac{\cos \theta_I - \sqrt{N_2^2 - \sin^2 \theta_I}}{\cos \theta_I + \sqrt{N_2^2 - \sin^2 \theta_I}} \quad (7.143)$$

for the two types of polarisation. For ease of notation write the individual derivatives of  $R$  at  $\zeta' = 0$  as

$$\left. \frac{d^m R(\zeta')}{d\zeta'^m} \right|_{\zeta'=0} = R_0^{(m)} \quad (7.144)$$

so the series becomes

$$R(\zeta') = R_0^{(0)} + R_0^{(1)} \zeta' + R_0^{(2)} \frac{\zeta'^2}{2!} + R_0^{(3)} \frac{\zeta'^3}{3!} + \dots + O(\zeta'^m) + \dots \quad (7.145)$$

then this series converges uniformly to  $R(\zeta')$ , [75], provided (by the ratio test) that for the  $m^{\text{th}}$  term  $R_0^{(m)} \frac{\zeta'^m}{m!}$ .

$$\lim_{m \rightarrow \infty} \left| \frac{R_0^{(m+1)}}{R_0^{(m)}} \right| \frac{|\zeta'|}{m+1} < 1 \quad (7.146)$$

provided this result is independent of  $x$  and the  $m^{\text{th}}$  term tends to zero in the limit as  $m \rightarrow \infty$ .

If this is the case we have a valid expansion for  $R$  about the mean plane and any solution of the scattering integral will be a valid solution provided it obeys the criterion (7.146) above. We will find this is fairly easily obeyed in certain cases we wish to study. The above is an extension of the work of Parkins, [61], who took only terms up to  $O(1)$  in the derivatives and did not consider the entire series as a valid representation of the scattering coefficient.

Substituting this series in the integrals, (7.140), we have the solution for the scattering coefficient as

$$\rho_S = -\frac{Wn}{2LR_0 \cos \theta_I} \left\{ (\sin \theta_I + \sin \theta_S) \int_0^T \zeta' e^{i\mathbf{k}^- \cdot \mathbf{r}_0} dx_0 + \right. \quad (7.147)$$

$$(\sin \theta_S - \sin \theta_I) \int_0^T \left( R_0^{(0)} + R_0^{(1)} \zeta' + R_0^{(2)} \frac{\zeta'^2}{2!} + \dots \right) \zeta' e^{i\mathbf{k}^- \cdot \mathbf{r}_0} dx_0 + \quad (7.148)$$

$$\left. (\cos \theta_I - \cos \theta_S) \int_0^T e^{i\mathbf{k}^- \cdot \mathbf{r}_0} dx_0 - (\cos \theta_I + \cos \theta_S) \int_0^T \left( R_0^{(0)} + R_0^{(1)} \zeta' + R_0^{(2)} \frac{\zeta'^2}{2!} + \dots \right) e^{i\mathbf{k}^- \cdot \mathbf{r}_0} dx_0 \right\} \quad (7.149)$$

we are presented with two types of integrals

$$\int_0^T \zeta'^m e^{i(k_x^- x_0 + k_z^- \zeta(x_0))} dx_0 \quad (7.150)$$

$m$  a positive integer, and

$$\int_0^T e^{i(k_x^- x_0 + k_z^- \zeta(x_0))} dx_0 \quad (7.151)$$

whose solution is possible with some assumptions on the values taken by  $\zeta$ .

### 7.8.2 The Case $\theta_S = \theta_I = 0$

Since we are interested in comparing the rough case with the smooth one and since the smooth case directs all of the scattered energy in the specular direction,  $\theta_S = \theta_I$ , we must observe the scattered energy from the rough case in the specular direction also. If this is

the case we find

$$\rho_S = -\frac{Wn}{2LR_0 \cos \theta_I} \left\{ (2 \sin \theta_I) \int_0^T \zeta' e^{i\mathbf{k}^- \cdot \mathbf{r}_0} dx_0 - (2 \cos \theta_I) \int_0^T \left( R_0^{(0)} + R_0^{(1)} \zeta' + R_0^{(2)} \frac{\zeta'^2}{2!} + \dots \right) e^{i\mathbf{k}^- \cdot \mathbf{r}_0} dx_0 \right\} \quad (7.152)$$

Now, if we only look at the normal angle of incidence,  $\theta_{I1} = 0$ , as preferred in industrial measurement, we find that  $p = 0 \Rightarrow W = 1$  and  $k_x^- = 0$ , then the scattering integral reduces to

$$\rho_S = \frac{n}{LR_0} \int_0^T \left( R_0^{(0)} + R_0^{(1)} \zeta' + R_0^{(2)} \frac{\zeta'^2}{2!} + \dots \right) e^{ik_z^- \zeta(x_0)} dx_0 \quad (7.153)$$

Now, obtaining the derivatives of the reflection coefficients  $R(\theta_I = 0)$

$$R^{\parallel}(\mathbf{r}_0) = \frac{N_2^2 - \sqrt{(N_2^2 - 1)\zeta'^2 + N_2^2}}{N_2^2 + \sqrt{(N_2^2 - 1)\zeta'^2 + N_2^2}} \quad (7.154)$$

$$R^{\perp}(\mathbf{r}_0) = \frac{1 - \sqrt{(N_2^2 - 1)\zeta'^2 + N_2^2}}{1 + \sqrt{(N_2^2 - 1)\zeta'^2 + N_2^2}} \quad (7.155)$$

Notice  $R$  is an even function of  $\zeta'$ . The derivatives are

$$\frac{dR^{\parallel}}{d\zeta'} = \frac{2N_2^2(1 - N_2^2)\zeta'}{\sqrt{(N_2^2 - 1)\zeta'^2 + N_2^2}(N_2^2 + \sqrt{(N_2^2 - 1)\zeta'^2 + N_2^2})^2} \quad (7.156)$$

and

$$\frac{dR^{\perp}}{d\zeta'} = \frac{2(1 - N_2^2)\zeta'}{\sqrt{(N_2^2 - 1)\zeta'^2 + N_2^2}(1 + \sqrt{(N_2^2 - 1)\zeta'^2 + N_2^2})^2} \quad (7.157)$$

evaluated at  $\zeta' = 0$

$$\left. \frac{dR^{\parallel, \perp}}{d\zeta'} \right|_{\zeta'=0} = 0 \quad (7.158)$$

the second derivatives evaluated at  $\zeta' = 0$  are

$$\left. \frac{d^2 R^{\parallel, \perp}}{d\zeta'^2} \right|_{\zeta'=0} = \frac{2(1 - N_2^2)}{N_2(1 + N_2)} \quad (7.159)$$

with  $R_0$  at  $\zeta' = 0$  being

$$R_0^{\parallel} = -\frac{1 - N_2}{1 + N_2} \quad (7.160)$$

$$R_0^\perp = \frac{1 - N_2}{1 + N_2} \quad (7.161)$$

Since  $R$  is an even function of  $\zeta'$  its odd order derivatives are all zero when evaluated at  $\zeta' = 0$ , leaving only those at the even orders, ie

$$R_0^{(0)} + R_0^{(2)} \frac{\zeta'^2}{2!} + R_0^{(4)} \frac{\zeta'^4}{4!} + \dots + R_0^{(2m)} \frac{\zeta'^{2m}}{(2m)!} + \dots \quad (7.162)$$

where the term  $R_0^{(0)}$  is the zeroth derivative at  $\zeta' = 0$ , in other words the function  $R(\zeta')$  is not differentiated but is evaluated at  $\zeta' = 0$ . Therefore  $R_0^{(0)} \equiv R(0) \equiv R_0$  the integral is now

$$\rho_S = \frac{n}{LR_0} \int_0^T \left( R_0^{(0)} + R_0^{(2)} \frac{\zeta'^2}{2!} + R_0^{(4)} \frac{\zeta'^4}{4!} + \dots + R_0^{(2m)} \frac{\zeta'^{2m}}{2m!} + \dots \right) e^{ik_z^- \zeta(x_0)} dx_0 \quad (7.163)$$

The integral becomes

$$= \frac{n}{LR_0} \int_0^T \sum_{m=0}^{\infty} R_0^{(2m)} \frac{\zeta'^{2m}}{2m!} e^{ik_z^- \zeta(x_0)} dx_0 \quad (7.164)$$

or

$$= \frac{n}{LR_0} \sum_{m=0}^{\infty} \frac{R_0^{(2m)}}{2m!} \int_0^T \zeta'^{2m} e^{ik_z^- \zeta(x_0)} dx_0 \quad (7.165)$$

interchanging as usual the order of integration and summation. Note, that the term by term integration is only possible if the series is uniformly convergent, [75], which we have established, provided the convergence condition, (7.146), is satisfied.

### 7.8.3 Edge Terms

As for the main integral making the substitutions for  $a$  and  $b$  in terms of  $\theta_S, \theta_I$  and  $R$ , and putting  $\theta_S = \theta_I = 0, \Rightarrow k_x^- = p = 0$  we find the edge integrals become

$$\frac{1}{2LR_0} \left\{ \int_0^{\eta T} R e^{ik^- \cdot r_0} dx_0 + \int_{-\eta T}^0 R e^{ik^- \cdot r_0} dx_0 \right\} \quad (7.166)$$

replacing  $R$  with the Taylor series from above

$$E(T) = \frac{1}{2LR_0} \left\{ \sum_{m=0}^{\infty} \frac{R_0^{(2m)}}{2m!} \int_0^{\eta T} \zeta'^{2m} e^{ik^- \cdot r_0} dx_0 + \sum_{m=0}^{\infty} \frac{R_0^{(2m)}}{2m!} \int_{-\eta T}^0 \zeta'^{2m} e^{ik^- \cdot r_0} dx_0 \right\} \quad (7.167)$$



$$= \frac{1}{2LR_0} \left\{ \sum_{m=0}^{\infty} \frac{R_0^{(2m)}}{2m!} \int_0^{\eta T} \zeta'(x_0)^{2m} e^{ik_z^- \zeta(x_0)} dx_0 + \sum_{m=0}^{\infty} \frac{R_0^{(2m)}}{2m!} \int_0^{\eta T} \zeta'(-x)^{2m} e^{ik_z^- \zeta(-x_0)} dx_0 \right\} \quad (7.168)$$

changing the variable in the second integral. Consider the odd and even cases

### Even Case

The integrals become, remembering  $\zeta(-x) = \zeta(x)$ ,  $\zeta'(-x) = -\zeta'(x)$

$$E(T) = \frac{1}{2LR_0} \left\{ \sum_{m=0}^{\infty} \frac{R_0^{(2m)}}{2m!} \int_0^{\eta T} \zeta'(x_0)^{2m} e^{ik_z^- \zeta(x_0)} (1 - 1) dx_0 \right\} = 0 \quad (7.169)$$

no edge term contribution from the even case.

### Odd Case

We get using  $\zeta(-x) = -\zeta(x)$ ,  $\zeta'(-x) = \zeta'(x)$

$$E(T) = \frac{1}{2LR_0} \sum_{m=0}^{\infty} \frac{R_0^{(2m)}}{2m!} \int_0^{\eta T} \zeta'(x_0)^{2m} (e^{ik_z^- \zeta(x_0)} + e^{-ik_z^- \zeta(x_0)}) dx_0 \quad (7.170)$$

$$= \frac{1}{LR_0} \sum_{m=0}^{\infty} \frac{R_0^{(2m)}}{2m!} \int_0^{\eta T} \zeta'^{2m} \cos k_z^- \zeta dx_0 \quad (7.171)$$

the edge terms only making a contribution, in the specular normal incidence case, when the surface profile is an odd function of distance.

## 7.9 Specific Periodic Surface Profiles

We choose the simple profile

$$\zeta(x_0) = A \sin \left( \frac{2\pi x_0}{T} \right) \quad (7.172)$$

Since this function agrees with the boundary values of the surface  $\zeta(L) = \zeta(-L) = 0$  if  $L = nT$  only, mentioned in section (7.3.2).  $A$ , is the amplitude or maximum height of the surface variation and  $T$ , the period of the surface undulation. These values are somewhat

analogous to the statistical parameters  $\sigma \sim A$  and  $\lambda_0 \sim A/T$ .

Then

$$\zeta'(x_0) = \frac{2\pi A}{T} \cos\left(\frac{2\pi x_0}{T}\right) \quad (7.173)$$

### 7.9.1 Solution Simplifications, $A = 0, T \rightarrow \infty$

If we substitute for this function into the original integral we have

$$\rho_S = -\frac{1}{4LR_0 \cos \theta_I} \int_{-L}^L (a\zeta' - b) e^{i(k_x^- x_0 + k_z^- \zeta(x_0))} dx_0 \quad (7.174)$$

with

$$\zeta(x_0) = A \sin\left(\frac{2\pi x_0}{T}\right), \zeta'(x_0) = \frac{2\pi A}{T} \cos\left(\frac{2\pi x_0}{T}\right) \quad (7.175)$$

two very obvious simplifications come to mind. If the amplitude of surface corrugations is very small or zero ( $A = 0$ ) the solution reduces to that of a flat surface and is expressed by (7.45) section (7.3.1). Similarly, if we let the period  $T \rightarrow \infty$  (provided  $x$  stays finite) the solution is also that of the flat case. This is true since

$$\lim_{A \rightarrow 0} \zeta = \lim_{A \rightarrow 0} \zeta' = 0 \quad (T > 0) \quad (7.176)$$

and

$$\lim_{T \rightarrow \infty} \zeta = \lim_{T \rightarrow \infty} \zeta' = 0 \quad (x \text{ finite}) \quad (7.177)$$

note that, strictly speaking, we are not considering surfaces with infinite period but as long as the ratio  $x/T \simeq 0$  this will suffice.

This implies that any solution must tend to the smooth case as either  $A \rightarrow 0$  or  $T \rightarrow \infty$ .

In addition, the periodic surface must obey the tangent plane criterion calculated in the appendix as

$$T \gg \sqrt{\pi A \lambda} \quad (7.178)$$

this being the criterion necessary for the valid use of Kirchhoff theory.

### 7.9.2 The Main Integral

Since  $\zeta$  is periodic with period  $2\pi$ , convert the range of integration by putting  $\frac{2\pi x_0}{T} \rightarrow x_0$  so the limits of the integral become  $x_0 : 0 \rightarrow 2\pi$  and  $dx_0 \rightarrow \frac{T}{2\pi} dx_0$  ie

$$\zeta = A \sin x_0 \quad (7.179)$$

$$\zeta^{2m} = \left(\frac{2\pi A}{T}\right)^{2m} \cos^{2m} x_0 \quad (7.180)$$

$$\rho_S = \frac{nT}{2\pi(n+\eta)R_0T} \sum_{m=0}^{\infty} \left(\frac{2\pi A}{T}\right)^{2m} \frac{R_0^{(2m)}}{(2m)!} \int_0^{2\pi} \cos^{2m} x_0 e^{ik_z^- A \sin x_0} dx_0 \quad (7.181)$$

$$= \frac{n}{2\pi(n+\eta)R_0} \sum_{m=0}^{\infty} \left(\frac{2\pi A}{T}\right)^{2m} \frac{R_0^{(2m)}}{(2m)!} \int_0^{2\pi} \cos^{2m} x_0 e^{ik_z^- A \sin x_0} dx_0 \quad (7.182)$$

The general solution for a periodic surface

### 7.9.3 Convergence Criteria for a Valid Solution

The series

$$\sum_{m=0}^{\infty} \frac{R_0^{(2m)}}{(2m)!} \zeta^{2m} \quad (7.183)$$

$$= \sum_{m=0}^{\infty} \left(\frac{2\pi A}{T}\right)^{2m} \frac{R_0^{(2m)}}{(2m)!} \cos^{2m} x_0 \quad (7.184)$$

is uniformly convergent provided (by the ratio test)

$$\lim_{m \rightarrow \infty} \left(\frac{2\pi A}{T}\right)^2 \left| \frac{R_0^{(2m+2)}}{R_0^{(2m)}} \right| \frac{|\cos^2 x_0|}{(2m+2)(2m+1)} < 1 \quad (7.185)$$

for  $m$  a positive integer and  $A, T$  positive and real. The result relies on

$$\left(\frac{2\pi A}{T}\right)^2 |\cos^2 x_0| \lim_{m \rightarrow \infty} \frac{1}{(2m+2)(2m+1)} \left| \frac{R_0^{(2m+2)}}{R_0^{(2m)}} \right| < 1 \quad (7.186)$$

Note that

$$\max |\cos^2 x_0| \leq 1 \quad (7.187)$$

so it is irrelevant for the determination of the criterion for convergence.

### Perpendicular Polarisation

The largest  $2m^{\text{th}}$  term for each  $R_0^{(2m)}$  in powers of  $N_2$  is given by (refer to appendix)

$$\frac{(2m)(2m-3)!}{2^{m-2}2^{m-2}(m-2)!} \left[ \frac{(N_2^2-1)^m}{N_2^{2m-3}(1+N_2)^3} \right] \quad (7.188)$$

where this term is the upper bound for each  $R_0^{(2m)}$ , for perpendicular polarisation. So the ratio  $R_0^{(2m+2)}/R_0^{(2m)}$  becomes

$$\frac{R_0^{(2m+2)}}{R_0^{(2m)}} = \frac{(2m+2)(2m-1)!}{2^{m-1}2^{m-1}(m-1)!} \frac{2^{m-2}2^{m-2}(m-2)!}{(2m)(2m-3)!} \times \left[ \frac{(N_2^2-1)^{m+1}}{N_2^{2m-1}(1+N_2)^3} \frac{N_2^{2m-3}(1+N_2)^3}{(N_2^2-1)^m} \right] \quad (7.189)$$

$$= \frac{(2m-1)(2m-2)(2m+2)}{4(2m)(m-1)} \left[ \frac{(N_2^2-1)}{N_2^2} \right] \quad (7.190)$$

$$= \frac{(2m-1)(m+1)}{2m} \left[ \frac{(N_2^2-1)}{N_2^2} \right] \quad (7.191)$$

the convergence criterion becomes

$$\left( \frac{2\pi A}{T} \right)^2 \lim_{m \rightarrow \infty} \left| \frac{(2m-1)(m+1)}{2m(2m+2)(2m+1)} \left[ \frac{(N_2^2-1)}{N_2^2} \right] \right| < 1 \quad (7.192)$$

then, since

$$\lim_{m \rightarrow \infty} \left| \frac{(2m+1)(m+1)}{2m(2m+2)(2m+1)} \right| = 0 \quad (7.193)$$

which implies the series is uniformly convergent independent of  $N_2$ . Notice also that for the  $2m^{\text{th}}$  term

$$\lim_{m \rightarrow \infty} \left( \frac{2\pi A}{T} \right)^{2m} \frac{R_0^{(2m)}}{(2m)!} \cos^{2m} x_0 \quad (7.194)$$

$$= \lim_{m \rightarrow \infty} \left( \frac{2\pi A}{T} \right)^{2m} \frac{(2m)(2m-3)!}{2^{2m-4}(2m+1)(2m+2)(m-2)!} \left[ \frac{(N_2^2-1)^m}{N_2^{2m-3}(1+N_2)^3} \right] \cos^{2m} x_0 = 0 \quad (7.195)$$

for  $A/T$  finite which is always true, this implies the series not only converges, but converges to the function  $R$ .

**Parallel Polarisation**

For parallel polarisation the  $2m^{\text{th}}$  term is

$$\frac{(2m)(2m-3)!}{2^{m-2}2^{m-2}(m-2)!} \left[ \frac{(N_2^2-1)^m}{N_2^{2m}(1+N_2)^3} \right] \quad (7.196)$$

substitute into the ratio  $R_0^{(2m+2)}/R_0^{(2m)}$

$$\frac{R_0^{(2m+2)}}{R_0^{(2m)}} = \frac{(2m+2)(2m-1)!}{2^{m-1}2^{m-1}(m-1)!} \frac{2^{m-2}2^{m-2}(m-2)!}{(2m)(2m-3)!} \times \left[ \frac{(N_2^2-1)^{m+1}}{N_2^{2m+2}(1+N_2)^3} \frac{N_2^{2m}(1+N_2)^3}{(N_2^2-1)^m} \right] \quad (7.197)$$

$$= \frac{(2m-1)(m+1)}{2m(m-1)} \left[ \frac{(N_2^2-1)}{N_2^2} \right] \quad (7.198)$$

the convergence criterion becomes

$$\left( \frac{2\pi A}{T} \right)^2 \lim_{m \rightarrow \infty} \left| \frac{(2m-1)(m+1)}{2m(2m+2)(2m+1)} \left[ \frac{(N_2^2-1)}{N_2^2} \right] \right| < 1 \quad (7.199)$$

the same as the one above. So the series converges as well. The higher power of  $N_2$  has no effect.

**7.9.4 Evaluation of the Integral  $\int_0^{2\pi} \cos^{2m} x_0 e^{ik_z^- A \sin x_0} dx_0$** 

Using the definition of cosine we have

$$\cos^{2m} x_0 = \left( \frac{e^{ix_0} + e^{-ix_0}}{2} \right)^{2m} \quad (7.200)$$

$$= \frac{e^{-2mix_0}}{2^{2m}} (1 + e^{2ix_0})^{2m} \quad (7.201)$$

$$= \frac{e^{-2mix_0}}{2^{2m}} \left( 1 + 2me^{2ix_0} + \frac{2m(2m-1)}{2!} e^{4ix_0} + \frac{2m(2m-1)(2m-2)}{3!} e^{6ix_0} + \dots \right. \\ \left. + \frac{2m(2m-1)\dots(1)}{(2m)!} e^{2mix_0} \right) \quad (7.202)$$

$$= \frac{1}{2^{2m}} \left( e^{-2mix_0} + 2me^{(2-2m)ix_0} + \frac{2m(2m-1)}{2!} e^{(4-2m)ix_0} + \dots \right. \\ \left. + \frac{2m(2m-1)(2m-2)}{3!} e^{(6-2m)ix_0} + \dots + 1 \right) \quad (7.203)$$

$$= \sum_{j=0}^{2m} \frac{1}{2^{2m}} \binom{2m}{j} e^{(2j-2m)ix_0} \quad (7.204)$$

where

$$\binom{2m}{j} = \frac{2m(2m-1)(2m-2)(2m-3)\dots(2m-j+1)}{(j)!} \quad (7.205)$$

by the binomial theorem which converges for all integer  $m$ . The integral becomes

$$\rho_S = \frac{n}{2\pi(n+\eta)R_0} \sum_{m=0}^{\infty} \left(\frac{2\pi A}{T}\right)^{2m} \frac{R_0^{(2m)}}{(2m)!R_0} \int_0^{2\pi} \cos^{2m} x_0 e^{ik_z^- A \sin x_0} dx_0 \quad (7.206)$$

$$= \frac{n}{2R_0\pi(n+\eta)} \sum_{m=0}^{\infty} \left(\frac{2\pi A}{T}\right)^{2m} \frac{R_0^{(2m)}}{(2m)!} \int_0^{2\pi} \sum_{j=0}^{2m} \frac{1}{2^{2m}} \binom{2m}{j} e^{(2j-2m)ix_0} e^{ik_z^- A \sin x_0} dx_0 \quad (7.207)$$

$$= \frac{n}{R_0(n+\eta)} \sum_{m=0}^{\infty} \left(\frac{2\pi A}{T}\right)^{2m} \frac{R_0^{(2m)}}{(2m)!} \sum_{j=0}^{2m} \frac{1}{2^{2m}} \binom{2m}{j} \frac{1}{2\pi} \int_0^{2\pi} e^{i[k_z^- A \sin x_0 - (2m-2j)x_0]} dx_0 \quad (7.208)$$

The integral is easily evaluated in terms of Bessel functions of the first kind (see, [95])

$$\frac{1}{2\pi} \int_0^{2\pi} e^{i[k_z^- A \sin x_0 - (2m-2j)x_0]} dx_0 = J_{(2m-2j)}(k_z^- A) \quad (7.209)$$

since  $k_z^- = -\frac{4\pi}{\lambda}$  because  $\theta_I = \theta_S = 0$ . Where  $J_{2j}$  is an even ordered Bessel function of the first kind. The final result being

$$\rho_S = \frac{n}{R_0(n+\eta)} \sum_{m=0}^{\infty} \sum_{j=0}^{2m} \left(\frac{2\pi A}{T}\right)^{2m} \frac{R_0^{(2m)}}{(2m)!} \frac{1}{2^{2m}} \binom{2m}{j} J_{(2m-2j)}\left(\frac{4\pi A}{\lambda}\right) \quad (7.210)$$

since  $J_{2j}(-x) = J_{2j}(x)$ , [95]. This forms the general solution to the scattering integral for periodic surface corrugations in the specular direction at normal incidence.

### 7.9.5 The Edge Terms

The edge terms are given in (7.171) as

$$= \frac{1}{LR_0} \sum_{m=0}^{\infty} \frac{R_0^{(2m)}}{(2m)!} \int_0^{\eta T} \zeta^{2m} \cos(k_z^- \zeta) dx_0 \quad (7.211)$$

substituting for  $\zeta$  as a sinusoid and changing the integration variable to  $X_0 = \frac{2\pi x_0}{\eta T}$ , provided  $\eta \neq 0$ . If  $\eta = 0$ , the edge terms may be ignored and the solution is that of the main integral only.

$$\zeta = A \sin X_0, \zeta' = \frac{2\pi A}{T} \cos X_0, dx_0 = \frac{\eta T}{2\pi} dX_0, X_0 : 0 \rightarrow 2\pi, \quad (7.212)$$

$$= \frac{\eta}{2\pi(n+\eta)R_0} \sum_{m=0}^{\infty} \left(\frac{2\pi A}{T}\right)^{2m} \frac{R_0^{(2m)}}{(2m)!} \int_0^{2\pi} \cos^{2m} \eta X_0 \cos(k_z^- A \sin \eta X_0) dX_0 \quad (7.213)$$

expressing the first cosine term as a series and the second by its definition we have two integrals both of which have been done in the previous section, ie (also putting  $X_0 \rightarrow x_0$  again)

$$= \frac{\eta}{4\pi(n+\eta)R_0} \sum_{m=0}^{\infty} \left(\frac{2\pi A}{T}\right)^{2m} \frac{R_0^{(2m)}}{(2m)!} \sum_{j=0}^{2m} \frac{1}{2^{2m}} \binom{2m}{j} \left\{ \int_0^{2\pi} e^{i[k_z^- A \sin \eta x_0 - \eta(2m-2j)x_0]} dx_0 + \right. \quad (7.214)$$

$$\left. \int_0^{2\pi} e^{i[-k_z^- A \sin \eta x_0 - \eta(2m-2j)x_0]} dx_0 \right\} \quad (7.215)$$

$$= \frac{1}{4\pi(n+\eta)R_0} \sum_{m=0}^{\infty} \left(\frac{2\pi A}{T}\right)^{2m} \frac{R_0^{(2m)}}{(2m)!} \sum_{j=0}^{2m} \frac{1}{2^{2m}} \binom{2m}{j} \left\{ \int_0^{2\pi} e^{i[k_z^- A \sin(\eta x_0) - (2m-2j)(\eta x_0)]} d(\eta x_0) + \right. \quad (7.216)$$

$$\left. \int_0^{2\pi} e^{i[-k_z^- A \sin(\eta x_0) - \eta(2m-2j)(\eta x_0)]} d(\eta x_0) \right\} \quad (7.217)$$

then integrating over the variable  $\eta x_0$  instead of  $x_0$  we find again

$$= \frac{1}{2(n+\eta)R_0} \sum_{m=0}^{\infty} \left(\frac{2\pi A}{T}\right)^{2m} \frac{R_0^{(2m)}}{(2m)!} \sum_{j=0}^{2m} \frac{1}{2^{2m}} \binom{2m}{j} \left\{ J_{(2m-2j)}(k_z^- A) + J_{(2m-2j)}(-k_z^- A) \right\} \quad (7.218)$$

since  $J_{2u}(-x) = J_{2u}(x)$

$$= \frac{1}{(n+\eta)R_0} \sum_{m=0}^{\infty} \left(\frac{2\pi A}{T}\right)^{2m} \frac{R_0^{(2m)}}{(2m)!} \sum_{j=0}^{2m} \frac{1}{2^{2m}} \binom{2m}{j} J_{(2m-2j)}(k_z^- A) \quad (7.219)$$

### 7.9.6 The Complete Solution

#### Edge Terms included, $\eta \neq 0$

The complete solution to the scattering problem being

$$\rho_S = \frac{n+1}{(n+\eta)R_0} \sum_{m=0}^{\infty} \sum_{j=0}^{2m} \left(\frac{2\pi A}{T}\right)^{2m} \frac{R_0^{(2m)}}{(2m)!} \frac{1}{2^{2m}} \binom{2m}{j} J_{(2m-2j)}\left(\frac{4\pi A}{\lambda}\right) (\eta \neq 0) \quad (7.220)$$

the only difference in the terms above, (7.219), being the absence of  $n$  in the edge term, the edge terms contribute significantly to the total scattering solution being of the same order as the original solution.

#### Edge Terms Excluded, $\eta = 0$

Note that if  $\eta = 0$  the edge integrals are zero leaving us with the original solution only, ie

$$\rho_S = \frac{1}{R_0} \sum_{m=0}^{\infty} \sum_{j=0}^{2m} \left(\frac{2\pi A}{T}\right)^{2m} \frac{R_0^{(2m)}}{(2m)!} \frac{1}{2^{2m}} \binom{2m}{j} J_{(2m-2j)}\left(\frac{4\pi A}{\lambda}\right) (\eta = 0) \quad (7.221)$$

This result cannot be obtained by a substitution of  $\eta = 0$  since the edge integral is only valid if  $\eta \neq 0$ . However recalling the original integral if  $\eta = 0$  the edge terms become zero leaving us only the main integral which has the solution given above.

#### Solution Check

The integral is obviously finite and the extension to infinite surfaces is straightforward. Applying the limit as  $n \rightarrow \infty$ , since  $L = (n+\eta)T$  and  $T$  is finite we get

$$\rho_S = \frac{1}{R_0} \sum_{m=0}^{\infty} \sum_{j=0}^{2m} \left(\frac{2\pi A}{T}\right)^{2m} \frac{R_0^{(2m)}}{(2m)!} \frac{1}{2^{2m}} \binom{2m}{j} J_{(2m-2j)}\left(\frac{4\pi A}{\lambda}\right) \quad (7.222)$$

identical to the edge free case. Similarly we may check for the simplifications  $A = 0$  and  $T \rightarrow \infty$ . Remembering that the first term of the series (7.184) is one (independent of  $T$ ,  $J_{2m}(0) = 1$ ), then, all other terms are zero if either  $A = 0$  or  $T \rightarrow \infty$ . As expected we



obtain the flat surface scattering coefficient  $\rho_S = 1$ . The solution satisfies all requirements, however it is only a special case, specular at normal incidence. For a more thorough investigation and graphical solutions portraying all aspects of the problem we need a numerical solution. This will be considered in the following chapters.

### 7.9.7 Comparison to Perfect Conducting Case

Substitute as above  $\theta_S = \theta_I = 0$ ,  $\zeta = A \sin(2\pi x_0/T)$  etc in the solution (7.133) for the perfectly Conducting case for an odd function we get

$$\begin{aligned} \rho^{\parallel,\perp}(\theta_I, \theta_S) &= \frac{\pm n}{(n + \eta)T} \int_0^T e^{ik^- \cdot r_0} dx_0 + \frac{\pm 1}{4(n + \eta)T} \int_0^{\eta T} (e^{ik_z^- \zeta} + e^{-ik_z^- \zeta}) dx_0 \quad (7.223) \\ &= \frac{\pm n}{(n + \eta)T} \int_0^T e^{ik_z^- A \sin(\frac{2\pi x_0}{T})} dx_0 + \frac{\pm 1}{4(n + \eta)T} \int_0^{\eta T} (e^{ik_z^- A \sin(\frac{2\pi x_0}{T})} + e^{-ik_z^- A \sin(\frac{2\pi x_0}{T})}) dx_0 \quad (7.224) \end{aligned}$$

again converting to  $x_0 : 0 \rightarrow 2\pi$

$$= \frac{\pm n}{2\pi(n + \eta)} \int_0^{2\pi} e^{ik_z^- A \sin x_0} dx_0 + \frac{\pm T}{4\pi(n + \eta)T} \int_0^{2\pi} (e^{ik_z^- A \sin(\eta x_0)} + e^{-ik_z^- A \sin(\eta x_0)}) d(\eta x_0) \quad (7.225)$$

$$= \frac{\pm n}{(n + \eta)} J_0\left(\frac{4\pi A}{\lambda}\right) + \frac{\pm 1}{n + \eta} J_0\left(\frac{4\pi A}{\lambda}\right) \quad (7.226)$$

$$= \frac{\pm(n + 1)}{(n + \eta)} J_0\left(\frac{4\pi A}{\lambda}\right) \quad (7.227)$$

using  $J_0(-x) = J_0(x)$ . This matches the solution with the expanded reflection coefficient when the reflection coefficient derivatives are all zero since  $R = \pm 1$ .

### 7.9.8 The Approximate Solution

As a first order correction (1st order in  $R_0^{(m)}$ ) to the solution take just the sum from  $m = 0 \rightarrow 1$  the solution becomes

$$\rho_S = \frac{n + 1}{R_0(n + \eta)} \sum_{m=0}^1 \sum_{j=0}^{2m} \left(\frac{2\pi A}{T}\right)^{2m} \frac{R_0^{(2m)}}{(2m)!} \frac{1}{2^{2m}} \binom{2m}{j} J_{(2m-2j)}\left(\frac{4\pi A}{\lambda}\right) \quad (7.228)$$

$$= \frac{n+1}{R_0(n+\eta)} \left\{ R_0^{(0)} J_0\left(\frac{4\pi A}{\lambda}\right) + \frac{R_0^{(2)}}{8} \left(\frac{2\pi A}{T}\right)^2 \left[ J_0\left(\frac{4\pi A}{\lambda}\right) + J_2\left(\frac{4\pi A}{\lambda}\right) \right] \right\} \quad (7.229)$$

The first approximation to the scattering integral is the first term in (7.229) or

$$\rho_S = \frac{n+1}{R_0(n+\eta)} \left\{ R_0^{(0)} J_0\left(\frac{2\pi A}{\lambda}\right) + O(R_0^{(2)}) \right\} \quad (7.230)$$

then approximately

$$\rho_S \simeq \frac{(n+1)J_0\left(\frac{4\pi A}{\lambda}\right)}{(n+\eta)} \quad (7.231)$$

if, in addition, the dimensions of the scattering surface are an exact integer multiple of the period, ie  $\eta = 0$  (for large  $n$ )

$$\rho_S \simeq J_0\left(\frac{4\pi A}{\lambda}\right) \quad (7.232)$$

This is a useful expression considering that the terms of  $O(2)$  and above are in powers of  $2\pi A/T$  which of course is already a small value. Similarly, higher order Bessel functions do not contribute much to the solution as it is well known that

$$\lim_{n \rightarrow \infty} J_n(x) \rightarrow 0 \text{ for } x \text{ finite} \quad (7.233)$$

(refer to appendix). In that case we find

$$R_S = R_0 J_0\left(\frac{4\pi A}{\lambda}\right) \quad (7.234)$$

then for a specific polarisation

$$R_y = R_0 R_0^* \left[ J_0\left(\frac{4\pi A}{\lambda}\right) \right]^2 \quad (7.235)$$

giving for the average reflectivity

$$R_y = \left[ J_0\left(\frac{4\pi A}{\lambda}\right) \right]^2 \frac{R_0^{\parallel} R_0^{*\parallel} + R_0^{\perp} R_0^{*\perp}}{2} \quad (7.236)$$

where this is only one kind of averaging technique, others such as the square root average is also possible, we will however use the simplest one. If we define

$$R_{y_0} = \frac{R_0^{\parallel} R_0^{*\parallel} + R_0^{\perp} R_0^{*\perp}}{2} \quad (7.237)$$

the flat surface reflectivity, then the rough surface emissivity is defined by

$$\epsilon = 1 - \left[ J_0 \left( \frac{4\pi A}{\lambda} \right) \right]^2 R_{y_0} \quad (7.238)$$

N.B. : If we were to have considered the order of the Bessel function rather than the derivatives of  $R$ , then we would obtain the expression

$$\rho_S \simeq J_0 \left( \frac{4\pi A}{\lambda} \right) \left[ 1 + \frac{1}{4N_2} \left( \frac{2\pi T}{T} \right)^2 \right] \quad (7.239)$$

since  $R_0^2 = \mp(2/N_2)R_0$ . Bessel function of order 2 or above have been discarded. This presents the solution to the scattering problem up to zero order Bessel functions and second order in the derivatives of  $R$ . It includes the effects of both optical roughness  $A/\lambda$  and correlation length  $A/T$ .

The influence of the second of these parameters will be discussed further in the next section. For the moment we will assume a solution of the form

$$\rho_S \simeq J_0 \left( \frac{4\pi A}{\lambda} \right)$$

with the second parameter assumed smaller than 1 in most instances.

### 7.9.9 Consequences of the Periodic Solution

The solution of the scattering problem is

$$\epsilon = 1 - \left[ J_0 \left( \frac{4\pi A}{\lambda} \right) \right]^2 R_{y_0} \quad (7.240)$$

this has several important consequences.

The Bessel function  $J_0$  has the properties of decaying rapidly with distance from the origin, it oscillates frequently with the zeros of the oscillation determined by the zeros of  $J_0$  which occur when  $\frac{4\pi A}{\lambda}$  is coincident with these zeros. They occur approximately when

$$A = \frac{\lambda}{4\pi} \times \{j_{0,1}, j_{0,2}, j_{0,3}, \dots\} , [1] \quad (7.241)$$

where  $j_{0,i}$  refers to the  $i^{th}$  zeros of the zero order Bessel function (refer to appendix). The first of these is the most important since this zero determines the point after which the emissivity is no longer influenced by the Bessel term and instead becomes solely dependent on the smooth surface reflection coefficient. This is true since as the ratio  $A/\lambda$  approaches zero  $J_0$  approaches one. As we move further away from the origin we meet several zeros of  $J_0$  and also note the decay of the amplitude of  $J_0$ . This implies strong oscillations for the emissivity as we approach the origin as well as a tendency to approach one as we get closer to the origin. In summary the emissivity :

- will oscillate severely for  $A/\lambda \rightarrow 0$
- will oscillate about one for small values of  $A/\lambda$
- will equal one when  $\lambda \rightarrow 0$
- oscillations will increase in period finally damping out at the first zero of  $J_0$ , ie  $4\pi A/\lambda = j_{0,1}$
- will approach that of the smooth case for values of  $4\pi A/\lambda > j_{0,1}$
- will be exactly that of the smooth case if  $A = 0$  or  $\lambda \rightarrow \infty$
- will vary more with roughness the larger the value of  $A/\lambda$

here our ratio,  $A/\lambda$ , plays the role of optical roughness  $\sigma/\lambda$ . These results are demonstrated in Figures 7.9.1-7.9.4. The first three figures are graphs drawn on a Macintosh computer using *Mathematica*. The function drawn is given by

$$1 - \left[ J_0 \left( \frac{4\pi A}{\lambda} \right) \right]^2 \quad (7.242)$$

(Note that we did not include the reflectivity  $R_{y_0}$  see below for a discussion) at the amplitudes  $A = 0.1\mu\text{m}, 1\mu\text{m}, 10\mu\text{m}$  for Figures 7.9.1, 7.9.2 and 7.9.3 respectively. As a comparison, the calculated result for a roughness amplitude of  $5\mu\text{m}$  is drawn in Figure 7.9.4. The similarity to Figure 7.9.2 is striking. We see immediately the accuracy of our

analysis regarding the effect of roughness on the graphs of emissivity verses wavelength. Small degrees of roughness produce minimal oscillations which decay away rapidly after the first zero is reached at about  $1\mu\text{m}$  in Figure 7.9.1. An increase in roughness to that of Figure 7.9.2 stretches out the wavelength region for oscillations until the point  $\lambda = 5\mu\text{m}$  is reached. Finally Figure 7.9.3 has the highest degree of roughness which oscillates near  $\epsilon = 1$  for a very long wavelength range. This result, in addition to being very accurate as a first order solution, also demonstrates that the emissivity is relatively independent of the reflection coefficient as compared with the roughness characteristics.

As regards the extra terms in the series they will contribute as first order corrections to solution above. Taking

$$\rho_S \simeq \frac{1}{R_0} \left\{ R_0^{(0)} J_0 \left( \frac{4\pi A}{\lambda} \right) + \frac{R_0^{(2)}}{8} \left( \frac{2\pi A}{T} \right)^2 \left[ J_0 \left( \frac{4\pi A}{\lambda} \right) + J_2 \left( \frac{4\pi A}{\lambda} \right) \right] \right\} \quad (7.243)$$

using the fact that

$$R_0^{(2)} = \mp \frac{2}{N_2} R_0 \quad (7.244)$$

$$\rho_S \simeq J_0 \left( \frac{4\pi A}{\lambda} \right) + \frac{1}{4N_2} \left( \frac{2\pi A}{T} \right)^2 \left[ J_0 \left( \frac{4\pi A}{\lambda} \right) + J_2 \left( \frac{4\pi A}{\lambda} \right) \right] \quad (7.245)$$

$$\simeq J_0 \left( \frac{4\pi A}{\lambda} \right) \left[ 1 + \frac{1}{4N_2} \left( \frac{2\pi A}{T} \right)^2 \right] + \frac{1}{4N_2} \left( \frac{2\pi A}{T} \right)^2 J_2 \left( \frac{4\pi A}{\lambda} \right) \quad (7.246)$$

The solution is dominated by the  $J_0$  term with the extra  $J_2$  being a smaller addition.  $J_2$  has a smaller amplitude and as such has less effect on the result than does the first term. The extra term in the first expression made up of the ratio  $2\pi A/T$  acts like the correlation length as it relates the surface height to the period (gradient). Depending on the size of this ratio its influence varies accordingly. For large periods the ratio becomes very small and as expected the smooth case is retrieved. Note that usually we are dealing with ratios less than 0.2 at the most. Their influence is certainly not negligible but its effect is reduced due to the squaring of the ratio. We must not neglect the presence of the refractive index which may effect the solution through its electrical properties and its temperature dependence. In effect, the extra term is like adding another oscillatory

function to the original  $J_0$  ie

$$J_0 \left( \frac{4\pi A}{\lambda} \right) + \frac{1}{4N_2} \left( \frac{2\pi A}{T} \right)^2 J_0 \left( \frac{4\pi A}{\lambda} \right) \quad (7.247)$$

the first of these is oscillatory and the second is oscillatory with the same period but differing amplitude, the result is to effectively increase the size of the oscillations depending on the size of  $T$ . That is, a large  $T$  value ensures a small increase in amplitude of oscillation, a smaller  $T$  value, such that the ratio  $A/T$  becomes comparable to about 0.3, will significantly increase the amplitude of oscillation and delay the decay of the wave generated by  $J_0$ . This means the emissivity oscillation for small wavelengths is strong and dies out over a longer wavelength range. The position at which the solution reverts to the smooth case is still the same but the amplitude variation is larger and the return to the smooth case is more gradual. This effect is added to with the addition of  $J_2$  which also alters the period of oscillation. So, the larger the size of  $A/T$  the more oscillation is produced. However, it must be stressed that its effect is nowhere near as significant as the ratio  $A/\lambda$  which to a good degree of approximation specifies the effect of roughness, and its influence on the emissivity. So, as already mentioned, the dominant roughness parameter is  $A/\lambda$  with the extra ratio  $A/T$  a secondary influence. This is equivalent to saying the optical roughness plays a dominating role and the correlation length being an added smaller contribution. This is supported by the presence of the refractive index which increases with wavelength therefore decreasing the effect of the second term  $\frac{1}{4N_2} \left( \frac{2\pi A}{T} \right)^2$ .

We should also note that since  $N_2$  also increases in size with temperature (through conductivity) the temperature effects on a rough surface is small.

### 7.9.10 Closer Analysis of the second order term $1/4N_2(2\pi A/T)^2$

The expression for the scattering coefficient

$$\rho_S = J_0 \left( \frac{4\pi A}{\lambda} \right) \left[ 1 + \frac{1}{4N_2} \left( \frac{2\pi A}{T} \right)^2 \right]$$

can be used to find the reflectivity as

$$R_y = J_0^2 \left( \frac{4\pi A}{\lambda} \right) R_0 R_0^* \left[ 1 + \left( \frac{\pi A}{T} \right)^4 \frac{1}{N_2 N_2^*} \right]$$

Therefore the second term in brackets, which acts as a second order contribution to the reflectivity, will be significant when

$$\left( \frac{\pi A}{T} \right)^4 \frac{1}{N_2 N_2^*} \geq 1$$

this occurs when

$$\frac{A}{T} \geq \frac{1}{\pi} (N_2 N_2^*)^{1/4}$$

where  $N_2 = n_2 + i\eta_2$ , therefore we find

$$\frac{A}{T} \geq \frac{1}{\pi} (n_2^2 + \eta_2^2)^{1/4}$$

Now, from section (2.4.2) we already know that both the real and complex parts of the refractive index  $N_2$  are proportional to  $\sqrt{\sigma_2 \lambda}$ . Therefore we find

$$T \leq \frac{\pi A}{(\sigma_2 \lambda)^{1/4}} \quad (A \neq 0)$$

Now, from the tangent plane criterion we already know that the period,  $T$ , is confined by the inequality

$$T \gg \sqrt{\pi A \lambda}$$

We can plot two graphs of  $T$  versus  $\lambda$  for each of the two inequalities above. Note that the graph of  $T = \pi A / (\sigma_2 \lambda)^{1/4}$  represents a family of curves for each particular value of  $\sigma_2$ . This term shifts the point at which the two graphs intersect from left to right as  $\sigma$  decreases in size. This behaviour can be observed in Figure 7.9.6. The shaded areas in Figure 7.9.5 represent the respective regions of validity of each inequality. The point of intersection may be determined by equating the two functions and we obtain

$$(\lambda_i, T_i) = \left[ \left( \frac{\pi^2 A^2}{\sigma_2} \right)^{1/3}, \left( \frac{\pi^5 A^5}{\sigma_2} \right)^{1/6} \right]$$

( $i \equiv \text{intersectionpoint}$ ). The region of intersection we wish to look at lies in the area defined by

$$0 < \lambda \leq \frac{(\pi A)^{2/3}}{\sigma_2^{1/3}}$$

The region of validity is the cross hatched area on the left of Figure 7.9.5. This region can be extended into longer wavelengths by extending the point of intersection. This can be done by changing the ratio  $A^2/\sigma_2$ , for example, strong conductors push this point close to the origin and insulators extend the region to infinity. Since  $A > 0$  and is usually a great deal less than  $\sigma_2$  the shape of each function is mainly controlled by the conductivity of the oxide except when the amplitude and conductivity are of the same order. This occurs when the conductivity is very small, of the order of  $\mu(\Omega m)^{-1}$ .

The different oxides vary in their conductivities a great deal. The conductivity of magnetite is very low at small temperatures, eg 200°C, whereas the conductivities of both haematite and wustite never reach very low values. Wustite maintains a relatively constant conductivity over a range of temperatures, 100-1000°C, of the order of  $10^4 (\Omega m)^{-1}$ . In that case the region where the second order term becomes significant is a small region confined close to the origin with small wavelengths and large periods. See Figures 7.9.7 and 7.9.8

This implies that the effect of this second order term is relatively small except at small wavelengths and lower temperatures. If the oxide is mainly wustite the ratio,  $A^2/\sigma_2$ , is always small and the reflectivity is controlled by the optical roughness in the main. The effects of correlation length should be minimal.



## Chapter 8

# Oxidised Rough Surfaces

### 8.1 Introduction

The work of Beckmann has been used in theoretical analyses of surfaces that are not only rough, but also possess an extra layer of material on top of a substrate. The film interfaces, film/steel & film/air, are considered rough, [58]. To the authors knowledge, no research has been carried out dealing with the emissivity of oxidised steel surfaces where the layer of oxide and the steel surface are treated as roughened. It has always been treated either as intractable to theoretical approaches or as too time consuming. The impression was one of, ‘ the work on flat oxidised surfaces was more than adequate for a full understanding ’. Of course, as has been noted earlier the research on rough steel surfaces alone brought out a considerably number of new aspects.

However, in terms of layered, rough surface scattering, a good deal has been considered. These aspects are

1. Absorption in the film is included.
2. The boundaries of both the film/air and film/substrate are assumed rough in some way. Two types are considered, one where both boundaries are identical in profile, and two, each boundary has a different profile shape.

3. Analytic solutions are not produced.
4. Sinusoidal surfaces are not considered.
5. The treatment is statistical.

This being the case, the method of Ohlidal, [58], is useful for further research on rough surface emissivity. The new research will consider

1. All the extra aspects considered in the previous two cases. Multilayer flat surface scattering and rough surface scattering of unoxidised surfaces are included. This means the electrical properties, the surface roughness, the film layer thickness, interference phenomena, absorption properties and semiconducting characteristics of iron-oxides are included.
2. Sinusoidal periodic profiles for both boundaries are analysed.
3. The interaction between the film's electrical properties and thickness are contrasted to the roughness characteristics of the two boundaries.
4. Interference effects and roughness aspects are analysed.
5. An analytic solution is found.

This problem involves the presence of an iron-oxide film on top of steel. In the following theoretical construction the film will be assumed periodically rough in the same sense as the substrate surface itself. This means that each boundary, the first between the substrate and the film, the second the film and air, will possess the same surface undulation. Both boundaries will then be described by the function,  $\zeta = \zeta(x)$ , except that the top boundary will be raised by the average thickness of the film. This kind of film is often called an identical film, [58], or a uniform film, [55].

We will follow the work of Ohlidal et al, [58], [59], [60], in the theoretical problem construction which is based on the scattering theory of Beckmann, used in the previous chapter.

It is just an extension of the Kirchhoff method.

It should be stated that we will only investigate the structure of identical films and not look at general thin films, leaving this for future study. Similarly, we will restrict ourselves to films which cover the substrate uniformly not partially, this aspect has been studied by, [55].

The chapter structure is as follows. First the basis of the work is considered, the extended reflection coefficients of single layer films is investigated, including the phase change on traversing the oxide film. The solution is then found via the very successful technique of the earlier chapter on rough unoxidised steel surfaces. Finally, its consequences are analysed with respect to an objects' emissivity.

## 8.2 Constraints of the Method

A plane monochromatic EM wave is incident upon a rough steel surface covered in a thin film of iron-oxide, also rough, both of these media are assumed homogeneous, isotropic and linear. Both media are assumed to be absorbing through the presence of a complex refractive index in each material. The electrical properties of the substrate will be assumed that of iron with conduction effects described by the conductivity,  $\sigma_{c_3} = \sigma_{c_3}(T)$ , and the other constants being kept at the free space values ie  $\mu = \mu_0, \varepsilon = \varepsilon_0$ . Similarly, the absorption characteristics of the thin oxide film will be governed by its conductivity  $\sigma_{c_2} = \sigma_{c_2}(T)$ , the subscripts  $\{1, 2, 3\}$  increasing from the top down, 1 = air, 2 = iron-oxide, 3 = iron, the other properties assumed identical to free space. Similarly the indices are given by  $N_1$  (air),  $N_2$  (oxide) and  $N_3$  (iron). The iron-oxide will be taken to be only *FeO* this being the dominant layer at high temperatures.

The problem will of course be a scalar diffraction problem with the rough surface one dimensional so that depolarisation does not enter the analysis. The polarisation will be considered parallel ( $\parallel$ ) and ( $\perp$ ). The Kirchhoff method assumptions will be used here as previously, ie

- The only scattering that takes place will be surface scattering with the possibilities of internal inhomogeneities in the film not considered.
- Diffraction effects are expected to occur due to the height variations.
- Shadowing and multiple scattering effects will be neglected.
- The scattered field is measured only in the Fraunhofer (far-field) zone of the body so that the dimensions of the irradiated surface are assumed much larger than the wavelength (incident radiation), ie

$$\frac{L}{r} \ll 1, \frac{kL^2}{r} \ll 1 \quad (8.1)$$

although much smaller than the observation distance.

- The Kirchhoff boundary conditions are obeyed on the surface of the scatterer, ie

$$E(\mathbf{r}_0) = (1 + R(\mathbf{r}_0))E_I(\mathbf{r}_0), \frac{\partial E(\mathbf{r}_0)}{\partial n_0} = i[(1 - R(\mathbf{r}_0))(\hat{\mathbf{n}}_0 \cdot \mathbf{k}_I)]E_I(\mathbf{r}_0) \quad (8.2)$$

These assumptions are of course subject to the tangent plane criterion such that

$$T \gg \sqrt{\pi A \lambda} \quad (8.3)$$

As in the unoxidised case the scattered field in the Fraunhofer zone is given by

$$E_S(\mathbf{r}) = \int_S E(\mathbf{r}_0) \frac{\partial G(\mathbf{r}, \mathbf{r}_0)}{\partial n_0} - G(\mathbf{r}, \mathbf{r}_0) \frac{\partial E(\mathbf{r}_0)}{\partial n_0} dS_0 \quad (8.4)$$

which reduces to

$$\rho_S = -\frac{1}{4LR_{f_0} \cos \theta_I} \int_{-L}^L (a\zeta' - b) e^{i(k_x^- x_0 + k_z^- \zeta(x_0))} dx_0 \quad (8.5)$$

the only difference being that the local reflection coefficient is the Fresnel coefficient for a smooth two layer structure, not just a flat surface. In the above case called  $R_f$  indicating a filmed surface.

### 8.2.1 Fresnel Coefficients

This is commonly expressed as

$$R_f = \frac{r_1 + r_2 e^{i\delta}}{1 + r_1 r_2 e^{i\delta}} \quad (8.6)$$

where  $r_1$  and  $r_2$  are the usual Fresnel coefficients at each surface,  $r_1$  the air/oxide boundary and  $r_2$  the oxide/iron boundary. The exponential factor represents the effect of thin film interference in the oxide layer. This is given by, [58]

$$\delta = \left( \frac{4\pi}{\lambda} \right) N_2 d \cos \vartheta \cos \theta_t \quad (8.7)$$

here  $N_2$  is now the refractive index of the oxide,  $d$ , the film thickness and  $\theta_t$  the angle of refraction just inside the film. The individual Fresnel coefficients are given by

$$r_1^{\parallel}(\mathbf{r}_0) = \frac{N_2 \cos \vartheta_1 - \cos \theta_{t1}}{N_2 \cos \vartheta_1 + \cos \theta_{t1}} \quad (8.8)$$

$$r_1^{\perp}(\mathbf{r}_0) = \frac{\cos \vartheta_1 - N_2 \cos \theta_{t1}}{\cos \vartheta_1 + N_2 \cos \theta_{t1}} \quad (8.9)$$

where the "1" subscript indicates the upper (oxide) boundary.

$$r_2^{\parallel}(\mathbf{r}_0) = \frac{N_3 \cos \vartheta_2 - N_2 \cos \theta_{t2}}{N_3 \cos \vartheta_2 + N_2 \cos \theta_{t2}} \quad (8.10)$$

$$r_2^{\perp}(\mathbf{r}_0) = \frac{N_3 \cos \vartheta_2 - N_3 \cos \theta_{t2}}{N_3 \cos \vartheta_2 + N_3 \cos \theta_{t2}} \quad (8.11)$$

$\vartheta_i, \{i = 1, 2\}$  are the local angles of incidence and angles of refraction at subsequent interfaces. The refractive indices are,  $N_2$ , oxide, and  $N_3$ , iron respectively. Since the surface slopes are small (tangent plane approximation), then the local angle of incidence,  $\vartheta_2$ , at the iron interface may be assumed to be approximately the refraction angle from the oxide interface ie

$$\vartheta_2 = \theta_{t1} \quad (8.12)$$

consequently, the angles will be renamed as follows

$$\vartheta_1 = \vartheta \quad \theta_{t1} = \theta_t \quad \vartheta_2 = \theta_t \quad \theta_{t2} = \theta'_t \quad (8.13)$$

then the reflection coefficients become

$$r_1^{\parallel}(\mathbf{r}_0) = \frac{N_2 \cos \vartheta - \cos \theta_t}{N_2 \cos \vartheta + \cos \theta_t} \quad (8.14)$$

$$r_1^{\perp}(\mathbf{r}_0) = \frac{\cos \vartheta - N_2 \cos \theta_t}{\cos \vartheta + N_2 \cos \theta_t} \quad (8.15)$$

$$r_2^{\parallel}(\mathbf{r}_0) = \frac{N_3 \cos \theta_t - N_2 \cos \theta'_t}{N_3 \cos \theta_t + N_2 \cos \theta'_t} \quad (8.16)$$

$$r_2^{\perp}(\mathbf{r}_0) = \frac{N_3 \cos \theta_t - N_3 \cos \theta'_t}{N_3 \cos \theta_t + N_3 \cos \theta'_t} \quad (8.17)$$

The refraction angles can be expressed with the aid of Snells law as

$$\sin \theta_t = \frac{1}{N_2} \sin \vartheta \quad \sin \theta'_t = \frac{N_2}{N_3} \sin \theta_t \quad (8.18)$$

or

$$\sin \theta'_t = \frac{1}{N_3} \sin \vartheta \quad (8.19)$$

then, expressing the local angles of incidence directly as

$$\vartheta = \theta_I - \beta \quad (8.20)$$

where

$$\beta = \tan^{-1} \zeta'(x) \quad (8.21)$$

$\zeta$ , the surface profile. Upon substitution of the above simplifications the local Fresnel coefficients are

$$r_1^{\parallel}(\mathbf{r}_0) = \frac{N_2^2(\cos \theta_I + \zeta'^2 \sin \theta_I) - \sqrt{(N_2^2 - \cos^2 \theta_I)\zeta'^2 + \sin 2\theta_I \zeta' + (N_2^2 - \sin^2 \theta_I)}}{N_2^2(\cos \theta_I + \zeta'^2 \sin \theta_I) + \sqrt{(N_2^2 - \cos^2 \theta_I)\zeta'^2 + \sin 2\theta_I \zeta' + (N_2^2 - \sin^2 \theta_I)}} \quad (8.22)$$

$$r_1^{\perp}(\mathbf{r}_0) = \frac{\cos \theta_I + \zeta'^2 \sin \theta_I - \sqrt{(N_2^2 - \cos^2 \theta_I)\zeta'^2 + \sin 2\theta_I \zeta' + (N_2^2 - \sin^2 \theta_I)}}{\cos \theta_I + \zeta'^2 \sin \theta_I + \sqrt{(N_2^2 - \cos^2 \theta_I)\zeta'^2 + \sin 2\theta_I \zeta' + (N_2^2 - \sin^2 \theta_I)}} \quad (8.23)$$

$$r_2^{\parallel}(\mathbf{r}_0) = \frac{N_3^2 \sqrt{(N_2^2 - \cos^2 \theta_I)\zeta'^2 - \sin 2\theta_I \zeta' + (N_2^2 - \sin^2 \theta_I)}}{N_3^2 \sqrt{(N_2^2 - \cos^2 \theta_I)\zeta'^2 - \sin 2\theta_I \zeta' + (N_2^2 - \sin^2 \theta_I)}}$$

$$\frac{-N_2^2 \sqrt{(N_3^2 - \cos^2 \theta_I) \zeta'^2 - \sin 2\theta_I \zeta' + (N_3^2 - \sin^2 \theta_I)}}{+N_2^2 \sqrt{(N_3^2 - \cos^2 \theta_I) \zeta'^2 - \sin 2\theta_I \zeta' + (N_3^2 - \sin^2 \theta_I)}} \quad (8.24)$$

where these equations are one equation with the fraction divided to fit on the page.

$$r_2^\perp(\mathbf{r}_0) = \frac{\sqrt{(N_2^2 - \cos^2 \theta_I) \zeta'^2 - \sin 2\theta_I \zeta' + (N_2^2 - \sin^2 \theta_I)} - \sqrt{(N_3^2 - \cos^2 \theta_I) \zeta'^2 - \sin 2\theta_I \zeta' + (N_3^2 - \sin^2 \theta_I)}}{\sqrt{(N_2^2 - \cos^2 \theta_I) \zeta'^2 - \sin 2\theta_I \zeta' + (N_2^2 - \sin^2 \theta_I)} + \sqrt{(N_3^2 - \cos^2 \theta_I) \zeta'^2 - \sin 2\theta_I \zeta' + (N_3^2 - \sin^2 \theta_I)}} \quad (8.25)$$

with the further simplification  $\theta_S = \theta_I = 0$  (specular normal incidence)

$$r_1^\parallel(\mathbf{r}_0) = \frac{N_2^2 - \sqrt{(N_2^2 - 1) \zeta'^2 + N_2^2}}{N_2^2 + \sqrt{(N_2^2 - 1) \zeta'^2 + N_2^2}} \quad (8.26)$$

$$r_1^\perp(\mathbf{r}_0) = \frac{1 - \sqrt{(N_2^2 - 1) \zeta'^2 + N_2^2}}{1 + \sqrt{(N_2^2 - 1) \zeta'^2 + N_2^2}} \quad (8.27)$$

$$r_2^\parallel(\mathbf{r}_0) = \frac{N_3^2 \sqrt{(N_2^2 - 1) \zeta'^2 + N_2^2} - N_2^2 \sqrt{(N_3^2 - 1) \zeta'^2 + N_3^2}}{N_3^2 \sqrt{(N_2^2 - 1) \zeta'^2 + N_2^2} + N_2^2 \sqrt{(N_3^2 - 1) \zeta'^2 + N_3^2}} \quad (8.28)$$

$$r_2^\perp(\mathbf{r}_0) = \frac{\sqrt{(N_2^2 - 1) \zeta'^2 + N_2^2} - \sqrt{(N_3^2 - 1) \zeta'^2 + N_3^2}}{\sqrt{(N_2^2 - 1) \zeta'^2 + N_2^2} + \sqrt{(N_3^2 - 1) \zeta'^2 + N_3^2}} \quad (8.29)$$

for the special cases of a flat surface,  $\zeta = 0$ , they are

$$r_{1_0}^\parallel(\mathbf{r}_0) = \frac{1 - N_2}{1 + N_2} \quad (8.30)$$

$$r_{1_0}^\perp(\mathbf{r}_0) = \frac{1 - N_2}{1 + N_2} \quad (8.31)$$

$$r_{2_0}^\parallel(\mathbf{r}_0) = \frac{N_3^2 \sqrt{N_2^2 - 1} - N_2^2 \sqrt{N_3^2 - 1}}{N_3^2 \sqrt{N_2^2 - 1} + N_2^2 \sqrt{N_3^2 - 1}} \quad (8.32)$$

$$r_{2_0}^\perp(\mathbf{r}_0) = \frac{\sqrt{N_2^2 - 1} - \sqrt{N_3^2 - 1}}{\sqrt{N_2^2 - 1} + \sqrt{N_3^2 - 1}} \quad (8.33)$$

(where the "0" subscript indicates a flat surface) so that

$$R_{f_0} = \frac{r_{1_0} + r_{2_0} e^{i\delta_0}}{1 + r_{1_0} r_{2_0} e^{i\delta_0}} \quad (8.34)$$

and  $\delta$  is

$$\delta = \left( \frac{4\pi d}{\lambda} \right) N_2 \frac{\cos \theta_I + \zeta' \sin \theta_I}{\sqrt{1 + \zeta'^2}} \frac{1}{N_2} \frac{\sqrt{N_2^2(1 + \zeta'^2) - (\zeta' \cos \theta_I - \sin \theta_I)^2}}{\sqrt{1 + \zeta'^2}} \quad (8.35)$$

$$= \left( \frac{4\pi d}{\lambda} \right) \left( \frac{\cos \theta_I + \zeta' \sin \theta_I}{1 + \zeta'^2} \right) \sqrt{(N_2^2 - \sin^2 \theta_I) + (N_2^2 - \cos^2 \theta_I)\zeta'^2 + \sin 2\theta_I \zeta'} \quad (8.36)$$

giving

$$= \left( \frac{4\pi d}{\lambda} \right) \frac{\sqrt{(N_2^2 - 1)\zeta'^2 + N_2^2}}{1 + \zeta'^2} \quad (8.37)$$

for specular normal incidence of the flat case,  $\zeta' = 0$

$$\delta_0 = \frac{4\pi N_2 d}{\lambda} \quad (8.38)$$

### 8.3 Solution for Periodically Rough Surfaces

Making the same assumptions as for the unoxidised case the solution of the scattering problem for periodically rough surfaces having surface profile  $\zeta(x) = A \sin \frac{2\pi x}{T}$  is exactly the same as the unoxidised case except for the replacement of the reflection coefficient with those above. Therefore, the general solution for an oxidised rough surface with an identical film of iron-oxide is

$$\rho_S = \frac{n+1}{R_{f_0}(n+\eta)} \sum_{m=0}^1 \sum_{j=0}^{2m} \left( \frac{2\pi A}{T} \right)^{2m} \frac{R_{f_0}^{(2m)}}{(2m)!} \frac{1}{2^{2m}} \binom{2m}{j} J_{(2m-2j)} \left( \frac{4\pi A}{\lambda} \right) \quad (\eta \neq 0) \quad (8.39)$$

when the edge terms are included and

$$\rho_S = \frac{1}{R_{f_0}} \sum_{m=0}^1 \sum_{j=0}^{2m} \left( \frac{2\pi A}{T} \right)^{2m} \frac{R_{f_0}^{(2m)}}{(2m)!} \frac{1}{2^{2m}} \binom{2m}{j} J_{(2m-2j)} \left( \frac{4\pi A}{\lambda} \right) \quad (\eta = 0) \quad (8.40)$$

for a surface an integer multiple of the period. This is of course only valid if the series containing the derivatives  $R_{f_0}^{(2m)}$  converges. This will be assumed and not be proved. The check on this solution will be made through comparison with numerical means.



This again allows us to approximate the solution up to the first term as

$$R_S \simeq R_{f_0} J_0 \left( \frac{4\pi A}{\lambda} \right) \quad (8.41)$$

finally giving the emissivity as

$$\epsilon_f \simeq 1 - \left[ J_0 \left( \frac{4\pi A}{\lambda} \right) \right]^2 R_{y_{f_0}} \quad (8.42)$$

where the average reflectivity

$$R_{y_{f_0}} = \frac{R_{f_0}^{\parallel} R_{f_0}^{*\parallel} + R_{f_0}^{\perp} R_{f_0}^{*\perp}}{2} \quad (8.43)$$

### 8.3.1 Consequences of the Oxidised Film Solution

We have already considered the influence of both film thickness and surface roughness on the emissivity, these effects being propagated by the refractive index of the film, and the term,  $e^{i\delta}$ , which produces interference phenomena, and the ratio  $A/\lambda$  (also  $A/T$  to some degree). Now we are interested in which one of these dominates in its effect on the emissivity. This effect is determined by the product

$$\left[ J_0 \left( \frac{4\pi A}{\lambda} \right) \right]^2 R_{y_{f_0}} \quad (8.44)$$

We have already stated for the unoxidised case that the influence of roughness lasts only over the range of wavelengths up until the first zero of  $J_0$ , this remains true in this case also. After this zero is passed the maximum size of  $J_0$  is reached when  $J_0 = 1$ , the emissivity is then controlled by the smooth surface single film reflection coefficient  $R_{f_0}$ .

The actual maximum size of the emissivity depends on the refractive index contained in  $R_{y_{f_0}}$  and the size of  $J_0$ . Note again the influence of the roughness ends when  $J_0 \rightarrow 1$ . Now both the surface roughness and the interference effects produce oscillations in the emissivity at small wavelengths. Both become negligible as the wavelength increases. The first depending on the first zero of  $J_0$  and the second on the ratio  $d/\lambda$ . Interference only occurs when this ratio is close to one. It can be shown that for products of the form

$$J_0 \left( \frac{4\pi A}{\lambda} \right) \left[ \frac{r_1 + r_2 e^{2i\delta}}{1 + r_1 r_2 e^{2i\delta}} \right] \quad (8.45)$$

- As in part 1 if the ratio  $d/\lambda$  is large enough no matter whether roughness exists or not, the decaying exponential will dominate the expression giving rise to the reflection coefficient given in the smooth case

$$\pm J_0 \left( \frac{4\pi A}{\lambda} \right) \frac{N_2 - 1}{N_2 + 1} \quad (8.46)$$

the roughness term in front has the effect of causing oscillations even though the interference oscillations have been eliminated. So, even at small wavelengths we expect quite strong oscillations due to the strong degree of roughness,  $A/\lambda$ , which is exhibited by  $J_0$  at small wavelengths. These oscillations will take place at quite large values of emissivity since we are dealing with the reflection coefficient of Scale, not steel.

- If  $d/\lambda \sim 0$  then we get a reflection coefficient approximately that of clean steel (iron)

$$\pm J_0 \left( \frac{4\pi A}{\lambda} \right) \frac{N_3 - 1}{N_3 + 1} \quad (8.47)$$

we get behaviour like the rough steel case already discussed.

- If  $d/\lambda \sim O(1)$  as for the smooth case the term of greatest interest is

$$J_0 \left( \frac{4\pi A}{\lambda} \right) \sin \left( \frac{4n_2 d\pi}{\lambda} \right) e^{-\frac{4\eta_2 d\pi}{\lambda}} \quad (8.48)$$

again, for larger ratios of  $d/\lambda$  in the decaying exponential the oscillations produced by both the sinusoidal and the Bessel function terms will decay away quickly. However because of the extra  $J_0$  term these oscillations may continue longer than expected. So, instead of decaying away over a thickness range given by the critical value

$$d_{critical} = \frac{\lambda C}{4\eta_2 \pi} \quad (8.49)$$

the Bessel function will contribute to stretch out this distance until it reaches its first zero after which it too will decay away reverting the reflection characteristics back to the other two functions  $\sin \left( \frac{4n_2 d\pi}{\lambda} \right), e^{-\frac{4\eta_2 d\pi}{\lambda}}$ . If the zero lies further out along the

wavelength axes than the range of wavelengths needed to reach the critical thickness then oscillations will continue until this zero is reached. If, on the other hand, the zero lies inside this region the critical thickness will be reached as controlled by  $e^{-\frac{4\eta_2 d\pi}{\lambda}}$ . Otherwise the critical thickness will be extended.

Observation of the behaviour of the zero order Bessel function shows a pronounced bump or an area of large width about the first zero, this too shall impose itself on the other terms above, although its effect will be diminished by the exponential decay term. Now the first zero is reached at

$$\frac{4\pi A}{\lambda} = j_{0,1} \quad (8.50)$$

that is when  $\lambda = \lambda_z$ , where the “ $z$ ” subscript indicates the wavelength at the first zero.

$$\lambda_z = \frac{4\pi A}{j_{0,1}} \quad (8.51)$$

so when we reach  $\lambda = \lambda_z$  then  $d_{critical}$  becomes

$$d_{critical} = \frac{AC}{\eta_2 j_{0,1}} \quad (8.52)$$

then the new distance depends on the roughness through  $A/\eta_2$  which of course is a function of wavelength. This extension of distance is an amount given by the difference between the two  $d$ 's

$$\left| \frac{C(4\pi A - \lambda j_0)}{4\pi \eta_2 j_{0,1}} \right| \quad (8.53)$$

- As such, the time for oscillations to cease will be longer. This is, as in part 1, a direct replacement of  $d_{critical}$  in the expression (3.137).

The general trend, therefore, is for the emissivity to behave in a similar way as to the smooth case. the differences are that for small thicknesses the behaviour is like the rough iron case, as the thickness increases oscillations are produced as a combination of roughness and interference effects. They decay out due to absorption where this decay may be

of a longer duration than in the flat case. After this episode of instability, the appearance is as of the flat layered case, that is, a relatively constant period where the emissivity is that of the iron oxide. As the wavelength is increased the roughness and layer effects diminish and the result is that of pure unlayered unroughened steel.

Note that, at long wavelengths, even though the emissivity of steel is approximated it will be very small,  $\epsilon \sim 0.05$  then the measurement of the radiation becomes very difficult because of its low intensity and very sensitive instruments will be required. In an industrial environment it is possible the true signal might be swamped by other external noise.

Multilayer films are not considered here but their behaviour is expected to follow qualitatively that of the single layer case with the exception that interference only take place for layers at that particular wavelength and thickness, whereas the roughness contributes anyway.

## Chapter 9

# Numerical Solution Scheme for Rough Surfaces

Calculation via computer of the scattering integral is achieved with the use of a commercially available NAG subroutine specially tailored for the solution of oscillatory integrals. Even though the scattering integral is not an extreme example of its kind, it was felt that the use of this routine improves accuracy in the solution rather than using simple Trapezoidal or Simpson's rules.

The scattering coefficient,  $\rho$ , was calculated from the scattering integral

$$\rho_S = -\frac{1}{4LR_0 \cos \theta_I} \int_{-L}^L (a\zeta' - b) e^{i(k_x^- x_0 + k_z^- \zeta(x_0))} dx_0 \quad (9.1)$$

with the reflection coefficients calculated from the term

$$R = \frac{r_1 + r_2 e^{2i\delta}}{1 + r_1 r_2 e^{2i\delta}} \quad (9.2)$$

for the layered case (one layer),  $d \neq 0$  and the expressions for the rough unlayered case,  $d = 0$ . The phase difference in interference inside the layer was calculated by

$$\delta = \left( \frac{4\pi d}{\lambda} \right) \frac{\cos \theta_I + \zeta' \sin \theta_I}{\sqrt{1 + \zeta'^2}} \frac{\sqrt{N_2^2(1 + \zeta'^2) - (\zeta' \cos \theta_I - \sin \theta_I)^2}}{\sqrt{1 + \zeta'^2}} \quad (9.3)$$

As in the theory the surface was considered sinusoidal  $\zeta = A \sin\left(\frac{2\pi x}{T}\right)$ . The solution involved the factors,  $d$ , average thickness of Scale layer,  $\lambda$ , wavelength of incident radiation,  $A$ , the amplitude of surface corrugations,  $T^o$ , the temperature of the surface and  $T$  the period of undulations of the surface. That is, after calculation of the reflection coefficient and the reflectivity the emissivity is

$$\epsilon = \epsilon(\lambda, T^o; A, T) \quad (9.4)$$

## 9.1 Interpretation and Discussion of Numerical Results : Unoxidised Surfaces

The variation of emissivity for unoxidised periodically rough surfaces is shown in Figures 9.1.1-9.1.6. All results are obtained at a temperature of  $T = 1000^\circ\text{C}$  over a wavelength range of  $\lambda : 0.0 - 10\mu\text{m}$  for an unoxidised steel (iron) surface ( $d = 0$ ). All calculations are carried out at a surface period of  $100\mu\text{m}$  and integration limits  $L : 0 \rightarrow 0.001\text{m}$ . This was considered more than large enough as a representation of scattering off a rough surface. This is far in excess of the first few Fresnel zones required to produce accurate results. The present graphs are evaluated over

$$\frac{\max(L)}{\lambda} = \frac{1000\mu\text{m}}{10\mu\text{m}} = 100 \quad \frac{\max(L)}{T} = \frac{1000\mu\text{m}}{100\mu\text{m}} = 10$$

therefore many more wavelengths than needed are included and 10 sets of periods are involved. For each graph the roughness parameter  $A/\lambda$  is increased and the results considered.

**Figure 9.1.1**,  $A = 0.01\mu\text{m}$ ,  $\frac{A}{\lambda} : 0.1 - 0.001$ ,  $\frac{A}{T} = 0.0001$

As a comparison, the (near) flat case was added. This was actually at an optical roughness of 0.1 or an amplitude of  $0.01\mu\text{m}$ , a very small surface undulation away from the mean ( $A = 0$ ). We see the usual behaviour for a smooth surface. There is a rapid fall in emissivity

### 9.1. INTERPRETATION AND DISCUSSION OF NUMERICAL RESULTS : UNOXIDISED SURFACES 17

from close to one at small wavelengths to 0.18 at longer wavelengths. The fall is of the form  $1/\sqrt{\lambda}$  as predicted by theory.

**Figure 9.1.2**,  $A = 0.1\mu\text{m}$ ,  $\frac{A}{\lambda} : 1 - 0.01$ ,  $\frac{A}{T} = 0.001$

The presence of roughness makes itself felt at very small wavelengths  $0.1 - 0.8\mu\text{m}$ . We expect contributions whenever the roughness parameter is comparable to the wavelength. There is a typical oscillation until the first zero of  $J_0$  is reached this occurs at about

$$\frac{4\pi A}{\lambda} = 2.405, \text{ or when } \lambda = 0.5\mu\text{m}$$

this is easily seen in the graph. A comparison to Figure 7.9.1 shows the similarity. The oscillations present in the *Mathematica* drawn graph are not seen because the resolution used in the numerical solution is not small enough to extract this information.

**Figure 9.1.3**,  $A = 0.5\mu\text{m}$ ,  $\frac{A}{\lambda} : 5 - 0.05$ ,  $\frac{A}{T} = 0.005$

As expected, the increase in surface amplitude increases the oscillations in the emissivity. The point at which the solution reverts back to the smooth surface reflection coefficient is reached at about  $\lambda = 2.5\mu\text{m}$  this lies well within the value given by theory which is  $\lambda = 2.6\mu\text{m}$ .

- We notice that the smooth surface reflection coefficients don't actually influence the result a great deal. It would seem that the earlier assertion, [8], that electrical properties marginally influence the scattered field is confirmed.
- Note also that on comparison with Figures 4.3.2 and 4.3.3 the graph of emissivity verses wavelength has the appearance of a filmed surface rather than a rough one. We may hypothesize that a rough surface is qualitatively equivalent to a smooth layered surface. A crude estimate would replace the rough surface as a single layer of oxide on steel with film thickness obtained by consideration of surface roughness. Since both surface roughness amplitude and film thickness induce oscillations when

they are of the same order as the wavelength we are led to the conclusion that a rough surface is equivalent to a filmed surface having, in the case of Figure 9.1.3, a thickness equal to about  $1\mu\text{m}$ .

- Since the ratio  $(2\pi A/T)^2 = 0.001$  is quite small, it is reasonable to assume that the influence of second order terms, which are always multiplied by this ratio, is very small indeed. In fact, this means that the representation of rough surface emissivity, as a function only of the ratio  $4\pi A/\lambda$ , is adequate provided the ratio  $A/T$  is always relatively small.

**Figure 9.1.4**,  $A = 1\mu\text{m}$ ,  $\frac{A}{\lambda} : 10 - 0.1$ ,  $\frac{A}{T} = 0.01$

This graph illustrates the same behaviour as the previous figure. Again oscillations cease at about  $\lambda = 5.5\mu\text{m}$  this is close to the theoretical value of  $5\mu\text{m}$ . It is now possible that the reflection coefficients play some part in the location of the points where oscillations decay away. The small discrepancy between theory and numerical solution may be due to the influence of the reflectivity multiplier. We may probably discount the effect of  $2\pi A/T$  as compared to the effect the smooth surface reflectivity has. Also, we again obtain an equivalent film thickness of about  $2 - 3\mu\text{m}$ .

**Figure 9.1.5 and 9.1.6**,  $A = 5 - 10\mu\text{m}$ ,  $\frac{A}{\lambda} : 50, 100 - 0.5, 1$ ,  $\frac{A}{T} = 0.05, 0.1$

These graphs are merely extensions of the earlier ones demonstrating the oscillatory behaviour for large roughness parameters. Compare these results with Figure 7.9.3 ( $A = 10\mu\text{m}$ ). The two graphs are almost identical, once again showing that at high degrees of optical roughness the ratio  $4\pi A/\lambda$  is the most important parameter describing emissivity characteristics.

### 9.1.1 Conclusions

We arrive at the following conclusions



1. Rough unoxidised surfaces act like a smooth oxidised surface with equivalent layer thickness determined by the roughness parameter.
2. The emissivity characteristics of unoxidised rough surfaces are governed by the optical roughness parameter in the main. The influence of electrical properties is relatively insignificant until the first zero of  $J_0$  is reached. After this point the emissivity is controlled by the smooth surface reflectivity. The effect of the second order roughness parameter,  $2\pi A/T$ , is usually very small although if it is of a significant size it may effect results. The effect of this parameter has so far not been very pronounced.
3. The roughness of a surface significantly increases the emissivity in the same sense that an oxidised smooth surface does through the refractive index of the oxide layer.
4. The effect of roughness on emissivity properties is most significant when the surface amplitude,  $A$ , is comparable to the wavelength used in the measurement.
5. Since the emissivity behaviour of rough surfaces is controlled by the smooth surface reflectivity when the wavelength exceeds  $4\pi A/j_{0,1}$ , then the emissivity must eventually tend to that of the smooth case. If the roughness parameter is small enough the entire behaviour is governed by the smooth reflectivity.

## 9.2 Interpretation and Discussion of Numerical Results : Oxidised Surfaces

The Figures 9.2.1-9.2.32 are organised as follows :

1. Figures 9.2.1-9.2.10 are graphs of emissivity verses thickness of oxide layer, demonstrating the effect of roughness for oxidised and unoxidised surfaces. A comparison is made between the effects of roughness increase and layer thickness increase.

2. Figures 9.2.11-9.2.32 are graphs of emissivity verses wavelength of measurement radiation for oxidised and unoxidised surfaces.

Each of the two sets of graphs considers various ranges of the other constant parameters : wavelength in 1. and thickness in 2. above.

All graphs are taken over a surface period of  $T = 100\mu\text{m}$  and at  $T^\circ = 1000^\circ\text{C}$ .

**Figures 9.2.1-9.2.2,  $A = 0, 0.05\mu\text{m}$ ,  $\lambda = 0.5\mu\text{m}$ ,  $d : 0 - 2\mu\text{m}$**

These two graphs compare how small degrees of roughness change the emissivity of filmed surfaces. The first graph, Figure 9.2.1, is a typical graph of emissivity verses film thickness extending from zero to  $2\mu\text{m}$  with zero roughness, the second applies a roughness amplitude of  $A = 0.05\mu\text{m}$ . That is

$$\frac{A}{\lambda} = 0.1 \quad \max\left(\frac{A}{d}\right) = 0.0025 \quad \frac{A}{T} = 0.0005$$

We see immediately that, as expected, the emissivity is increased even for very small roughness parameters. This has the effect of decreasing the amplitude of interference oscillations at small wavelengths (this of course being the property of smooth oxidised surfaces). Notice that there is no net increase in the final converged value of emissivity which remains constant over the latter part of the graph at 0.99 or so. The number of peaks and troughs remains constant and the period of oscillation is also not changed. However, the smooth surface graph rises from the initial real emissivity of iron,  $\epsilon = 0.43$  at  $\lambda = 0.5\mu\text{m}$ ,  $d = 0\text{m}$ , whereas the rough graph never even starts from this point, commencing instead, from an emissivity of 0.77. At no time can we say the rough oxidised graph obtains the emissivity of steel itself.

**Figures 9.2.3-9.2.5,  $A = 0, 0.01, 0.03\mu\text{m}$ ,  $\lambda = 0.1\mu\text{m}$ ,  $d : 0 - 2\mu\text{m}$**

This time we considered the same situation as the previous graphs except for a smaller range of wavelengths. The original graph, Figure 9.2.3, has interference oscillations about

the mean emissivity curve not as in the previous curves where the oscillations dominated the graph. We have for Figure 9.2.3

$$\frac{A}{\lambda} = 0.1 \quad \max\left(\frac{A}{d}\right) = 0.0005 \quad \frac{A}{T} = 0.0001$$

For Figure 9.2.4

$$\frac{A}{\lambda} = 0.3 \quad \max\left(\frac{A}{d}\right) = 0.0015 \quad \frac{A}{T} = 0.0003$$

The same behaviour as in Figures 9.2.1-9.2.2 is noticed again even for very small ratios of surface amplitude to thickness. The behaviour seems to be solely controlled by the optical roughness ratio. We may discount the effect of second order roughness parameters as these are very small  $(2\pi A/T)^2 = 3.5 \times 10^{-6}$ .

**Figures 9.2.6-9.2.10**,  $A = 0, 0.5, 1, 3, 5\mu\text{m}$ ,  $\lambda = 10\mu\text{m}$ ,  $d : 0 - 2\mu\text{m}$

This time we study emissivity behaviour at longer wavelengths starting again from the smooth surface oxidised case and proceeding through larger and larger roughness ratios. For example we start from, Figure 9.2.7 :

$$\frac{A}{\lambda} = 0.05 \quad \max\left(\frac{A}{d}\right) = 0.025 \quad \frac{A}{T} = 0.005$$

to Figure 9.2.10 :

$$\frac{A}{\lambda} = 0.5 \quad \max\left(\frac{A}{d}\right) = 0.25 \quad \frac{A}{T} = 0.05$$

Note that this time the effects of second order roughness parameters may not be so small. This time the ratio of surface amplitude to depth of oxide film is no longer small. In Figure 9.2.10 we see that at large roughness parameters the initially small emissivity in earlier graphs, Figures 9.2.6, 9.2.7 is completely eliminated and there is a flattening out of the graph until almost a constant emissivity is obtained over all film thicknesses, whether small (near zero) or large  $2\mu\text{m}$ . This time, we also notice a large increase in the converged emissivity from about 0.64 (Figure 9.2.6) to 0.98 (Figure 9.2.10). We must attribute this

increase to, first, higher degrees of optical roughness and, second, to the possible influence of second order roughness. This time the difference in size of  $A/\lambda$  and  $A/T$  is only 1 order of magnitude rather than 3 or 2.

**Figures 9.2.11-9.2.18**,  $A = 0\mu\text{m}$ ,  $d = 0, 0.1, 0.2, 0.3, 0.4, 0.5, 1, 5\mu\text{m}$ ,  $\lambda : 0.03 - 3\mu\text{m}$

These graphs demonstrate the change in emissivity over wavelength as the thickness of the oxide layer (single-layer of  $FeO$ ) is varied from zero up to  $5\mu\text{m}$ . They are included for comparison with the corresponding rough cases to be studied forthwith.

**Figures 9.2.19-9.2.24**,  $A = 0, 0.01, 0.02, 0.08, 0.1, 0.2\mu\text{m}$ ,  $d = 0.4\mu\text{m}$ ,  $\lambda : 0.03 - 3\mu\text{m}$

These graphs start from Figure 9.2.19 with a thickness of  $0.4\mu\text{m}$  and zero roughness, that is, a graph chosen from the previous set : Figure 9.2.15. The graphs progress as follows :

$$\frac{A}{\lambda} = 0 \quad 0.33 - 0.003 \quad 0.66 - 0.0066 \quad 2.66 - 0.0266 \quad 3.3.3 - 0.033 \quad 6.66 - 0.066$$

$$\frac{A}{d} = 0, 0.025, 0.05, 0.2, 0.25, 0.5$$

$$\frac{A}{T} = 0, 0.0001, 0.0002, 0.0008, 0.001, 0.002$$

for each Figure, 9.2.11-9.2.18, in increasing order. We should also note the point at which roughness oscillations cease these occur at  $\lambda = 4\pi A/j_{0,1}$ , for each graph they are

$$\lambda = 0.05, 0.1, 0.42, 0.52, 1.04\mu\text{m}$$

We first note that until we reach a surface amplitude of  $A = 0.08\mu\text{m}$  (Figure 9.2.22) there is virtually no change in the behaviour of the emissivity. This is due to the fact that the oscillations, due to roughness, decay away much earlier than do the interference oscillations, until the surface amplitude reaches  $0.08\mu\text{m}$ . At this stage the oscillatory contributions from both interference and roughness factors seem to be of the same order and in fact cancel each other out giving the approximate straight line in the early part of Figure 9.2.22. The rest of the graph then behaves according to interference theory

described in section (3.3.2) and equation (3.137). Beyond this optical roughness value the surface undulation continues to increase the emissivity and eliminates all but one oscillation. The first zero of  $J_0$  shifts further towards the right of the graphs causing this extended behaviour.

**Figures 9.2.25-9.2.28**,  $A = 0, 0.5, 1, 2\mu\text{m}$ ,  $d = 10\mu\text{m}$ ,  $\lambda : 0.1 - 10\mu\text{m}$

The next set of graphs start with zero surface amplitude at  $d = 10\mu\text{m}$  and increase the roughness progressively up to  $A = 2\mu\text{m}$ . The various parameters are

$$\frac{A}{\lambda} = 0, 5 - 0.05, 10 - 1, 20 - 2$$

$$\frac{A}{d} = 0, 0.05, 0.1, 0.2$$

$$\frac{A}{T} = 0, 0.005, 0.01, 0.02$$

$$\lambda_{crit} = 2.6, 5.2, 10.4\mu\text{m}$$

Note that the optical roughness is now much larger than in previous graphs. This is why we see an immediate increase in emissivity as soon as the surface amplitude is increased to  $0.5\mu\text{m}$ . The behaviour is very similar to that of previous graphs with the last one extending emissivity oscillations just past the endpoint,  $10\mu\text{m}$ . Note the presence of extra oscillations induced by the roughness. This was not present in the original graph, Figure 9.2.25, which had passed the point where interference oscillations take place.

**Figures 9.2.29-9.2.32**,  $A = 0, 0.2, 0.3, 0.5\mu\text{m}$ ,  $d = 1\mu\text{m}$ ,  $\lambda : 0.1 - 10\mu\text{m}$

The next set of graphs start with zero surface amplitude at  $d = 1\mu\text{m}$  and increase the roughness progressively up to  $A = 0.5\mu\text{m}$ . The various parameters are

$$\frac{A}{\lambda} = 0, 2 - 0.02, 3 - 0.03, 5 - 0.05$$

$$\frac{A}{d} = 0, 0.2, 0.3, 0.5$$

$$\frac{A}{T} = 0, 0.002, 0.003, 0.005$$

$$\lambda_{crit} = 1, 1.6, 2.6\mu\text{m}$$

There is no relevant change in behaviour from earlier graphs. These graphs were included in order to observe how emissivity changed if the interference region had been bypassed. All previous explanations are confirmed in these set of graphs.

### 9.3 Conclusions

As regards oxidised rough surfaces it is reasonable to state that :

1. As for smooth oxidised surfaces, oxidised rough surfaces undergo a significant increase in emissivity due not only to the interference phenomena but also the roughness considerations. These two effects combine to increase the emissivity of real (rough, oxidised) surfaces to such an extent that at no time other than at very long wavelengths does the emissivity approach that of steel.
2. The effect of surface roughness,  $A/\lambda$ , can be confined to three regions of interest for oxidised surfaces :
  - when roughness,  $A/\lambda$ , is smaller than interference,  $d/\lambda$ .
  - when roughness and thickness factors are comparable,  $A/\lambda \sim d/\lambda$ .
  - when roughness,  $A/\lambda$ , is greater than interference,  $d/\lambda$ .

The first case shows that interference effects dominate with almost no contribution from surface roughness. This is expected as long as  $A/\lambda$  is small and  $A/d$  is of order one. So a relatively smooth oxidised surface has the characteristics of smooth layered surfaces and so is governed by the optical laws used for smooth layered media. That is the surface is oxidised but not rough.

The second case allows an interaction between both phenomena often resulting in a very high emissivity that remains constant over a large range of wavelengths.

The third case is dominated by the roughness parameter,  $A/\lambda$ , which accounts for oscillation effects and the general behaviour. However the presence of the oxide layer contributes by the initial raising of the emissivity and forming the basis for the addition of the roughness properties. In other words, the roughness effects are added on top of the original smooth surface oxide effects.

### 9.3.1 Summary

In reality we are always presented with a steel surface that is rough and is covered by three separate layers of iron-oxide. However, in industry, the simplest possible model is both financially and time-wise preferable to any complex simulation representing the 'real' situation. Similarly, it makes sense to use a simple model because its inherent simplicity allows much greater physical comprehension, rather than an involved model where the effects of relevant properties can not be easily extracted.

Upon consideration of the conclusions drawn about the various models studied, we find that

1. The more accurate three-layer model of smooth surface emissivity variation can under appropriate conditions be simplified to a single-layer model of oxide on steel. This is true provided the wavelength of measurement is larger than the thickness of  $FeO$ .
2. The case of a rough unoxidised steel surface can be approximated by a single smooth layer of a material whose thickness is determined by the roughness parameter  $4\pi A/\lambda$  and whose refractive index may be extracted by consideration of the function  $J_0(4\pi A/\lambda)$ .
3. An oxidised surface with substrate/oxide and oxide/air boundaries having identical surface roughness may be approximated as two flat (smooth) layers upon an iron substrate. The first layer is the smooth layer of oxide and the second layer represents the roughness properties of both boundaries.

## 9.4 Future Directions in Research

There are several avenues of research to follow :

1. The obvious first step is to extend the analysis in a straightforward manner to deal with the full three-layer problem. This of course makes the simulation more realistic.
2. Firstly, the last conclusion above leads to the possibility of considering all rough oxidised surfaces as simply two smooth layers on a steel substrate. It would then be possible to model all such surfaces in this way and lead to considerable simplification for realistic emissivity simulation.

For example, we would contend with three simple cases. The first of these deals with a thick oxide layer and a thin layer on top of the oxide representing the roughness properties. We expect some slight variations in behaviour from a pure single-layer of oxide on steel, but in the main, the behaviour would be described by interference theory due to the oxide layer only. The second case occurs where the oxide layer and roughness layer are both contributing equally, they are of similar thickness, or rather, both interact with the incident wavelength to produce combined two layer behaviour. The last case involves mainly the upper layer with only a thin oxide layer underneath. The properties are then governed by this layer in the main.

Other possibilities are that both layers are very thin corresponding to minimal roughness and little oxidation. As it is this two layer model should be investigated for its validity and use in modelling real surfaces reliably.

3. The previous work on rough surfaces may be extended to surfaces rough in both  $x$  and  $y$  directions rather than just the  $x$  direction used currently. Two possibilities arise, first, if the new 2-D surface does not induce depolarisation upon scattering the extension to 2-D surfaces is straightforward application of the theory discussed in this thesis. Second, if depolarisation does take place then the scattering problem



must be constructed as a vector theory rather than as a scalar theory which is used in this thesis.

4. Consideration of surface shadowing is possible with the inclusion of shadowing functions, [8]. This would improve the accuracy of Kirchhoff theory.
5. It is possible to extend Kirchhoff theory to fractal surfaces and periodic surfaces having more than one scale of roughness. This extension is not difficult and in the case of periodic functions could lead to very generalised solutions which may be obtainable in closed form.
6. Other effects, such as multiple scattering, and any extension away from the Kirchhoff assumptions require a new theory such as integral equation methods or the partial differential equation solution of the original scattering problem.



# Appendix A

## A.1 Derivatives of odd and even functions

Given an odd function

$$\zeta(-x) = -\zeta(x) \tag{A.1}$$

then it is relatively straightforward to show that the derivative of this function must be even. Define the derivative of a function  $\zeta(x)$  as at some point  $x$  by

$$\zeta'(x) = \lim_{h \rightarrow 0} \frac{\zeta(x+h) - \zeta(x)}{h} \tag{A.2}$$

for an odd function

$$\zeta'(-x) = \lim_{h \rightarrow 0} \frac{\zeta(-x+h) - \zeta(-x)}{h} \tag{A.3}$$

$$= \lim_{h \rightarrow 0} \frac{-\zeta(x-h) + \zeta(x)}{h} \tag{A.4}$$

$$= -\lim_{h \rightarrow 0} \frac{\zeta(x-h) - \zeta(x)}{h} \tag{A.5}$$

$$= -\lim_{-h \rightarrow 0} \frac{\zeta(x+h) - \zeta(x)}{-h} \tag{A.6}$$

$$= \lim_{h \rightarrow 0} \frac{\zeta(x+h) - \zeta(x)}{h} \tag{A.7}$$

$$= \zeta'(x) \tag{A.8}$$

so the derivative of an odd function is an even function. Similarly it is easily shown that if  $\zeta$  is even

$$\zeta'(-x) = -\zeta'(x) \tag{A.9}$$

or the derivative of an even function is odd. In fact it is also possible to show that generally for

- $\zeta$  odd ie  $\zeta(-x) = -\zeta(x)$

$$\zeta'(-x) = \zeta'(x), \zeta^2(-x) = -\zeta^{(2)}(x), \zeta^{(3)}(-x) = \zeta^{(3)}(x), \dots \quad (\text{A.10})$$

or

$$\zeta^{(2n+1)}(-x) = \zeta^{(2n+1)}(x) \quad (\text{A.11})$$

$$\zeta^{(2n)}(-x) = -\zeta^{(2n)}(x) \quad (\text{A.12})$$

$n$  an integer

- $\zeta$  even ie  $\zeta(-x) = \zeta(x)$

$$\zeta'(-x) = -\zeta'(x), \zeta^{(2)}(-x) = \zeta^{(2)}(x), \zeta^{(3)}(-x) = -\zeta^{(3)}(x), \dots \quad (\text{A.13})$$

or

$$\zeta^{(2n+1)}(-x) = -\zeta^{(2n+1)}(x) \quad (\text{A.14})$$

$$\zeta^{(2n)}(-x) = \zeta^{(2n)}(x) \quad (\text{A.15})$$

$n$  an integer

## A.2 Derivatives of Reflection Coefficients

### Perpendicular Polarisation

The derivatives of the reflection coefficients of a rough surface with incident radiation at normal incidence are given by

$$R_0^{(2)} = \left. \frac{d^2 R}{d\zeta'^2} \right|_{\zeta'=0} = \frac{(1-N^2)(1-N)}{2N(1+N)^2} + \frac{1-N^2}{2N(1+N)^2} \quad (\text{A.16})$$

$$R_0^{(4)} = \frac{(N^2-1)^2(1-N)}{2N^2(1+N)^3} + \frac{(N^2-1)^2}{2N^2(1+N)^2} + \frac{(N^2-1)^2(1-N)}{4N^3(1+N)^2} + \frac{(N^2-1)^2}{4N^3(1+N)} \quad (\text{A.17})$$

$$R_0^{(6)} = \frac{-3(N^2-1)^3(1-N)}{4N^3(1+N)^4} - \frac{3(N^2-1)^3}{4N^3(1+N)^3} - \frac{3(N^2-1)^3(1-N)}{4N^4(1+N)^3} - \frac{3(N^2-1)^3}{4N^4(1+N)^2} - \frac{3(N^2-1)^3(1-N)}{8N^5(1+N)^2} - \frac{3(N^2-1)^3}{8N^5(1+N)} \quad (\text{A.18})$$

$$R_0^{(8)} = \frac{3(N^2-1)(1-N)}{2N^4(1+N)^5} + \frac{3(N^2-1)^4}{2N^4(1+N)^4} + \frac{9(N^2-1)^4(1-N)}{4N^5(1+N)^4} + \frac{15(N^2-1)^4}{8N^6(1+N)^3} + \frac{15(N^2-1)^4}{8N^6(1+N)^2} + \frac{15(N^2-1)^4(1-N)}{16N^7(1+N)^2} + \frac{15(N^2-1)^4}{16N^7(1+N)} \quad (\text{A.19})$$

$$R_0^{(10)} = \frac{-15(N^2-1)^5(1-N)}{4N^5(1+N)^6} - \frac{15(N^2-1)^5}{4N^5(1+N)^5} - \frac{15(N^2-1)^5(1-N)}{2N^6(1+N)^5} - \frac{15(N^2-1)^5}{2N^6(1+N)^4} - \frac{135(N^2-1)^5(1-N)}{16N^7(1+N)^4} - \frac{135(N^2-1)^5}{16N^7(1+N)^3} - \frac{105(N^2-1)^5(1-N)}{16N^8(1+N)^3} - \frac{105(N^2-1)^5}{16N^8(1+N)^2} - \frac{105(N^2-1)^5(1-N)}{32N^9(1+N)^2} - \frac{105(N^2-1)^5}{32N^9(1+N)} \quad (\text{A.20})$$

$$R_0^{(12)} = \frac{45(N^2-1)^6(1-N)}{4N^6(1+N)^7} + \frac{45(N^2-1)^6}{4N^6(1+N)^6} + \frac{225(N^2-1)^6(1-N)}{8N^7(1+N)^6} + \frac{225(N^2-1)^6}{8N^7(1+N)^5} + \frac{315(N^2-1)^6(1-N)}{8N^8(1+N)^5} + \frac{315(N^2-1)^6}{8N^8(1+N)^4} + \frac{315(N^2-1)^6(1-N)}{8N^9(1+N)^4} + \frac{315(N^2-1)^6}{8N^9(1+N)^3} + \frac{945(N^2-1)^6(1-N)}{32N^{10}(1+N)^3} + \frac{945(N^2-1)^6}{32N^{10}(1+N)^2} + \frac{945(N^2-1)^6(1-N)}{64N^{11}(1+N)^2} + \frac{945(N^2-1)^6}{64N^{11}(1+N)} \quad (\text{A.21})$$

for perpendicular polarisation. The largest terms in each of the derivatives  $R_0^{(2m)}$  form the basis for an analysis of the convergence of the total series, (7.184). For example, the largest terms in the 10<sup>th</sup> and 12<sup>th</sup> derivatives are given by :

$$\frac{135(N^2-1)^5}{16N^7(N+1)^3} \quad \frac{315(N^2-1)^6}{8N^9(1+N)^3} \quad (\text{A.22})$$

this is true provided  $|N| \geq 1$  ( $N$  complex), this being a refractive index for which the minimum value is 1, that of free space, and the maximum, infinite, a perfect conductor. Any materials of refractive indices less than 1 are unphysical for the current problem. It is difficult to generate the  $2m^{\text{th}}$  largest term, such as the two above, in a consistent formula. However it is relatively easy to find the  $2m^{\text{th}}$  term for the last term in each series above. For example the last terms for the 10th and 12th derivatives are :

$$\frac{945(N^2-1)^6}{64N^{11}(1+N)} \quad \frac{105(N^2-1)^5}{32N^9(1+N)}$$

$$\frac{(2m-3)!}{2^{m-2}2^m(m-2)!} \left( \frac{(N^2-1)^m}{N^{2m-1}(1+N)} \right) \quad (\text{A.23})$$

for example the substitution of  $m = 6$  reproduces the last term in  $R_0^{(12)}$ . Now, it is possible to construct a series such as the ones we are dealing with by taking the generator of the last term, which we know, and make this the largest term of the series merely by altering the denominator so that the largest term now reads

$$\frac{(2m-3)!}{2^{m-2}2^{m-2}(m-2)!} \left( \frac{(N^2-1)^m}{N^{2m-3}(1+N)^{m-3}} \right) \quad (\text{A.24})$$

the new term for  $m = 6$  now becomes

$$\frac{(9)!}{2^4 2^4 (4)!} \left( \frac{(N^2-1)^6}{N^9(1+N)^3} \right) = \frac{945(N^2-1)^6}{16N^9(1+N)^3} \quad (\text{A.25})$$

which is now larger than the previous equivalent largest term  $\frac{315(N^2-1)^6}{8N^9(1+N)^3}$ . It is then possible to generate the largest term for each series above so that this new series, which must be larger than the previous one, can be used to test the convergence of the earlier one. If this new series converges then so must the previous one since it is the larger of the two, [75]. Now, since the largest term is larger than any other of the terms in the series for  $R_0^{(2m)}$  above, then for any of the other terms in the series

$$\text{1st term} < \textit{largest}, \quad \text{2nd term} < \textit{largest}, \quad \dots, \text{largest term} \leq \textit{largest} \quad (\text{A.26})$$

and so on up to the last term. Now, in each series there are always  $2m$  terms so adding all terms

$$\text{1st} + \text{2nd} + \text{3rd} + \dots + \text{largest} < 2m \times \textit{largest} \quad (\text{A.27})$$

therefore, we may propose that the  $2m \times$  the largest term can represent each series for each  $R_0^{(2m)}$  above. Then the approximate  $2m^{\text{th}}$  term of each derivative is

$$\sim \frac{(2m)(2m-3)!}{2^{m-2}2^{m-2}(m-2)!} \left( \frac{(N^2-1)^m}{N^{2m-3}(1+N)^3} \right) \quad (\text{A.28})$$

**Parallel Polarisation**

For parallel polarisation the  $2m^{th}$  term changes only as regards the presence of a higher power of  $n$  in the denominator. For example, the previous largest term for perpendicular polarisation was given by

$$\frac{315(N^2 - 1)^6}{8N^9(1 + N)^3} \quad (\text{A.29})$$

whereas the one for parallel polarisation is

$$\frac{315(N^2 - 1)^6}{8N^{12}(1 + N)^3} \quad (\text{A.30})$$

this merely changes the new general  $2m^{th}$  term from that above to

$$\sim \frac{(2m)(2m - 3)!}{2^{m-2}2^{m-2}(m - 2)!} \left( \frac{(N^2 - 1)^m}{N^{2m}(1 + N)^3} \right) \quad (\text{A.31})$$

**A.3 Properties of Bessel Functions**

The Bessel function of the first kind of order  $m$  is defined by the series

$$J_m(x) = \sum_{s=0}^{\infty} \frac{(-1)^s}{s!(m + s)!} \left(\frac{x}{2}\right)^{m+2s} \equiv \left(\frac{1}{2}x\right)^m \sum_{s=0}^{\infty} \frac{(-\frac{1}{4}x^2)^s}{s!\Gamma(m + s + 1)} \quad (\text{A.32})$$

For integer  $m$

$$J_m(x) = (-1)^m J_{-m}(x) \quad (\text{A.33})$$

now for  $m = 0$  from above

$$(-1)^0 J_{-0}(x) = J_0(x) \quad (\text{A.34})$$

and for  $x$  negative comparison with the series above with  $m = 0$  gives

$$J_0(-x) = J_0(x) \quad (\text{A.35})$$

in fact for  $m$  even

$$J_{2m}(-x) = J_{2m}(x) \quad (\text{A.36})$$

and using the representation for  $m$  integral

$$J_m(x) = \frac{1}{\pi} \int_0^\pi \cos(x \sin \theta - m\theta) d\theta \quad (\text{A.37})$$

$$J_{-2m}(-x) = \frac{1}{\pi} \int_0^\pi \cos(-x \sin \theta - (-2m)\theta) d\theta \quad (\text{A.38})$$

since

$$\cos(-x \sin \theta - (-2m)\theta) = \cos[-(x \sin \theta - 2m\theta)] = \cos(x \sin \theta - 2m\theta) \quad (\text{A.39})$$

therefore

$$\frac{1}{\pi} \int_0^\pi \cos(-x \sin \theta - (-2m)\theta) d\theta = \frac{1}{\pi} \int_0^\pi \cos(x \sin \theta - 2m\theta) d\theta \quad (\text{A.40})$$

or

$$J_{-2m}(-x) = J_{2m}(x) \quad (\text{A.41})$$

we will also use the results

$$J_m(x) = \frac{1}{2\pi} \int_\theta^{\theta+2\pi} e^{i(x \sin t - mt)} dt \quad (\text{A.42})$$

$$i^m J_m(x) = \frac{1}{2\pi} \int_\theta^{\theta+2\pi} e^{i(x \cos t + mt)} dt \quad (\text{A.43})$$

$$(-1)^m J_m(x) = \frac{1}{2\pi} \int_\theta^{\theta+2\pi} e^{i(x \sin t + mt)} dt \quad (\text{A.44})$$

### Asymptotic Expansions

Note that for two extremes the Bessel function  $J_0(x)$  has two asymptotic expansions. For the case where

$$x \rightarrow 0 \quad (\text{A.45})$$

the zero order Bessel function of the first kind  $J_m$  has the expansion for  $m \geq 0$

$$J_m(x) \sim \frac{(\frac{1}{2}x)^m}{\Gamma(m+1)} \quad (\text{A.46})$$

on the other hand when

$$|x| \rightarrow \infty \quad (\text{A.47})$$

$$J_m(x) \sim \sqrt{\frac{2}{\pi x}} \cos\left(x - \frac{m\pi}{2} - \frac{\pi}{4}\right) \quad (\text{A.48})$$



so

$$\lim_{x \rightarrow 0} J_0(x) = 1, \quad \lim_{|x| \rightarrow \infty} J_0(x) = \sqrt{\frac{2}{\pi x}} \cos\left(x - \frac{\pi}{4}\right) \quad (\text{A.49})$$

Note that for large order

$$\lim_{m \rightarrow \infty} J_m(x) \sim -\sqrt{\frac{2}{\pi m}} \left(\frac{ex}{2m}\right)^m \quad (\text{A.50})$$

obviously if  $x$  is finite the result approaches zero.

### Zeros of Bessel Functions

The Bessel Function of integer order all have an infinite number of zeros. The first few zeros of the zero order Bessel function of the first kind are designated  $j_{0,i}$ , that is, the zero subscript representing the zero order Bessel function and the  $i$  representing the  $i^{\text{th}}$  zero. The first few zeros are

$$j_{0,1} = 2.40482 \quad (\text{A.51})$$

$$j_{0,2} = 5.52007 \quad (\text{A.52})$$

$$j_{0,3} = 8.65372 \quad (\text{A.53})$$

All information was obtained from, [1] and, [95].

## A.4 Tangent Plane Criterion

According to Ogilvy, [57], Beckmann & Spizzichino, [8], Bass & Fuks, [6] and originally Brekhovskikh, [17], the Kirchhoff method is only valid provided the radius of curvature of each scattering element is small compared with the incident wavelength that is

$$4\pi r_c \cos \vartheta \gg \lambda \quad (\text{A.54})$$

Another often quoted result, [57], is the condition

$$\left(\frac{kr_c}{2}\right)^{\frac{1}{3}} \cos \vartheta \gg 1 \quad (\text{A.55})$$

This is the less strict condition for local angles of incidence not too near grazing incidence.

The extra, stricter condition can be stated, [17], as

$$\frac{1}{\cos \vartheta} \frac{\lambda^2}{6} \frac{d}{dx} \left( \frac{1}{r_c} \right) \ll 1 \quad (\text{A.56})$$

Now, for sinusoidal surfaces such as the one used in our calculations, that is

$$\zeta = A \sin \left( \frac{2\pi x}{T} \right), \quad \zeta' = \frac{2\pi A}{T} \cos \left( \frac{2\pi x}{T} \right), \quad \zeta'' = -\frac{4\pi^2 A}{T^2} \sin \left( \frac{2\pi x}{T} \right) \quad (\text{A.57})$$

defining the radius of curvature as

$$r_c = \frac{(1 + \zeta'^2)^{\frac{3}{2}}}{|\zeta''|} \quad (\text{A.58})$$

then, since  $\vartheta = \theta_I - \tan^{-1} \zeta'$ , we may calculate for the condition above

$$\frac{4\pi(1 + \zeta'^2)^{\frac{3}{2}}}{|\zeta''|} \cos(\theta_I - \tan^{-1} \zeta') \gg \lambda \quad (\text{A.59})$$

or using the fact that

$$\cos \vartheta = \frac{\cos \theta_I + \zeta' \sin \theta_I}{\sqrt{1 + \zeta'^2}} \quad (\text{A.60})$$

for angles of incidence at the normal,  $\theta_I = 0$

$$\frac{4\pi(1 + \zeta'^2)^{\frac{3}{2}}}{|\zeta''|} \frac{1}{\sqrt{1 + \zeta'^2}} \gg \lambda \quad (\text{A.61})$$

$$= \frac{4\pi(1 + \zeta'^2)}{|\zeta''|} \quad (\text{A.62})$$

substituting for  $\zeta'$

$$= \frac{T^2(1 + \left(\frac{2\pi A}{T}\right)^2 \cos^2\left(\frac{2\pi x}{T}\right))}{A\pi \left| \sin\left(\frac{2\pi x}{T}\right) \right|} \quad (\text{A.63})$$

this must be equally true when the minimum value of this function is much greater than  $\lambda$ . The minimum occurs when the sine term is 1 and the cosine 0. That is when

$$\sin \left( \frac{2\pi x}{T} \right) = 1 \quad (\text{A.64})$$

or

$$x = \frac{T}{4} \quad (\text{A.65})$$

then the condition reads

$$\frac{T^2}{\pi A} \gg \lambda \quad (\text{A.66})$$

or

$$T \gg \sqrt{\pi A \lambda} \quad (\text{A.67})$$

the period must be much larger than amplitude multiplied by the wavelength. For an example, consider the values  $A = 1\mu\text{m}$  and a wavelength of the same order  $\lambda = 1\mu\text{m}$ . Then we find

$$T \gg \sqrt{\pi \times 10^{-12}} = \sqrt{\pi} \times 10^{-6} \simeq 1\mu\text{m} \quad (\text{A.68})$$

since our range of amplitudes will be much lower than this value periods of the order of  $100\mu\text{m}$  are more than adequate. For arbitrary angles of incidence  $\theta_I \neq 0$  we find

$$T \gg \sqrt{\pi A \lambda \sec \theta_I} \quad (\text{A.69})$$

valid provided  $\theta_I \neq \pi/2$ , this restriction is also used to avoid surface shadowing and multiple scattering, [8].

Now as regards the stricter condition

$$\frac{1}{\cos \vartheta} \frac{\lambda^2}{6} \frac{d}{dx} \left( \frac{1}{r_c} \right) \ll 1 \quad (\text{A.70})$$

It has been shown, [8], [17], that this condition is satisfied for sinusoidal surfaces when

$$\frac{\lambda^2 A}{T^3} \ll \cos \theta_I \quad (\text{A.71})$$

or

$$\frac{\lambda^2 A}{T^3} \ll \frac{\cos \theta_I + \zeta' \sin \theta_I}{\sqrt{1 + \zeta'^2}} \quad (\text{A.72})$$

This condition will be most critical at the points of inflection of the function,  $\zeta = A \sin \left( \frac{2\pi x}{T} \right)$ , these occur at  $2\pi x/T = m\pi$ ,  $m$  integer. Then  $\cos m\pi = (-1)^m$  and we have

$$\frac{\lambda^2 A}{T^3} \ll \frac{\cos \theta_I + (-1)^m \frac{2\pi A}{T} \sin \theta_I}{\sqrt{1 + \left( \frac{2\pi A}{T} \right)^2}} \quad (\text{A.73})$$

for  $\theta_I = 0$

$$\lambda^2 \ll \frac{T^4}{A\sqrt{T^2 + 4\pi^2 A^2}} \quad (\text{A.74})$$

or

$$4\pi^2 \lambda^4 A^4 + T^2 \lambda^4 A^2 - T^8 \ll 0 \quad (\text{A.75})$$

a quadratic in  $A$  with solutions

$$A^2 = \frac{T^2}{8\pi^2 \lambda^2} (-\lambda^2 \pm \sqrt{\lambda^4 + 16\pi^2 T^4}) \quad (\text{A.76})$$

then since  $A \geq 0, T > 0, \lambda > 0$  we must choose the positive square root. Therefore

$$A^2 = \frac{T^2}{8\pi^2 \lambda^2} (\sqrt{\lambda^4 + 16\pi^2 T^4} - \lambda^2) \quad (\text{A.77})$$

rearranging this becomes

$$A^2 = \frac{T^2}{8\pi^2 \lambda^2} \left[ 4\pi T^2 \sqrt{\left(\frac{\lambda^2}{4\pi T^2}\right)^2 + 1} - \lambda^2 \right] \quad (\text{A.78})$$

$$= \frac{T^4}{2\pi \lambda^2} \left[ \sqrt{\left(\frac{\lambda^2}{4\pi T^2}\right)^2 + 1} - \left(\frac{\lambda}{2\sqrt{\pi T}}\right)^2 \right] \quad (\text{A.79})$$

note that the squared term in brackets is usually much smaller than 1, this is the case if

$$\frac{\lambda^4}{16\pi^2 T^4} \ll 1 \quad (\text{A.80})$$

or

$$T \gg \frac{\lambda}{2\sqrt{\pi}} \quad (\text{A.81})$$

this is often the case, if for example  $\lambda = 1\mu\text{m}$ , then  $T \gg 0.4\mu\text{m}$  approximately. If this is

so

$$A^2 \ll \frac{T^4}{2\pi \lambda^2} \quad (\text{A.82})$$

approximately. This means

$$T \gg (2\pi)^{\frac{1}{4}} \sqrt{A\lambda} \quad (\text{A.83})$$

a very similar condition to the previous one. There is little difference and the top one will be used. The above conditions form the criteria which determine at least to a partial extent the accuracy of the Kirchhoff method and its applicability in our surface profile.

# Bibliography

- [1] Abramowitz, M., Stegun, I. A., 1958, Handbook of Mathematical Functions with Formulas, Graphs and Mathematical Tables, Dover, New York
- [2] Adler, D. in Kirk-Othmer Encyclopedia of Chem. Tech., 3rd ed., Vol 5, John Wiley, New York
- [3] Angell, T. S., Kleinman, R. E., Hettlich, F., 1990, SIAM J. Appl. Math., 50, 1607-1622
- [4] Bahar, E., 1978, IEEE Trans. Ant. Prop., AP-28, 11-21
- [5] Barrick, D. E., 1968, IEEE Trans. Ant. Prop., AP-16, 449-454
- [6] Bass, F.G., Fuks, I.M., 1979, Wave Scattering from Statistically Rough Surfaces, Pergamon, New York
- [7] Baud, J., Ferrier, A., Manenc, J., 1978, Oxid. Met., 12, 331-342
- [8] Beckmann, P., Spizzichino, A., 1963, The Scattering of Electromagnetic Waves from Rough Surfaces, Pergamon Press, London
- [9] Bennet, H. E., Bennet, J. M., 1966, Optical Properties and Electronic Structure of Metals and Alloys, Abeles, F. (ed), North Holland, Amsterdam
- [10] Bennet, H. E., Porteus, J. O., 1961, J. Opt. Soc. Am., 51, 123-129
- [11] Birkebak, R. C., Eckart, E. R. G., 1965, J. Heat Transf. Trans. ASME, 87, 85-94

- [12] Bleistein, N., Handelsman, R. A., 1986, *Asymptotic Expansions of Integrals*, Dover, New York
- [13] Born, M, Wolf, E., 1989, *Principles of Optics*, Macmillan, New York
- [14] Bousquet, par P., 1962, *Rev. de Opt.*, 41, 277-294
- [15] Bowman, J. J., Senior, B. A., Uslenghi, P. L. E., 1969, *Electromagnetic and Acoustical Scattering by Simple Shapes*, North-Holland, Amsterdam
- [16] Brannon, R. R., Goldstein, R. J., 1970, *J. Heat Transf. trans. ASME*, 92, 257-263
- [17] Brekhovskikh, L. M., 1952, part I & II, *Zh. Eksper. i Teor. Fiz.*, 23, 275-289
- [18] Brown, G. S., 1982, *IEEE Trans Ant. Prop.*, AP-30, 1135-1144
- [19] Browne, K., 1989, BHP Tech note
- [20] Chen, J., 1991, BHP rep. 3
- [21] Cho, S. K., 1990, *Electromagnetic scattering*, Springer, Berlin
- [22] Collin, R. E., 1991, *Field Theory of Guided Waves*, IEEE Press, New York
- [23] Da Silva, E. P., Farias, G. A., Maradudin, A. A., 1987, *J. Opt. Soc. Am.*, 4, 2023-2024
- [24] Davies, , 1954, *Proc. Inst. Elect. Eng.*, 101, 209-213
- [25] Davies, M. H., Simnad, M. T., Birchenall, C. E., 1952, *J. Meta.*, *Trans. AIME*, 536-540
- [26] Davis, J. R., 1990, *Metals Handbook Vol 2 : Properties and Selection - non-ferrous Alloys and Special Purpose Materials*, ASM Materials Information Society
- [27] Deryugin, L. N., 1952, *Dokl. Akad. Nauk. SSSR*, 87, 913-916
- [28] DeSanto, J. A., 1985, *J. Opt. Soc. Am.*, A2, 2202-2207

- [29] Dorren, H. J. S., Tip, A., 1991, *J. Math. Phys.*, 32, 3060-3070
- [30] Eastman, J. M., 1978, *Phys. Thin Films*, 10, 167-226
- [31] Elson, J. M., 1977, *Appl. Opt.*, 16, 2872-2881
- [32] Family, F., Vicsek, J. (ed), 1991, *Dynamics of Fractal Surfaces*, World Scientific, Singapore
- [33] Fontana, M. G., 1987, *Corrosion Engineering*, McGraw-Hill, Singapore
- [34] Fung, A. K., 1970, *Can J. Phys.*, 48, 127-136
- [35] Gulbransen, E. A., Andrew, K. F., 1954, *J. Electrochem. Soc.*, 101, 560
- [36] Harrington, R. F., 1968, *Field Computation by Moment Methods*, Macmillan, New York
- [37] Harrison, J. R., 1960, *Radiation Pyrometry and its Underlying Principles of Heat Transfer*, John Wiley, New York
- [38] Hauffe, K., 1965, *Oxidation of Metals*, Plenum Press, New York
- [39] Haupt, R. L., Cote, M., 1993, *IEEE Trans. Ant. Prop.*, AP-41, 227-230
- [40] Hecht, E., Zajac, A., 1974, *Optics*, Addison Wesley, London
- [41] Hill D. P. et al, 1989, *SPIE 1165*, 62-71
- [42] Hussey, R. J. et al, 1977, *Oxid. Met.*, 11, 65-79
- [43] Iuchi, T., Ohno, J., Kusaka, R., 1976, *Trans, ISIJ*, 16, 195-203
- [44] Kofstad, P., 1988, *High Temperature Corrosion*, Elsevier, London
- [45] Kriezis, E. E., Chrissoulides, D. P., Papagiannakis, A. G., *Electromagnetics and Optics*, World Scientific, Singapore

- [46] Kreyszig, E., 1988, *Advanced Engineering Mathematics*, John Wiley, New York
- [47] Lekner, J., 1987, *Theory of Reflection of Electromagnetic and Particle Waves*, Martinus-Nijhoff, Dordrecht
- [48] Liebert, C. H., 1965, NASA TN D-3115
- [49] Lutter, A., Ferencz, K., 1979, *Thin Sol. Films*, 57, 185-189
- [50] Maxwell Garnett, J. C., 1906, *Phil. trans. R. Soc. Lon., Ser A*, 205, 237
- [51] Maystre, D., 1984, *Progress in Optics XXI*, Elsevier, Amsterdam
- [52] McGer, T. D., 1988, *Principles and Methods of Temperature Measurement*, John Wiley, New York
- [53] Meakin, P., 1993, *Phys. Rep.*, 235, 189-289
- [54] Meecham, W. C., 1956, *J. Appl. Phys.*, 27, 361-367
- [55] Nagata, K., Nishiwaki, J., 1967, *Jap. J. Appl. Phys.*, 6, 251-257
- [56] Nakayama, J., Mitzutani, K., Ogura, H., Hayashi, S., 1984, *J. Appl. Phys.*, 56, 1465-1472
- [57] Ogilvy, L. A., 1991, *Theory of Wave Scattering from Random Rough Surfaces*, Adam Hilger, Boston
- [58] Ohlidal, I., Navratil, K., Lukes, F., 1971, *J. Opt. Soc. Am.*, 61, 1631-1639
- [59] Ohlidal, I., Lukes, F., 1972, *Optica Acta*, 1972, 817-843
- [60] Ohlidal, I., Navratil, K., Lukes, F., 1979, *Thin Sol. Films*, 57, 179-184
- [61] Parkins, B. E., 1967, *J. Ac. Soc. Am.*, 41, 126-134
- [62] Petit, R., *Nouv. Rev. Optique*, 1975, 6, 129-135



- [63] Plonus, M.A., 1978, Applied Electromagnetics, McGraw-Hill, New York
- [64] Popova, O. R., 1983, High Temp., 21, 58-64
- [65] Porteus, J. O., 1963, J. Opt. Soc. Am., 53, 1394-1402
- [66] Rellich, F., 1943, Jahresbericht. Deutscher Math. Vereinigung, 54, 57-65
- [67] Rice, S. O., 1951, Comm. Pure. Appl. Math., 4, 351-378
- [68] Richmond, J. C., DeWitt, D. P., 1985, Applications of Radiation Thermometry, ASTM Publ., Philadelphia
- [69] Sadiku, M. N. O., 1992, Numerical Techniques in Electromagnetics, CRC Press, Boca Raton
- [70] Saint-Jacques, R. G., Arnoux, C., Rheault, F., 1991, J. Appl. Phys., 69, 7876-7880
- [71] Shreir, L. L., Jarman, R. A., Burstein, G. T. (ed), 1994, Corrosion Vol 1 : Metal/Environment Reactions, Butterworth Heinemann, Oxford
- [72] Siegel, R., Howell, J. R., 1972, Thermal Radiation Heat Transfer, Hemisphere Publ. Co., New York
- [73] Sneddon, I. N., 1957, Elements of Partial Differential Equations, McGraw-Hill, New York
- [74] Smith, T. F., Hering, R. G., 1981, , 429-435
- [75] Sokolnikoff, I. S., Redheffer, R. M., 1965, Mathematics of Physics and Modern Engineering, McGraw-Hill, Tokyo
- [76] Spetner, A., 1958, IRE Trans. Ant. Prop., AP-6, 88-94
- [77] Starnes, J. J., 1986, Waves in Focal Regions, Adam Hilger, Boston
- [78] Stott, F. H., Rep. Prog. Phys., 50, 861-913

- [79] Stover, J. C., 1975, *Appl. Opt.*, 14, 1796-1802
- [80] Stratton, J.A., 1941, *Electromagnetic Theory*, McGraw-Hill, New York
- [81] Szczyrbowski, J., Czaplan, A., 1979, *J. Phys. D : Appl. Phys.*, 12, 1737-1751
- [82] Tanaka, F., DeWitt, D. P., 1989, *Nat. Heat Transf. Conf.*, HTD vol 112, 69-75
- [83] Tanaka, F., Ohira, H., Naganuma, Y., 1989, *IEEE*, 89, 24-28
- [84] Tannhauser, D. S., 1962, *J. Phys. Chem. Solids*, 23, 25
- [85] Thorsos, E. T., Jackson, D. R., 1989, *J. Ac. Soc. Am.*, 86, 261-277
- [86] Tokunaga, Y., Yamada, M., 1982, *JSIJ*, 70, 43-50
- [87] Torkov, E. Y., 1988, *High Pressure Phase Transformations : a handbook*, vol 2, Gordon Breach, Philadelphia
- [88] Torrance, K. E., Sparrow, E. M., 1967, *J. Opt. Soc. Am.*, 57, 1105-1114
- [89] Touloukian, Y. S., DeWitt, D. P., 1970, *Thermal Radiative Properties : Metallic Elements and Alloys*, Plenum, New York
- [90] Verein Deutscher Eisenhüttenleute (ed), 1993, *Steel : A Handbook for Materials Research and Engineering*, vol VI, Fundamentals, Springer, Berlin
- [91] Verhaeghe, M. F., 1972, *Optica Acta*, 19, 905-940
- [92] von Esser, F., 1965, *Neue Hütte*, 5, 302-304
- [93] Wagner, C., Koch, E., 1936, *Z. Physikal. Chem.*, B, 32, 439-446
- [94] Wangness, R.K., 1986, *Electromagnetic Fields*, John Wiley, New York
- [95] Watson, G. N., 1958, *A Treatise on the Theory of Bessel Functions*, Cambridge Uni Press, London

[96] Wilton, D. R., 1992, *Electromagnetics*, 12, 287-341

[97] Wirgin, A., 1980, *J. Ac. Soc. Am.*, 68, 692-699

[98] Zipin, R. B., 1966, *Appl. Opt.*, 5, 1954-1957